University of Nevada, Reno

Black Carbon Nanoparticles in Paleo-Records: A Combustion Proxy

A dissertation submitted in partial fulfillment of the requirements for the degree of Doctor of Philosophy in Hydrogeology

by

Marion Mathilde Anne Bisiaux

Dr. P. Ross Edwards/Dissertation Advisor

December, 2011

University of Nevada, Reno
Statewide • Worldwide

THE GRADUATE SCHOOL

We recommend that the dissertation
prepared under our supervision by

Marion Mathilde Anne Bisiaux

entitled

Black Carbon Nanoparticles in Paleo-Records: A Combustion Proxy

be accepted in partial fulfillment of the
requirements for the degree of

DOCTOR OF PHILOSOPHY

Prof. Dr. P. Ross Edwards, Advisor

Prof. Dr. Joseph R. McConnell, Committee Member

Prof. Dr. Alan C. Heyvaert, Committee Member

Prof. Dr. Joyce E. Penner, Committee Member

Prof. Dr. W. Patrick Arnott, Graduate School Representative

Marsha H. Read, Ph. D., Dean, Graduate School

December, 2011

ABSTRACT

Emitted to the atmosphere through fire and fossil fuel combustion, refractory black carbon nanoparticles (rBC) impact the global climate, atmospheric chemistry, human health, and the carbon cycle.

In the Southern Hemisphere (SH), rBC is transported in the atmosphere from low latitudes to Antarctica and deposited to the polar ice sheet, preserving a history of the variability of emissions and atmospheric transport. Here we present a total of eight records of rBC over the polar continent, covering a period ranging from the pre-industrial era to the modern era. These new records represent one of the first surveys of rBC deposition variability over Antarctica for that period of time. Firstly, two high-resolution rBC records from the West Antarctic Ice Sheet divide (WAIS) and Law Dome, on the periphery of the East Antarctic ice sheet, spanning calendar years 1850-2001, are investigated. Highly correlated over the past 60 years, the records show that coherent large-scale changes in rBC deposition to Antarctica occurred at decadal to inter-annual time scales, notably in ENSO-like periodicities. Since ~1940, the records show decadal trends similar to the inventories of SH rBC emissions from grass fires and biofuels. The two records suggest a large-scale reduction in rBC deposition from 1950 to 1990 to WAIS and Law Dome.

In order to better understand the spatial and temporal variability in rBC deposition to the polar continent, those high resolution records are compared to six other rBC ice core records from the East-Antarctic Plateau. Located on the Dronning Maud Land, those additional records are characterized by a lower accumulation and thereby lower temporal resolution compared to the WAIS and Law Dome sites. Temporal and spatial analysis of rBC concentrations and fluxes in the East-Antarctic ice cores for the period 1800-2000 reveals high variability of concentrations, and a slightly increasing general trend. Some of the variability recorded at those sites is similar to the high resolution records and suggests a link with short and long-term variability of ENSO.

Once emitted to the atmosphere, rBC particles also enter aquatic environments, where they may affect the fate of other pollutants. However, measurements of very low rBC-concentrated waters

have almost never been investigated for that purpose. Here, a study determining rBC in waters of the Lake Tahoe watershed in the western United States from 2007 to 2009 are presented. The study period spanned a large fire within the Tahoe basin, seasonal snow-melt, and a number of storm events, which injected urban runoff into the Lake with rBC concentrations up to four orders of magnitude higher than background concentrations. The results show that rBC pulses from both the wildfire and urban runoff were rapidly attenuated within the lake, suggesting unexpected removal from the water column or aggregation to sizes outside of analysis detection capability. Those processes prevent rBC concentrations from building up in the clear and oligotrophic Lake Tahoe. Results obtained for the Tahoe study are compared to similar measurements performed in other oligotrophic lakes, and interpreted to characterize rBC transfer to sediments. Additionally, we measure rBC concentrations in a sediment core from Lake Tahoe, to evaluate the potential of this archive as a combustion record. Despite loss of rBC particles observed in the water column, rBC is transferred to sediments which preserve a local-to-regional scale history of its emissions as revealed by comparison with other pollutant records.

Shall I refuse my dinner because I do not fully understand the process of digestion?

Oliver Heaviside (1850-1925),

English mathematician and physicist

Acknowledgments

I would like to express by deepest gratitude and thanks to my doctoral advisor Dr. Ross Edwards. Throughout my doctoral work, he has been very supportive and encouraged me to develop research skills and independent work. Thanks for asking “are you looking for a PhD?” one day in a DRI’s hallway. Did I really look lost?

I have many other “thanks” to say:

Thanks to the committee members, Drs. Joe McConnell, Alan Heyvaert, Joyce Penner and Patrick Arnott, for having been relaxed with last minute proposal presentations, video-conferenced comprehensive exam, and three-months-ahead organized defense. Thanks for your stimulating comments that have strengthened the manuscript. Thanks to Dr. Ken Taylor for your help at DRI once Ross had left. Thanks for being so supportive. Thanks to Dr. Paul Verburg for your offer of my first job at DRI, this is how it all started.

Thanks to the DRI ice core team: Dan, Kelley, Aja, Ryan, Orion, Tommy and Kelsey. I thought you were really good at keeping the warmth in the freezer. Thanks to the WAIS drilling team, the NorUS traverse team and the Tahoe sampling team, even if sometimes I wished I could have been one of you. Thanks to the Combatant Gang: yes the book will be super fantastic!

Thanks again to Dan for accepting to spend hours preparing the cryospheeere class, and for being on time while teaching. Thanks also to all the (four..) students who enrolled in this class and for not paying attention that I was, by far, the youngest in the room. Thanks to Dr. Greg Pohll for having let us teach this class.

Thanks to Drs. Jean-Luc Jaffrezo and Paolo Laj at LGGE for having given me an office during almost a year in Grenoble (should I leave the Greenland and sediment samples there as an excuse to come back?). Thanks also to the LGGE-camp-d’altitude colleagues notably: Julie, Aude, Giom, Julien, Saehee, Marco, DDA, Antonin, Paolo, Lucie, Mounir and associated animals for listening to me talking about black carbon, air pollution, biking Grenoble under rain and snow,

organic food and cancerogenous parabens. Thanks to Jean-Robert Petit for his valuable guidance and enthusiasm for my black carbon data. To all: I owe you one or two giraffes at least.

Thanks to Elisabeth Adamska, Pam Love, Cindy Littlefield, Margie Stuart and DRI administration for helping with graduate assistantship, international paperwork and general help throughout the GPHS. Thanks to Dr. John Warwick for the fluid mechanic class waver… Thanks to DHS, Dr. George B. and Jane C. Maxey for the Maxey award.

Thanks to Sabrina for sharing fundamental scientific experiments such as cheese ripening, whipped-cream skin cares and compost efficiency. Thanks to Daniel, Jimmy, Hans, Mark, Dave… for showing us the countryside of Reno and helping us while we were homeless/carless/bikeless or beerless (less often).

Merci à Moune qui m'a toujours encouragée et discrètement conseillée, et qui, surtout, m'a transmis sa curiosité. Merci à mes grands-parents pour leur soutien et intérêt même en anglais. Merci au reste de la famille et à la belle famille pour les encouragements. Merci aux amies de toujours Marie et Pauline d'avoir vraiment essayé de comprendre. Merci aux compagnons de galère de la filière « TUE » (un nom qui…) : Notamment Sam, Alesk, Elo, Orèl, Daf, Isa, Manu…Bon courage à ceux qui rament encore. Merci aux copains de Grenoble et aux breuvages de la Bonbonne Fêlée pour les décompressages à répétition. Merci à Mandou pour les fusibles.

et enfin Xav, merci. Sans toi y'aurait rien eu de tout ça et avec toi y'a tout qui va

Table of Contents

Acknowledgments iv

Table of Contents vi

List of Tables xi

List of Figures xii

List of abbreviations xviii

Chapter I. Introduction 1

Chapter II. Introduction to black carbon and fire sciences 3

II.1. Black carbon cycling and characteristics 3

II.1.1. Formation of black carbon 3

II.1.2. Sources and sinks of black carbon 6

II.1.3. Environmental impacts of black carbon 9

II.2. Using black carbon as a proxy 14

II.2.1. Black carbon in ice-cores and firn 14

II.2.2. Black carbon in fresh and marine waters 19

II.2.3. Black carbon in sediments 20

II.3. Nature and impact of biomass burning 21

II.3.1. What is a fire? 21

II.3.2. Today's fires 24

II.3.3. Fire emissions to the atmosphere 28

II.3.4. Fires and climate interactions 29

II.3.5. Past forest fires –records and modeling 32

II.4. Objectives of the dissertation 35

II.5. Dissertation organization 36

Chapter III. Methods 39

III.1. Black carbon measurements 39

III.1.1. The single particle soot photometer 39

III.1.2. Calibration of the instrument and protocol 42

III.2. Continuous Flow analysis 45

III.2.1. Ice core analysis at the Desert Research Institute 45

III.2.2. Protocol of analysis 47

III.3. Ice core dating 48

III.3.1. Annual layer counting 48

III.3.2. Identification of remarkable horizons 49

III.3.3. Cross-comparisons with other ice core records 50

III.3.4. Utilization of ice thinning and ice flow modeling 50

Chapter IV. High resolution rBC records from low elevation sites of Antarctica, cal. yr. 1850-2001 52

IV.1. Introduction 53

IV.2. Ice core locations and methods 54

IV.3. Results and discussion 56

IV.3.1. Concentrations and fluxes 56

IV.3.2. Decadal variability: Unprecedented period of low variance 60

IV.4. Conclusions 61

IV.5. Supplementary information to Chapter IV 63

IV.5.1. Black carbon measurements 63

IV.5.2. Dating 63

IV.5.3. Fluxes 64

IV.5.4. Spectral analysis 64

IV.5.5. Additional figures: 66

Chapter V. rBC ice core records from the Eastern Antarctic Plateau, cal. yr 1800-2000 69

V.1. Article: Variation of accumulation rates over the last eight centuries on the East Antarctic Plateau derived from volcanic signals in ice cores 69

V.1.1. Introduction 70

V.1.2. Data and Methods 72

V.1.3. Results 75

V.1.4. Discussion 79

V.1.5. Conclusions 88

V.2. Article: Variability of black carbon deposition to the East Antarctic Plateau, A.D. 1800-2000 90

V.2.1. Introduction 91

V.2.2. Drilling sites and methods 93

V.2.3. Results and Discussion 97

V.2.4. Conclusions 105

Chapter VI. rBC sources to oligotrophic lakes and transfer processes to sediments 107

VI.1. Context of study 107

VI.2. Article: Stormwater and fire as sources of black carbon nanoparticles to Lake Tahoe ... 109

VI.2.1. Introduction 110

VI.2.2. Materials and Methods 112

VI.2.3. Results and Discussion 115

VI.3. Investigation of rBC transfer in lake waters at other sites 124

VI.3.1. Castle Lake 124

VI.3.2. Crater Lake 125

VI.3.3. Great Lakes 126

VI.4. Interpretation of rBC sources to oligotrophic lakes and transfer processes to sediments 128

Chapter VII. rBC in lake sediments: a potential archive to investigate past fire history 130

VII.1. Lake Tahoe sediments analysis 130

VII.1.1. rBC measurements. 131

VII.1.2. Dating 132

VII.2. Results and discussion 132

VII.2.1. rBC concentrations in sediments 132

VII.2.2. Comparison with the charcoal record 133

VII.2.3. Comparison with lead and mercury records 134

VII.3. Conclusions and perspectives to rBC in lake sediments 135

Chapter VIII. Conclusions and perspectives 137

Appendices 140

References 148

List of Tables

Table II.1: Surface (S) and percentage (S%) cover of regions and sub-regions considered here, as well as corresponding average burning area (B, Mha yr^{-1}) and the percentage it represents within the global burned area (B%), FRI indicates the Fire Return Interval (in years) (Adapted from Mouillot & Field 2005). 27

Table IV.1: Ranges and averages of annual rBC concentrations for this study and previous work in Greenland and Antarctica (snow and ice). Approximate location of WDC06A and DSSW19K sites are shown on the map on left hand corner. [a]: For this work only, annual concentrations are calculated from the log values of monthly data and the average is the geometric mean of those annual concentrations. For Law Dome, out-layer year 1910 has been excluded of range estimation. [b]: Altitude measured by Digital Elevation Model from (Bamber et al. 2009). 57

Table V.1: Snow depths of volcanic peaks in the cores from the first leg. All depth units are in meters and the date refers to the year of eruption as this is more certain than the year of deposition (see text). 75

Table V.2: Snow depths of volcanic peaks in the cores from the second leg. All depth units are in meters and the date refers to the year of eruption. 76

Table V.3: Accumulation over the most recent decades, 200-year mean and long-term mean in the NUS cores, compared with the results by Arthern et al. [2006]. The 200-year values for sites NUS07-1, -3, ... 76

Table V.4: Sites characteristics for NUS records, rBC concentrations, accumulation and fluxes. a: multiplicative standard deviation; b: from section V.1; c : we assume same accumulation rate for the 1800-1815 periods..... 94

Table VI.1: rBC concentrations and discharge data at the storm water monitoring stations for four storm events. *indicates a gap in data for total discharge estimations, thus, those numbers have to be used with caution and just as indications. 117

List of Figures

Figure II.1: The black carbon combustion continuum (Thevenon et al. 2010, adapted from Masiello 2004). rBC measurements conducted for this dissertation would be found at very right of this continuum. 4

Figure II.2: BC nanoparticles collected from within a house (photo: www.tms.org) 6

Figure II.3: A schematic drawing of the carbon cycle and black carbon sources: gray arrows represent natural CO_2 emissions and red arrows represent CO_2 emissions due to land-use change and fossil-fuel use in gigatonnes of carbon per year (Thevenon et al. 2010). 7

Figure II.4: Global average radiative forcing (RF) in 2005 (best estimates and 5 to 95% uncertainty ranges) with respect to 1750 for CO_2, CH_4, N_2O and other important agents and mechanisms, together with the typical geographical extent (spatial scale) of the forcing and the assessed level of scientific understanding (LOSU). Aerosols from explosive volcanic eruptions contribute an additional episodic cooling term for a few years following an eruption. The range for linear contrails does not include other possible effects of aviation on cloudiness (IPCC 2007). 10

Figure II.5: Fraction of organic pollutant (PAHs, POPs) bound to BC as a function of aqueous concentration, for 1%, 5%, 10% and 20% BC (of TOC). The curves are modeled based on in situ sorption observations (Koelmans el al. 2006). 14

Figure II.6: Firn densification processes as a function of density (adapted from M. Van den Broeke) 15

Figure II.7: rBC record in an Himalayan ice core (Kaspari et al. 2011) showing increased rBC deposition from anthropogenic pollution in the last 30 years. 17

Figure II.8: Greenland record of rBC showing increased emissions in the 1930's due to increase use of coal as energy source in the U.S.A. (McConnell et al. 2007). 18

Figure II.9: Types of wildfires and sources of fuel (Modified from Scott, 1989) 23

Figure II.10:Schematic showing carbon-cycle, atmospheric-chemistry and biogeophysical feedbacks from fire to the climate system (adapted from Harrison et al. 2010) 30

Figure II.11: Overview of paleo-fire archives, recording fire occurrences at different scales and resolution (adapted from Whitlock and Tinner, 2010) 33

Figure III.1: Schematic of a USN CETAC UT5000 (left) and picture of this USN in operation (right). The white cloud in the aerosol chamber (glass) is visible and shows the aerosolization of the water sample. 40

Figure III.2: Schematic of the coupled SP2-FIA analytical system. 40

Figure III.3: Schematic of the SP2 (Droplet Measurement Technologies, Denver, CO) system used at DRI (adapted from Schwarz et al. 2006). 41

Figure III.4: A typical SP2 daily calibration at DRI. Peak areas of each standard (blue square) are reported on the graphs on the right as a function of known rBC concentrations. The top-right hand corner displays the bending of the calibration curve after ~20-30 µg/l. A zoom of the linear part is shown in the bottom graph. 44

Figure III.5: Schematic of the snow and ice chemistry facilities system used at DRI, including the CFA-side and trace element measurements (courtesy of Joe McConnell). 46

Figure III.6: (Left) Example of annual layers visible on an ice fall (Alpine glacier); brown layers mark summer layers. (Right) Illustration of the use of annual cycles for WAIS core: maximas and minimas correspond to specific periods of the year, depending on the proxy used (blue bands indicate winter-spring periods centered over September, red bands indicate summer periods centered over December) 49

Figure III.7: A visible layer in a WAIS divide ice core (depth ~2500m) of unknown nature yet (likely Tephra or dust). Courtesy of Peter Neff from the NiCL facility. 50

Figure IV.1: 1970-2000 monthly (dots) and annual smoothing (line) for rBC at WAIS and Law Dome. 56

Figure IV.2: Smoothed rBC concentrations (thick) and decimal (thin) for WAIS (top) and Law Dome (bottom), re-sampled with a piece-wise linear interpolation integration. Red dash line is 21-yr smoothing with R implementation of Nadaraya-Watson kernel regression estimate. K marks the Krakatoa volcanic eruption used for dating. 58

Figure IV.3: Spectrums obtained by Multi taper Method (MTM), for WAIS (a) and Law Dome (b) monthly rBC records for 1850-2001 period and confidence levels in red lines (90, 95, 99%). Significant periodicities (notably in ENSO and QBO band) an corresponding values in years are indicated as numbers on the graph. 59

Figure IV.4: a,b: rBC records for WAIS and Law Dome. In gray, concentrations re-sampled to annual resolution with a piece-wise linear interpolation integration. Dark thick lines are 21-yr smoothing with R implementation of Nadaraya–Watson kernel regression estimate. c: comparison with reconstructed rBC emissions from SH fossil fuel anthropogenic use, Australian grass fires, South American grass fires (Lamarque et *al*. 2010) –left scale- and from Australian biofuels (Ito and Penner 2005) –right scale. The vertical bar highlights the beginning of fire prevention in Australia. 61

Figure IV.5: 1970-2000 monthly (dots) and annual smoothing (line) for Na at WAIS and Law Dome. 66

Figure IV.6: Distribution of rBC (left) and Na (right) data points at WAIS (top) and Law Dome (bottom)..... 66

Figure IV.7: Top. Average (thick) and max-min (thin) coherence coefficients for 1970-2001 period between rBC and Na records for WAIS(a) and LD(c). Non zero coherence is > 0.38 and shaded. Time resolution is 0.4yr (Blackman Tukey spectrum using Bartlett window, band .. 67

Figure IV.8: Spectrum obtained with Multi Taper Method for WAIS (a) and LD (b) monthly Na records for 1850-2001 period and confidence levels in red lines (90, 95, 99%). Numbers on graph indicate significant periodicities in years. 67

Figure IV.9: Average coherence (thick) and max/min (thin) between LD and WAIS periodicities for rBC (a) and Na (b) for the 1970-2001 period at a 0.4yr time resolution (Blackman Tukey spectrum using a Bartlett window, bandwidth 0.098, non-zero coherence >0.38). ENSO 68

Figure IV.10: Moving variance (on log values) calculated for 21 months, from 1850 to 2000 at WAIS (a, c) and LD (b, d), for rBC (a, b) and Na (c, d). A period of low variance from 1955 to 1985 is common to the two sites, but only in rBC record. 68

Figure V.1:Map of the traverse route 2007/2008 (green line) and 2008/2009 (blue line) with drill sites from both legs indicated (NUS07-X and NUS08-X). The South Pole Queen Maud Land Traverse routes [*Picciotto et al.*, 1971] are indicate by the yellow-orange lines and relevant stations in the area of investigation are shown as well. Other dots indicate science stops along the traverse routes not relevant for this paper but shown for the sake of completeness. Elevation contour lines are in 100 m intervals. The map was compiled by K. Langley and S. Tronstad (Norwegian Polar Institute). 73

Figure V.2: Records of chemistry data for the cores NUS07-2 (a: nss-sulfur, b: electrolytical conductivity, c: sodium), NUS07-5 (d: nss-sulfur) and NUS07-7 (e: nss-sulfur). The two-fold standard deviation is indicated by the grey line in the sulfur records. A: Agung 1963, Kr: Krakatau 1883, T: Tambora 1815, U1: Unknown 1695, H: Huaynaputina 1600, Ku: Kuwae 1453, EC: El Chichón 1342, U3: Unknown 1259. Note that only the top 50 m are shown here as they fully cover the time period we are concerned with here..... 77

Figure V.3: The Agung eruption in the deep cores from the first leg. a) NUS07-2, b) NUS07-5, c) NUS07-7. Since the peak in NUS07-2 is just at the two-fold standard deviation (see Figure V.2) and also less clear than in the other cores, it is displayed with a question mark here. .. 80

Figure V.4: Normalized DEP-based conductivity for the cores NUS08-2, -3, -4 and -6 from the second leg. The volcanoes discussed in the text are indicated. DI: Deception Island 1641, U2: Unknown 1622; other abbreviations see Figure V.2. The negative spikes in parts of the records are due to varying core quality and slightly differing diameter and are not eliminated here completely as full elimination would induce data gaps..... 80

Figure V.5: Sulfur data for the cores NUS08-4 (a) and NUS08-5 (b) from the second leg. The two-fold standard deviation is indicated by the grey line. Same abbreviations as in Figure V.2.

Note that only the top 50 m of NUS08-5 are displayed here, covering the period back to about 1250 AD that we are concerned with in this paper. 81

Figure V.6: Radargram of the stretch between NUS08-5 and -6. The Tambora layer is highlighted by 83

Figure V.7: Temporal variability of accumulation rate in the cores from the first leg. Top: DEP cores; bottom: chemistry cores. 84

Figure V.8: Temporal variability of accumulation rate in the cores from the second leg. Top: DEP cores; bottom: chemistry cores. 84

Figure V.9: Map of the traverse route 2007/2008 (black line) and 2008/2009 (blue line) with drill described in this study sites from both legs indicated (NUS07-X and NUS08-X). Relevant stations in the area of investigation are shown as well. Elevation contour lines are in 100 m intervals. The map was compiled by K. Langley and S. Tronstad (Norwegian Polar Institute) and adapted for this study, and adapted from Anschütz et al. (2011) for this study. Complete map can be found in section V.1. 93

Figure V.10: Time series of rBC concentrations. Black line is annual (piece-wise linear integration interpolation of log raw data) and red line is 21 yr k-smooth on annual (calculated in log space). 99

Figure V.11: Z-scores of non-linear trends (Kspectra software, Kendall significance =95%) for the six NUS rBC records, as a function of time. Corresponding fraction of record variability is indicated next to record name (%). Top: comparison of twin sites 08-4 and 08-5, re-scaled from 07-1 dating (plain curve). Original dating is shown as dotted line. Middle: other three records 07-2, 07-5 and 07-7. Shaded areas highlight specifically common features and/or trends. Bottom: comparison of Z-scores from sites 07-1, 08-4, 08-5 with NADA variance (dotted line, scale inverted). 100

Figure V.12: Geometric mean rBC (a) and Na (b) concentrations ~since cal. yr. 1963 as a function of site altitude. For Na, regression line was calculated without the maritime site “Law Dome”. (c) Geometric mean rBC concentrations as a function of accumulation after cal. yr.1963 (Anschütz et al. 2011). Uncertainty bars refer to table V.4. Regression lines and coefficients are based on geometric mean values. R^2 indicates the coefficient of determination. * Indicates values for Law Dome and WAIS from Bisiaux et al. (2011, accepted), Chapter IV. 101

Figure V.13: Cross correlation coefficients between Na and rBC from the same record. Na leads rBC for delays >0 and rBC leads Na and for delay <0. 103

Figure V.14: Spectral power (red) of rBC NUS records and coherence coefficients (black) between rBC and Na investigated for the whole period (since 1800). Non-zero coherence is above 0.38. Letters “NT” stand for “Non Transport” and indicates periodic signal in the rBC record that is not coherent to Na (no black peak) and that is likely related to rBC emissions rather than regional to long-range atmospheric transport. The red numbers below “NT” show the corresponding periodicity (in years). 105

Figure VI.1: Map of sample locations around Lake Tahoe. A: In orange are the SWM sites and in red the MLTP station. The Figure B shows a drawing of the Angora neighborhood with the two sampling sites. The Figure C is a map of sampling sites at South Lake Tahoe, for stream sampling sites (Upper Truckee River (UT) sites) and near shore sampling sites (Regan, South Beach, Bijou). 113

Figure VI.2: Schematic of the coupled SP2-FIA analytical system. 114

Figure VI.3: Total rBC in Lake Tahoe mid-lake site water column (in g /m^2) from February 2007 to January 2009. The red line shows the timing of the Angora fire, which damaged 12.5 km^2 of land in the Southern Lake Tahoe area. The gray dashed lines display the error envelope for total rBC data points. On the insert on the top right hand corner is shown two rBC mid-lake profiles for the specific months of May and August 2007 (in µg/l), illustrating the disturbance induced by the fire on rBC concentrations. 116

Figure VI.4: Distribution of rBC concentrations in µg/l during the single storm event of January 22, 2009 at three SWM sites (Kings Beach, Incline Village and Tahoe Airport). A first “flushing” effect is visible, followed by a tail of steady concentrations. 119

Figure VI.5: rBC concentrations in µg/l in runoff at the five South Lake Tahoe sites and the days (year 2009) and weather conditions during sampling. 120

Figure VI.6: rBC concentration for near shore samples (lake samples) at the four South Lake Tahoe sites for the three storm events and one clear day monitored in the spring 2009, averaged for distances 1m and 10m away from shore. 121

Figure VI.7: Map of Crater Lake (OR), Castle Lake (CA) and Lake Tahoe (NV, CA) locations in the western United States. 124

Figure VI.8: Fall 2009 rBC concentrations lake profiles of Castle Lake (left) and Crater Lake (right). Watch the difference in depth scale. 125

Figure VI.9: Map of Lake Superior sampling sites (stars). Two sites are open lakes (East, orange and West, green), one is at the mouth of the Ontonagon River (magenta), and the last one is at the mouth of the Baptism River (red). 127

Figure VI.10: rBC concentrations in the Lake Superior, for isothermal and thermally stratified periods. Orange and green are open lake samples, magenta is at the mouth of the Ontonagon River, and red the mouth of the Baptism River. 128

Figure VII.1: Bathymetric profile of Lake Tahoe (modified from Heyvaert et al. (2000)). Sediment sampling locations are indicated for cores (1) LT-91-1, (3) LT-91-3, and (4) LT-91-4. Core #1 was used for rBC measurements (in yellow), all the cores were used for Hg and Pb. Depth contours are given in meters. 131

Figure VII.2: Median rBC concentrations (circles) versus core depth. Lines show 10 and 90%percentiles. Time scale (cal. yr.) is reported on the right axe. 133

Figure VII.3: Comparison of rBC concentrations in µg/g (left) and charcoal counts in # of grains per gram (right) in the top 20 cm of the sediment core. Dated layers are indicated on the right scale. 134

Figure VII.4: Lake Tahoe profiles (LT-91-1) of rBC, Pb and Hg concentrations, with the data smoothed by a three-term moving average, and of charcoal counts, smoothed by a five-term moving average. Approximate deposition dates are shown for reference on the right scale. 135

List of abbreviations

A.D.: Anno domini

ASL: Above sea level

BC: Black carbon

rBC: Refractory black carbon

BP: Before present

CFA: Continuous flow analysis

CH_4: Methane

CO: Carbon monoxide

CO_2: Carbon dioxide

Cpy: Cycle per year

CTO-375: Chemothermal oxidation method

DEP: Dielectric profiling

DOC: Dissolved organic carbon

DMA: Differential mass analyzer

DOM: Dissolved organic matter

DRI: Desert Research Institute

EC: Elemental carbon

ENSO: El Niño Southern Oscillation

FIA: Flow injection analysis

GC: Graphitic carbon

GPR: Ground penetrating radar

HR-ICP-MS: High resolution inductively coupled plasma mass spectrometry

ITCZ: Inter-tropical convergence zone

ICP-MS: Inductively coupled plasma-mass spectroscopy

IPY: International Polar Year

LD: Law Dome

NADA: North American Drought Atlas

NHZ: Near shore zone

Nss: Non sea-salt

NUS: Abbreviation for Norwegian-US traverse sites

PAHs: Polycyclic aromatic hydrocarbon

POM: Particulate organic matter

USN: Ultrasonic nebulizer

SCFCS: Segmented application of the constant flux with constant sedimentation rate model

SP2: Single particle soot photometer

WAIS: West Antarctic Ice Sheet

Chapter I. Introduction

Concerns about recent global warming are increasing and are “unequivocal, as is now evident from observations of increases in global average air and ocean temperatures, widespread melting of snow and ice and rising global average sea level” (IPCC 2007). Origin of this increase is, at least in the recent decades, attributed to the intensification of greenhouse gas emissions that have increased by 70% between 1970 and 2004, and which is much higher than natural variations observed in recent millennia. Projections of emissions for the future are rather pessimistic. If anthropogenic emissions continue to increase at the same rate as today, increase in temperature should be amplified during the 21st century (IPCC 2007). Consequences of this warming are numerous, since they induce disequilibrium of the global climatic system impacting directly ecosystems, meteorology and human society organization and life.

Fire is part of this climatic system and is also likely to be affected by climate change through modification of precipitations and temperature patterns. The effect of rapidly changing climate conditions such as global warming on fire intensity, repartition and frequency is not well understood, notably because there is a lack of understanding on the interactions between climate and fires. The global history of fires is not well constrained even in the last century. Fire is, however, a fundamental process of the Earth system, disturbing landscapes, ecosystems, carbon balance and energy balance notably through the emissions of greenhouse gases and light absorbing particles (Bowman et al. 2009). High resolution records of fire variability as a function of climate evolution since the industrial revolution would help to assess whether fire can amplify global warming or reduce it (positive or negative feedback).

In this context, refractory black carbon nanoparticles (rBC) produced by biomass burning and fossil fuel combustion, and staying unaltered in sediments and ice for thousands of years (Masiello and Druffel 1998) constitutes a suitable proxy to examine past-fires variability and their

anthropogenic disturbance. However, due to analytical limitations, the measurements such individual rBC nanoparticles has only been possible until recently in ice (McConnell et al. 2007; Kaspari et al. 2011) and yet never for sediments, rather analyzed as bulk rBC (Masiello and Druffel 1998; Elmquist et al. 2007). Nonetheless, the study of rBC as a combustion proxy in paleo-records is a “hot topic”. Its formation in the gas phase and subsequent small size allows it to be transported over longer distances than charcoal. Moreover, its high refractory characteristic makes it an important component of the carbon cycle of which it could represent parts of what is called the “missing sink” of carbon in global carbon cycle models (Shrestha et al. 2010). The duality of its sources (fossil fuels and biomass burning) implies that rBC can be used to investigate both natural and anthropogenic combustions. rBC records in ice cores are not subject to smoothing as gaseous species, and thus can reveal recent changes in emissions (last decades) with high temporal resolution (seasonal to sub-annual). rBC short atmospheric residence time, however, renders these records very dependent on atmospheric transport and source location (Kaspari et al. 2011). However, its unique origin from biomass burning prior to the industrial revolution makes it a direct tool for paleo-fire reconstructions.

Reconstruction of rBC histories from both the sediment records and the ice core records may thereby help to understand the processes linking fires and climate. Moreover, those deposition records at given locations, provide constraints for modeled scenarios of rBC emission and deposition, as a function of increased anthropogenic emissions. Together with global climate models, rBC records may significantly improve the prediction of emissions from fires and their climatic feedbacks.

Chapter II. Introduction to black carbon and fire sciences

II.1. BLACK CARBON CYCLING AND CHARACTERISTICS

II.1.1. Formation of black carbon

Black carbon (BC) is not one material but rather a continuum of materials related by pyrolysis. These materials have different properties and are operationally defined by the sample matrix and the method used to characterize them. Common names include (i) elemental carbon (EC) due to its thermally refractory nature (operationally quantified through thermo-optical methods), (ii) graphitic carbon (GC) due to its graphitic lattice structure (operationally quantified through Raman spectroscopy or X-ray diffraction), or (iii) insoluble carbon (operationally quantified as the soot fraction insoluble in polar and non-polar solvents) (Moosmüller et al. 2009). In soil sciences, BC is defined by a “combustion continuum model”, which depends on fuel material, availability of oxygen during combustion and the temperature of combustion (Masiello 2004). The BC continuum ranges from slightly charred material (char-BC) to soot-BC, which is formed by distinctly different processes (Masiello 2004), Figure II.1.

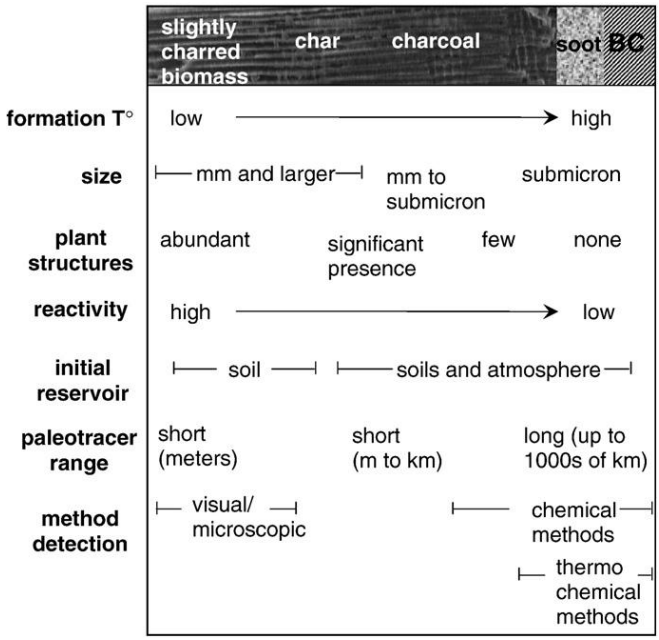

Figure II.1: The black carbon combustion continuum (Thevenon et al. 2010, adapted from Masiello 2004). rBC measurements conducted for this dissertation would be found at very right of this continuum.

Char-BC is defined as the residual phase left after relatively low temperature combustion of carbonaceous material. Char-BC tends to be formed from woody biomass and exhibits some of the morphological features of the original material (Nguyen et al. 2004). The particle diameters of char-BC typically range from 1 to 100 µm, with highly variable surface areas (1.3 to 424 m^2/g for synthetically produced particles) (Nguyen et al. 2004) dependent upon the original material, combustion temperature and duration of combustion.

In contrast, **soot-BC** is formed during the incomplete combustion of gaseous hydrocarbon at higher temperature than char-BC and above ~450°C (Andreae and Gelencser 2006). Soot formation process can occur during biomass burning (forest and grass wild fires, fire places) and fossil fuel combustion (coal, charcoal, gasoline, diesel fuel), which emit hydrocarbon pyrolysis gases. Ongoing research into soot formation has yielded a generalized formation mechanism (Moosmüller et al. 2009 and references therein). Stages of soot formation include: i) formation of precursor species; ii) particle inception; and iii) particle surface growth and agglomeration. During

the stage i), pyrolysis hydrocarbons condense at high temperature forming sub-micron aerosol particles. In step ii), polycyclic aromatic hydrocarbons (PAHs) form and grow within the aerosols, transitioning from a molecular phase to a solid particle which reacts with other precursors and gas phase molecules until becoming large enough to act as a nuclei for further growth and graphitization. The nuclei are constituted of a randomly ordered inner core and a more crystallized outer shell (Ishiguro et al. 1997; Schmidt and Noack 2000; Stanmore et al. 2001). The step iii) consists of the collision and agglomeration of particles (inside the flame) due to Brownian motion. As the particles leave the flame and cool, hydrocarbon species may condense on the surface as organic surface coatings (Glassman 1996).

The soot-BC formation in gas-phase results in much smaller size of “primary” particles (20-40nm) compared to char-BC (micron-sized particles) and chain-like aggregates with spherical equivalent diameters in the range of 60-150 nm that are difficult to characterize (Seinfeld 1998; Moosmüller et al. 2009), Figure II.2. Particles in this size range can be transported in the free troposphere for an average of a week (Cooke and Wilson 1996), which is long enough to be dispersed over distant areas. Most of rBC formed is initially hydrophobic, but becomes hydrophilic through reactions with ozone and condensation of sulfuric acid and can be mixed with water droplets or ice (Cooke and Wilson 1996).

In the atmosphere BC is primarily comprised of soot-BC and referred to as refractory BC (rBC) (Schwarz et al. 2010). Defined as soot with a melting point between ~ 3500 and 4000 K and an almost-unique non-zero imaginary part k (i.e., k~0.79) of its refractive index (wavelength independent over the visible and near-visible spectral regions), rBC is differentiated from brown carbon aerosols –or light absorbing organic carbon- which have a much lower melting point and different optical properties (Andreae and Gelencser 2006; Bond and Bergstrom 2006; Moosmüller et al. 2009). This present doctoral dissertation focuses specifically on rBC nanoparticles and does not address other forms of BC.

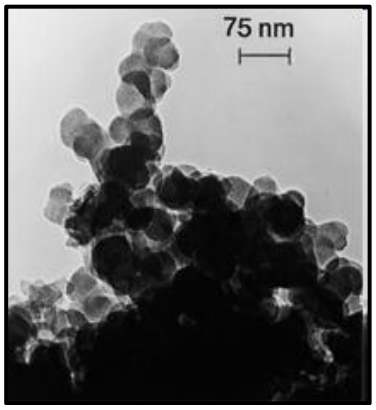

Figure II.2: BC nanoparticles collected from within a house (photo: www.tms.org)

II.1.2. Sources and sinks of black carbon

A schematic view of the global BC cycle is represented in Figure II.3. This figure also reports interactions of BC with the climatic system that will be discussed in section II.1.3. Natural and anthropogenic BC sources impact two main environmental compartments interacting together: terrestrial/marine environments and the atmospheric reservoir. For terrestrial and marine environments, both char-BC and rBC have to be considered. For atmospheric sources, only rBC.

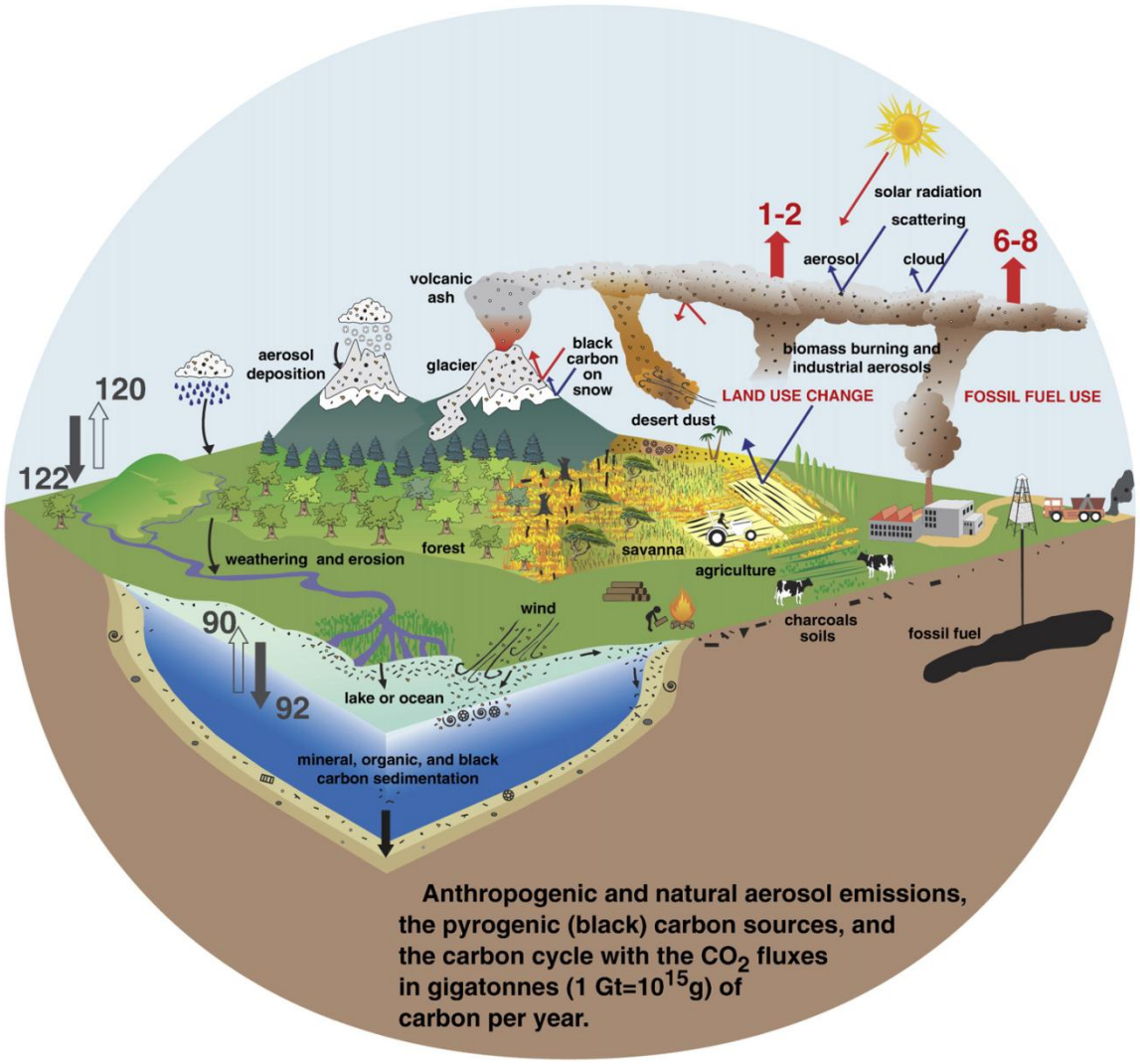

Figure II.3: A schematic drawing of the carbon cycle and black carbon sources: gray arrows represent natural CO_2 emissions and red arrows represent CO_2 emissions due to land-use change and fossil-fuel use in gigatonnes of carbon per year (Thevenon et al. 2010).

Sources and sinks to terrestrial and marine ecosystems

Globally, 0.05 to 0.27 Gt of BC are produced every year mainly through natural biomass burning (spontaneous forest and grass fires occurring during dry seasons) and land use changes (land-clearing practices, deforestation, agriculture) (Kuhlbusch and Crutzen 1995). About 80% of this global amount is considered to accumulate on the site of production. Indeed, big char-BC is not likely to be transported over long distances in the atmosphere and may thus accumulate in soil and sediments. Owing to their resistance to decomposition (Nguyen et al. 2004), char and rBC

have been reported comprising a substantial (up to 20%) fraction of sedimentary carbon in various marine sediments (Masiello and Druffel 1998), harbor sediments (Gustafsson et al. 1997; Gustafsson and Gschwend 1998) and soils (Schmidt et al. 2001). Moreover, fossil forms of BC are commonly found in sandstone, limestone, and other sedimentary rocks (Allen-King et al. 2002). BC was found to persist in marine sediments for at least 13,900 years (Masiello and Druffel, 1998), and can be 1300 to 2600 yrs old in some Australian soils (Lehmann et al. 2008).

Char-BC and rBC can both be transported by water from on-site runoff to streams, rivers and oceans (Hockaday et al. 2007). For instance, mean BC influx to West Equatorial pelagic Pacific is estimated to be 0.76 μg cm^{-2} yr^{-1} (Thevenon et al. 2010). However, concentrations in water have proven more challenging to analyze, probably because of the difficulties to measure highly dilute concentrations (Kim et al. 2004; Dittmar 2008). Sources and sinks of BC to the freshwater system are thus still poorly characterized.

Even though BC appears to be relatively stable, it must eventually mineralize; otherwise global organic C stocks would be converted to BC on Earth's surface within 80,000 years (Kim et al. 2004; Nguyen and Lehmann 2009). BC decomposition thus has been found to occur in soils and sediments through microbial degradation (Shneour 1966; Baldock and Smernik 2002; Hamer et al. 2004) and abiotic oxidation (Cheng et al. 2006; Cohen-Ofri et al. 2007). Hamer et al. (2004) suggested that some microbes could even be able to use BC as unique carbon source. In addition to environmental conditions, such as soil moisture and oxygenation, the nature of char (biomass type and charring temperature) may also control BC degradation.

In the water system, where microbial activity is lower than in soils, the fate of BC particles and its transfer to the oceans has not been much investigated and is still quasi-unknown. In addition to sedimentation, the processes removing BC from the water column may be alteration by UV irradiation (Lee et al. 2009; Hwang and Li 2010), uptake and agglomeration by biota (Baun et al. 2008; Tervonen et al. 2010), disaggregation and eventual mineralization (Nguyen et al. 2010).

Sources and sinks to the atmosphere

Char is not likely to be transported over long distances in the atmosphere. However, rBC particles have a mean atmospheric residence time of about eight days (Cooke and Wilson 1996), and can eventually reach several weeks. Sources of rBC to the atmosphere can be divided into two main categories which are biomass burning (fires) and fossil fuel combustion (charcoal, coal, gasoline, diesel fuel…), Figure II.3. Current and historical emissions of atmospheric BC (usually rBC) have recently been reviewed and, based on 1996 energy consumption data, global rBC emissions are ~0.008 Gt/yr with ~0.003 Gt/yr from fossil fuel and ~0.005 Gt/yr from biofuel and biomass combustion (Bond et al. 2004; Lamarque et al. 2010). Wet deposition may account for ~95% of the total deposition of rBC (Jacobson 2001), thus representing the main sink of atmospheric rBC and a contribution to rBC in terrestrial and marine environments.

Importance of black carbon in the global carbon cycle

The detection of BC in several soils worldwide and its high stability and long lifetime raise the question of the importance of BC in the global carbon cycle. In soils, the BC ^{14}C ages are indeed found to be greater than the most stable non-BC organic carbon pool (Pessenda et al. 2001) and suggests that the chemical and biological availability of carbon may be affected by the presence of BC (Skjemstad et al. 1996; Schmidt et al. 1999). Lehmann et al. (2008) even advised that current models of global climate change postulating that global warming is likely to increase decomposition of soils organic carbon and increase CO_2 emissions, are inaccurate if the large fraction of slowly decomposing BC is not included. Likewise, these authors show that by including realistic stocks of BC in prediction models, CO_2 emissions are reduced by 18.3 and 24.4% in two Australian savanna regions in response to a warming of 3°C over 100 years.

II.1.3. Environmental impacts of black carbon

II.1.3.1. Impact of black carbon on the climatic system

BC solar absorption increases inversely with wavelengths from near-infrared (1 μm) to ultraviolet wavelengths with a power law of one (Ramanathan and Carmichael 2008) and can affect the radiative properties of the atmosphere, snow, ice, in local and remote locations from their sources. The IPCC (IPCC 2007) reports an overall radiative forcing of +0.1 W/m^2 only due to the effect of rBC deposition on snow (Figure II.4). On the other hand, Ramanathan and Carmichael (2008) estimate that the radiative effects of rBC in the atmosphere could be as high as ~+0.9 W/m^2. This value is as much as ~55% of the CO_2 forcing and is larger than the forcing due to the other GHGs such as CH_4, CFCs, NO_2 or tropospheric ozone (Figure II.4). The following section gives an overview (not exhaustive) of the main processes driving the radiative forcing of rBC in atmosphere.

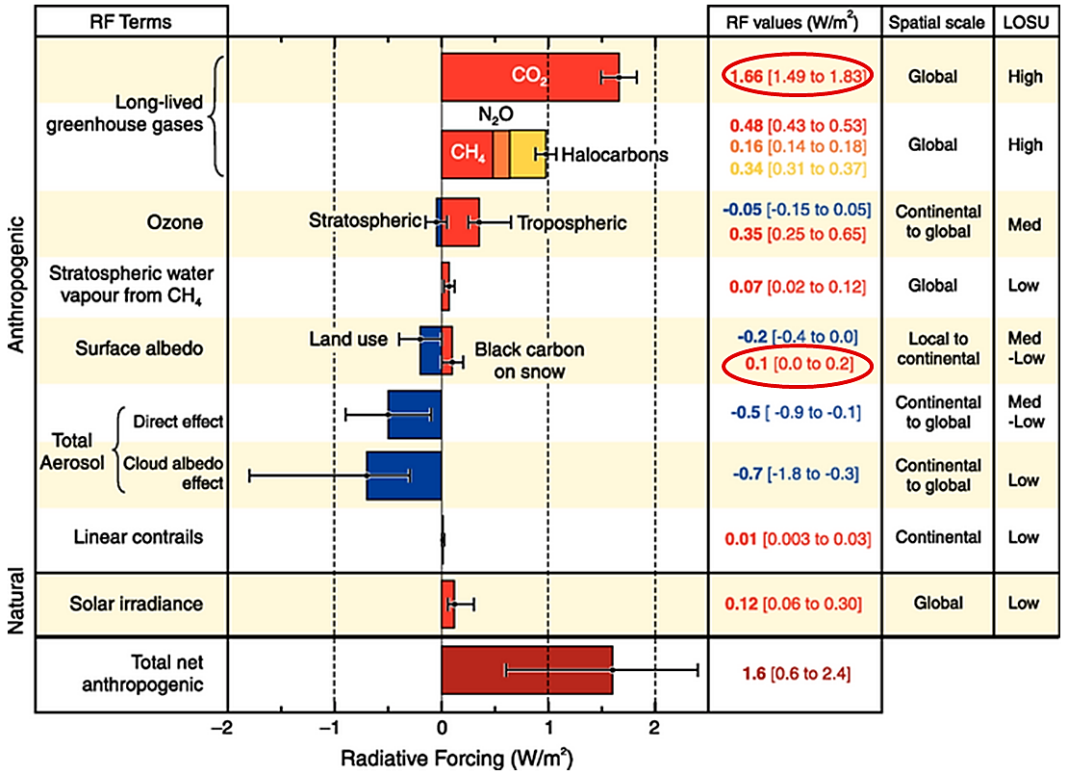

Figure II.4: Global average radiative forcing (RF) in 2005 (best estimates and 5 to 95% uncertainty ranges) with respect to 1750 for CO_2, CH_4, N_2O and other important agents and mechanisms, together with the typical geographical extent (spatial scale) of the forcing and the assessed level of scientific understanding (LOSU). Aerosols from explosive volcanic eruptions contribute an additional episodic cooling term for a few years following an eruption. The range for linear contrails does not include other possible effects of aviation on cloudiness (IPCC 2007).

Effect of rBC on air temperature

The light-absorption properties of rBC often impact the media in which the particles are mixed. In the atmosphere, rBC particles affect the temperature of their surrounding air. The more rBC particles in the air, the more light (directly coming from the sun or reflected from the Earth) is absorbed to warm up the adjacent environment (Jacobson 2001). This radiative effect of rBC on atmosphere temperature is influenced by the degree of mixture of the particles. Indeed, externally mixed particles (rBC particles rather distinct from other aerosol constituents) have a lesser effect on direct-radiative forcing than an internal mixture (aerosol directly coagulated on rBC) (Jacobson 2001). Locally, where rBC emissions are important or where the particles can accumulate due to low atmospheric mixing such as in narrow valleys, the effect of the warming has to be considered. Global forcing on air temperature in the atmosphere is estimated to +2.6 W/m^2 according to Ramanathan and Carmichael (Ramanathan and Carmichael 2008). In high emissions regions where forcing by rBC may reach ~+15 W/m^2, overall increase of air temperature due to rBC could even attain 50%. India and Eastern China are considered as examples of those “hot spots” for rBC emissions, mainly due to the widespread use of coal for cooking and heating. In the southern hemisphere, the more prononced “hot spots” are on the contrary almost exclusively driven by savanna burning such as in sub-Saharan Africa. On the other hand, the “interception” of the direct solar radiation by rBC subsequently reduces solar radiation reaching the surface causing dimming which has a global surface cooling effect as high as -1.2 W/m^2 (Kaufman and Koren 2006; Ramanathan and Carmichael 2008) and affects cloud formation.

Effect of rBC on cloud formation

In the case of the tropical forest, dimming decreases evaporation from vegetation and generates a more stable and drier air, thus inducing a lower amount of clouds, which affects in turn the albedo of the Earth’s surface (Koren et al. 2004). In drier areas, dimming would on the contrary increase the formation of clouds by keeping the below lying air from getting too hot. By warming the ambient air, rBC also increases the amount of water vapor in the air, and thus decreases the

amount of liquid water. This affects more directly the formation of clouds and their characteristics such as thickness, size of the droplets, altitude and temperature. rBC has an indirect effect on cloud albedo (ratio of light reflection over light absorption) since all those parameters have to be taken into account when looking at cloud light absorption and reflectivity.

Effect of rBC on precipitations

The presence itself of hygroscopic rBC nanoparticles can modify the number of droplets or ice crystals in a cloud. Indeed, small particles favor the condensation of water vapor on their surface, increasing the number of droplets: the more particles in a cloud, the more droplets. Nonetheless, rBC does not seem to be a particularly efficient condensation nucleus when present in a pure form, but it becomes attractive to water droplets when mixed with other hydrophilic chemicals such as sulfates cloud condensation nuclei (Weingartner et al. 1997). The degree of mixture influences the properties of the particles to act as a condensation nucleus, and therefore the amount of scavenged particles by precipitation. In general, scavenging of rBC increases with the age of the particle (Cozic et al. 2007). However, in any case, more droplets do not usually induce more rain, since small droplets do not come together well to form larger ones through collision and coalescence. Thus, they have longer lifetimes because they fall out slower to fall and form precipitation. Consequently, high concentrations of rBC may overall reduce precipitations (Albrecht 1989).

Effect of rBC on cloud albedo

On the other hand, clouds with smaller droplets usually have higher albedo than those with bigger drops (Seinfeld 1998), thus increased number of small water droplets in a cloud decreases the cloud absorption and increases the fraction of light reflected back to space. Nevertheless, once incorporated to cloud particles, rBC also decreases the albedo of clouds by enhancing absorption of light by drops and ice crystals (Chýlek et al. 1984), Figure II.3.

Effect of rBC on albedo of snow and ice surfaces

The hygroscopy acquired by rBC particles after a few hours or days, allows them to be transported by rain or snow in the atmosphere and deposited everywhere on the Earth surface including on oceans, alpine snow, glaciers or remote ice caps. Because the absorption contrast between snow and rBC is enormous (snow is a strongly multiple scattering medium), rBC deposited on snow substantially affects the albedo of the snow surface (Clarke and Noone 1985; Hadley 2010): less solar radiation is reflected back to the atmosphere while more is absorbed by the snowpack, increasing snow temperature and melting rates. In addition, snow-melt itself increases sizes of snow grains, which in turn increases the solar radiation absorbed by snow (Flanner et al. 2007). This effect is stronger for higher sun incidence in the inter-tropical zones. Thus, snow and ice in the Andes, at the Kilimanjaro or in the Himalayas, would be much more sensitive to rBC deposition than snow and ice of the Alps, the United States, the Arctic, and Antarctica (Grenfell et al. 1981). Overall, the radiative forcing of rBC deposition on snow/ice surface is close to ~0.1 W/m^2 according to IPCC (Figure II.4) and ~0.05 W/m^2 according to Flanner et *al*. (2007). Considering only forcing from fossil fuel and biofuel anthropogenic sources, rBC radiative forcing by deposition on snow surfaces is ~0.04 W/m^2, and is thus estimated to contribute to total albedo change of snow surfaces by at least 80% (Flanner et al. 2007).

II.1.3.2. Impact of black carbon on transport and fate of pollutants

The large surface area of BC particles renders them potent adsorbers of polycyclic aromatic hydrocarbons (PAHs) and persistent organic pollutants (POPs) (Gustafsson et al. 1997; Moermond et al. 2005), Figure II.5. The apportionment of those organic pollutants between the water column and BC particles may thus affect pollutant transport and fate in the aquatic environment (Allen-King et al. 2002; Buckley et al. 2004).

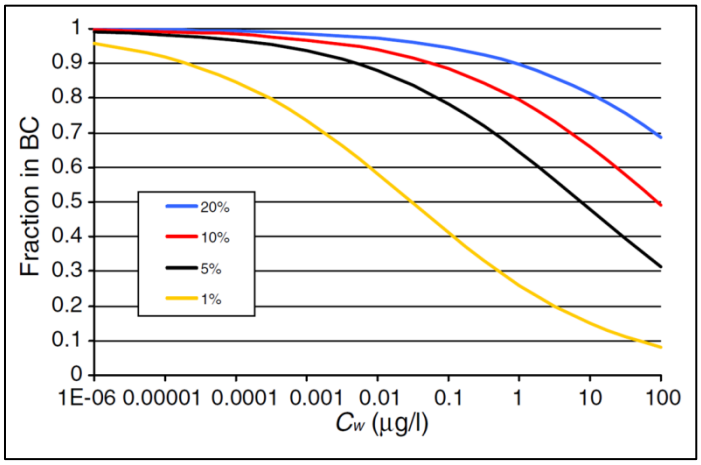

Figure II.5: Fraction of organic pollutant (PAHs, POPs) bound to BC as a function of aqueous concentration, for 1%, 5%, 10% and 20% BC (of TOC). The curves are modeled based on in situ sorption observations (Koelmans el al. 2006).

In the atmosphere, rBC particles are also often found bound to some pollutants which are known to be carcinogenic such as benzo[a]pyrene, when inhaled (Kuhlbusch 1995; Zielinska et al. 2004).

II.2. USING BLACK CARBON AS A PROXY

BC is ubiquitous in the environment and is present in the atmosphere, water, snow, ice, soils and sediments. The dual origin of its sources (fossil fuels and biomass burning) makes it an attractive tool for many environmental studies.

II.2.1. Black carbon in ice-cores and firn

II.2.1.1. Ice cores

Aerosols such as rBC aerosols are transported by atmospheric circulation to high elevations and low latitudes, and as far as the South and North Poles. There, they are deposited by wet and dry processes and mixed in snow layers. If the elevation or latitude of the deposition location is sufficiently high to preserve the site from summer melt, snow accumulates year after year. Under its own weight, snow, composed of air and ice crystal, starts to densify gradually as firn until

forming joined ice crystals where air is trapped and cannot circulate any longer. The depth at which air stops circulating from pore to pore is called the close-off, Figure II.6.

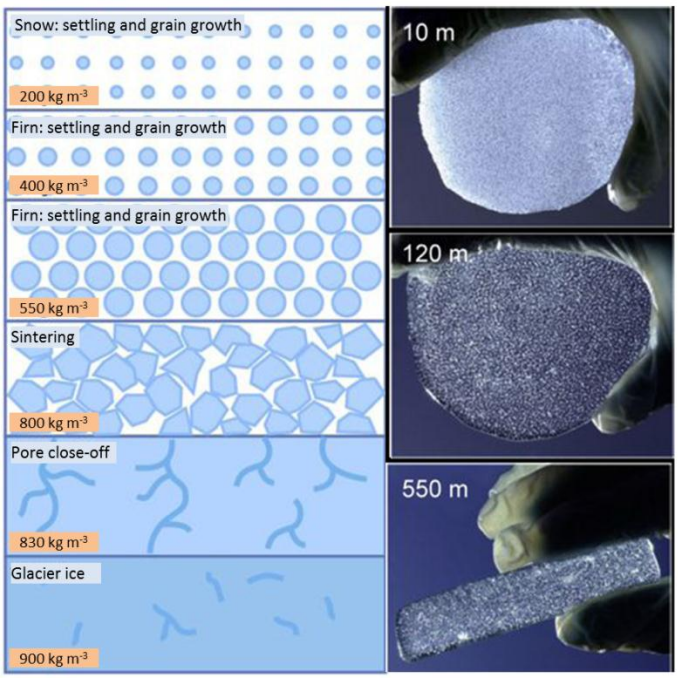

Figure II.6: Firn densification processes as a function of density (adapted from M. Van den Broeke)

Close-off depth depends on several parameters such as:

-i) the speed of densification (called snow metamorphism), which is mostly dependent on surface snow temperature (faster in warmer locations).

-ii) the annual snow accumulation (depending on snow falls and on snow ablation), which also influences snow metamorphism (i).

The formation of Alpine Glaciers, ice fields or ice caps, thus depends on elevation and latitude of the site (geography), but also on geological morphology. However, in any case, the ice starts to flow towards lower elevations due to gravity and at a rate depending on the annual accumulation, and the slope of the bedrock on which the glacier is resting, and on air/ice temperatures. This flowing activity is known to affect the ice core dating, and in some extreme cases to turn ice layers upside-down. The choices of ice drilling sites consequently depend on various parameters. First, sites with minimal flow are always preferred; divides, saddles and local elevation maximums

are thus typical drilling sites. Depending on the temporal resolution requested for the records (age versus resolution), a site with low or high annual snow accumulation is chosen. Low-accumulation site allows one to recover older ice (more years accumulated in the same ice thickness), but on the contrary, higher temporal resolution is obtained in high-accumulation sites, although maximal age obtained is decreased due to limits in drilling depths. Ice core records can cover various times scales ranging from ~100 to ~1000yrs in Alpine glaciers, to ~10,000 to ~80,000 yrs at Law Dome, Antarctica (Morgan et al. 2002), and up to ~800,000 years at EPICA Dome C, Antarctica (Jouzel et al. 2007). The drilling location also depend on the proxy and problematic investigated: Alpine or Equatorial ice cores provide more local information on the area studied, while Antarctica or Greenland ice cores record preferentially information on emissions over larger scales. The analysis of gases trapped in the ice, and reconstruction of past atmospheric composition has only relied on ice caps ice (Barnola et al. 1987; Chappellaz et al. 1990), while aerosol and ion studies has been conducted on more numerous locations (Alps, Andes, Himalayas…). Ice core records extracted from glaciers and ice caps ice have altogether widely improved the knowledge of the Earth climatic system, notably providing evidence of the link between greenhouse gases and temperature evolution (Lorius et al. 1993).

II.2.1.2. Himalaya and Alpine rBC ice core records

Since rBC atmospheric lifetime is in the order of few days to few weeks, particles found in an ice field are extensively influenced by the closest source. In the Himalayas for instance, rBC is expected to be dominated by the wide use of charcoal in upwind populations from China or India. A recent 1860-2000 rBC record of from Mount Everest illustrated this effect of pollution on Tibetan snows and confirmed the potential to use of high resolution rBC measurements (Kaspari et al. 2011), Figure II.7. However, the comparison of this rBC record with ice core records from other regions of the Himalaya and Tibetan Plateau over the last 50 years (Liu et al. 2008; Ming et al. 2008) showed spatial heterogeneity of rBC concentrations. The complicated geography of Alpine valley is indeed expected to induce differences in precipitation seasonality, dust

deposition, snow and ice melt and thus to influence rBC deposited and recorded in ice cores (Kaspari et al. 2011). The association of several atmospheric circulation tracers or other biomass burning proxy can thus be a precious advantage. Dust and isotope measurements were indeed added to rBC measurements in an ice core record from Colle Gnifetti glacier (Monte Rosa, Swiss-Italian Alps) spanning the last millennium (Thevenon et al. 2009). This analysis allowed the authors to conclude that: i) ice core rBC variability was primarily constrained by regional biomass burning prior to the industrial revolution; ii) agricultural anthropogenic grass burning was largely slowed down during the cold period of the Little Ice Age, and iii) rBC deposition have been overall in an increasing trend since the industrial revolution.

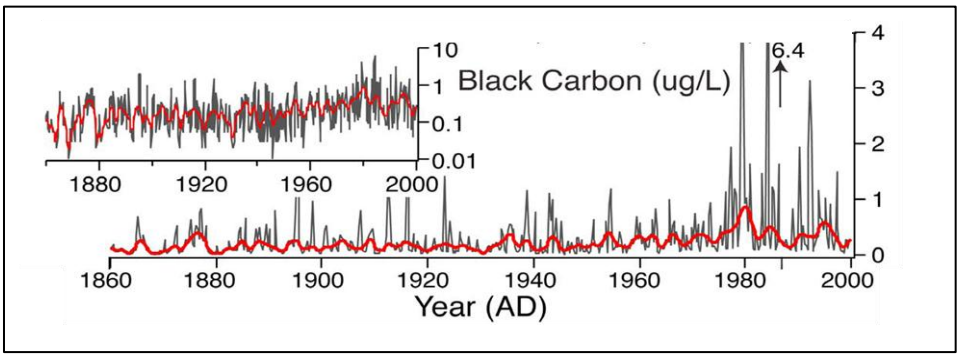

Figure II.7: rBC record in an Himalayan ice core (Kaspari et al. 2011) showing increased rBC deposition from anthropogenic pollution in the last 30 years.

II.2.1.3. Greenland rBC ice core record

In comparison with Alpine ice core, Greenland or Antarctic aerosol ice core records present the opportunity of a simpler geography located away from sources and thus are expected to reflect larger scale emission variability (regional to hemispheric). Moreover, the guaranteed absence of melt in the summer ensures the retrieval of unperturbed signal (notably in the first hundred meters), and low annual snow accumulations allow reconstructions over 1000 to 100,000yrs time scales.

However, atmospheric circulation always modulates both spatially and temporally the transport of particles to the ice caps. In Greenland, the existence of a “polar dome” isolating the cold lower

troposphere from the rest of the atmosphere complicates the atmospheric transport to the Arctic (Law and Stohl 2007; McConnell 2010). Variability between drilling sites in and out of the polar dome and under the influence of different dominant winds is thus expected. Consequently, investigation of atmospheric circulation patterns with global circulation models (GCM) is a valuable tool to link remote natural and anthropogenic sources to deposition at a specific ice drilling site. A study from McConnell et al. (2007) combining rBC ice core records from central Greenland and GCM analysis have shown that rBC emissions during the 20th century were most likely influenced by North America and northern Europe, Figure II.8. Nowadays, however, it is expected that Asia and notably China will have an increasing influence on the amount of rBC deposited to Greenland, although this increase is too recent to be already observed in Greenland ice (McConnell 2010). Moreover, the association of rBC records with another biomass burning marker (vanillic acid) or lead (Pb) emissions allowed McConnell and others (2007) to apportion between industrial sources of rBC and natural sources and to show that the rBC increase observed in the 1930's was linked to coal burning and not wood burning.

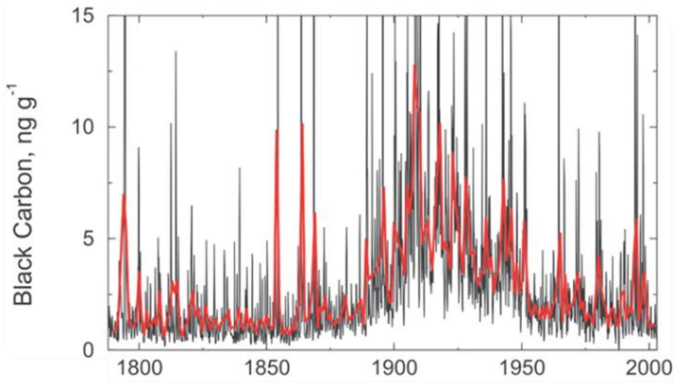

Figure II.8: Greenland record of rBC showing increased emissions in the 1930's due to increase use of coal as energy source in the U.S.A. (McConnell et al. 2007).

II.2.1.4. Antarctica rBC ice core records

The southern hemisphere is less populated, and rBC residence time in the troposphere is too short to allow it to travel from northern latitudes to Antarctica. Consequently, Antarctic records of 20th century rBC are expected to reflect more biomass burning than fossil fuel combustion

histories, in contrast to Greenland. Antarctic rBC records could thus be used to investigate the variability of forest fires as a function of recent climate change. However, few rBC measurements have been made in Antarctic snow (Chýlek et al. 1987; Warren and Clarke 1990; Grenfell et al. 1994; Wolff and Cachier 1998), only one rBC record covering the 13,000-700 yrs BP (Before Present) was reconstructed from an ice core archive from Byrd station (Chýlek et al. 1992). The remote location of Antarctica has rendered difficult the analysis of rBC (small size and low concentrations) and the understanding of atmospheric circulation patterns to and over the continent. Indeed, while low coastal regions are more influenced by storm systems and connected mainly with the lower tropospheric transport, the large area of highly elevated land at the interior ice sheet is affected by continental temperature inversion and influenced by complex upper tropospheric and tropospheric transport (Chýlek et al. 1987). In brief, the continental origin of rBC emission (i.e. Africa, Australia or South America) and their influences on rBC deposition at specific Antarctic sites is still uncertain. In addition, the association of rBC measurements with other biomass burning proxies (PAHs, vanillic acid, carbon isotopes) has not been performed yet due to current detection limitations.

II.2.2. Black carbon in fresh and marine waters

The low levels and small sizes of BC particles present as suspensions in marine and fresh-water bodies have render difficult the measurements of its concentrations and the understanding of its transport from sources to sinks (Mitra et al. 2002; Forbes et al. 2006). In relatively turbid waters, however, BC concentrations as particulate organic matter (POM) can be high enough to perform analysis with the standard filters methods. For instance, Mitra et al. (2002) were able to evaluate BC concentrations in suspended sediments of the Mississippi river and estimated the annual flux of BC to 50 megatons, corresponding to ~5% of BC discharged annually to the oceans. A complementary study of PAHs in the same samples allowed the authors to determine that ~27% of that BC discharged was originating from fossil fuel combustion (notably coal), and raised the question of water pollution from BC.

To measure BC occurrence as dissolved organic matter (DOM, particle diameters under 0.45 µm), Mannino and Harvey (2004) used the CTO-375 method (Gustafsson et al. 1997) in water samples from the Delaware river and estuary (U.S.A.). They found that BC was ~3-15% of dissolved organic carbon (DOC) and was associated with localized sources, possibly from atmospheric deposition or released from re-suspended sediments. Kim et al. (2004) applied another technique - based on indirect detection of BC degradation products (hydrogen deficient molecules) – to estimate BC concentrations in the McDonalds river (North-East U.S.A) and a tributary river of the Amazon (Rio Negro). They also proved the existence of BC in riverine DOM. More recently, a technique based on indirect detection of molecular BC degradation products such as benzenepolycarboxylic acids (BPCAs) have proven possible the estimation of BC concentrations in less concentrated riverine waters and open oceans (Hockaday et al. 2007; Dittmar 2008; Ziolkowski and Druffel 2010). However, improved detection limit from these new methods does not yet solve the enigma of the BC cycle: the known BC sinks are too low compared to sources and known residence time in the oceans (Masiello 2004; Ziolkowski and Druffel 2010). Ziolkowski and Druffel (2010) suggested that high concentrations of BC could even rest in extremely low molecular weight DOC, currently difficult to estimate. To conclude, the abundance and degradation of BC in rivers and oceans are still not well constrained as well as the environmental processes associated with these water systems. These processes include: water pollution; inputs from natural and anthropogenic fires; apportionment of hydrophobic contaminants (Burkhard et al. 2008); importance of BC in the carbon cycle (Kuhlbusch 1998) and micro-organisms cytotoxicity (Yang et al. 2009) (cf. section II.1.3.3).

II.2.3. Black carbon in sediments

Masiello and Druffel (1998) showed that BC can be found in deep Atlantic and Pacific Ocean sediments where, in some cases, it can constitute 12-47% of the sedimentary organic carbon (OC). Its refractory nature makes it a suitable candidate for environmental archives, where it can

be preserved thousands of years notably in marine sediments (Middelburg et al. 1999; Forbes et al. 2006) (cf. section II.1.2.).

However, the apportionment between char-BC and rBC particles, which reflect long-range transport of atmospheric fire emissions, is still the focus of ongoing research. Elmquist et al. (2006) suggest the use of the CTO-375 method (ChemoThermal Oxidation method) (Elmquist 2004) to distinguish char-BC versus soot-BC based on the difference in resistance to oxidation (higher for soot-BC). This method was applied to reconstruct a 700-yrs record from a sediment core drilled in a Swedish lake, showing a sharp increase in the 1920s followed by a constant decrease until recent years, which is likely the signature of the evolution of coal and coke burning in Sweden (Elmquist et al. 2008). In a review paper, Thevenon et al. (2010) suggest the use of combined optical and chemical methods to establish inter-comparative records of BC, and to apportion better the effect of transport variability from the effect of sources variability. In their study, they combine results of charcoal particle counts (area >0.2 μm^2) and chemical oxidative treatments and obtain “pyrogenic carbon records” from three sediment core-based case studies in Tanzania, Switzerland and West Equatorial Pacific Ocean. They find high sensitivity of the pyrogenic record to anthropogenic activities and correlations with human settlement, societal changes, and climate change.

Despite those promising results, they point out the necessity to build data sets of pyrogenic carbon storage, to consider the sources, transport mechanisms, and potential impact of human activities to assess better the contribution of pyrogenic carbon influxes in the global carbon cycle.

II.3. NATURE AND IMPACT OF BIOMASS BURNING

II.3.1. What is a fire?

According to the definition of the National Wildfire Coordinating Group (NWCG) a fire is the “rapid oxidation, usually with the evolution of heat and light, heat fuel, oxygen and interaction of the three” (NWCG). If the fire can maintain itself with enough combustible to burn, and if oxygen is

present in sufficiently high amounts, a flame can appear. The process of pyrolysis occurs when a temperature threshold is reached -related to the percentage of carbon and water in the type of combustible- and in the presence of oxygen. For forest fires, three types of fires can be distinguished depending on fire-type and combustible (Scott 1989, according to Davis 1959), Figure II.9: (a) surface fire, "*a fire that burns surface litter, other loose debris of the forest floor and small vegetation*"; (b) aerial fire, "*a fire that advances from top to top of trees or shrubs more or less independently of the surface fire*"; and (c) ground fire, "*a fire that consumes the organic material beneath the surface litter of the forest floor*." In such fires, the temperatures are highly variable and can reach 700°C in chaparral shrubland fires, to 800-1000°C in a forest canopy (Scott 1989). Heat emitted during large fires creates deep convection currents which can drag vegetation debris from trees up to 5km of elevation and 10km to 20km away horizontally in the atmosphere. In grassland and savannah wildfires, ground temperatures are lower and vary from 100°C to 300°C (Scotter 1970; Scott 1989). Propagation of fires for those types of biomes is usually highly dependent upon wind speed and stability of direction. The spreading time of grass/savannah fires is the fastest of all wildfires and can reach 20km/h (Cheney and Sullivan 2008). For all fire types, the burning of soils can cause the loss of its water absorption capacity and can hence drastically alter the hydrology of the area by increasing runoff (Martin and Moody 2001).

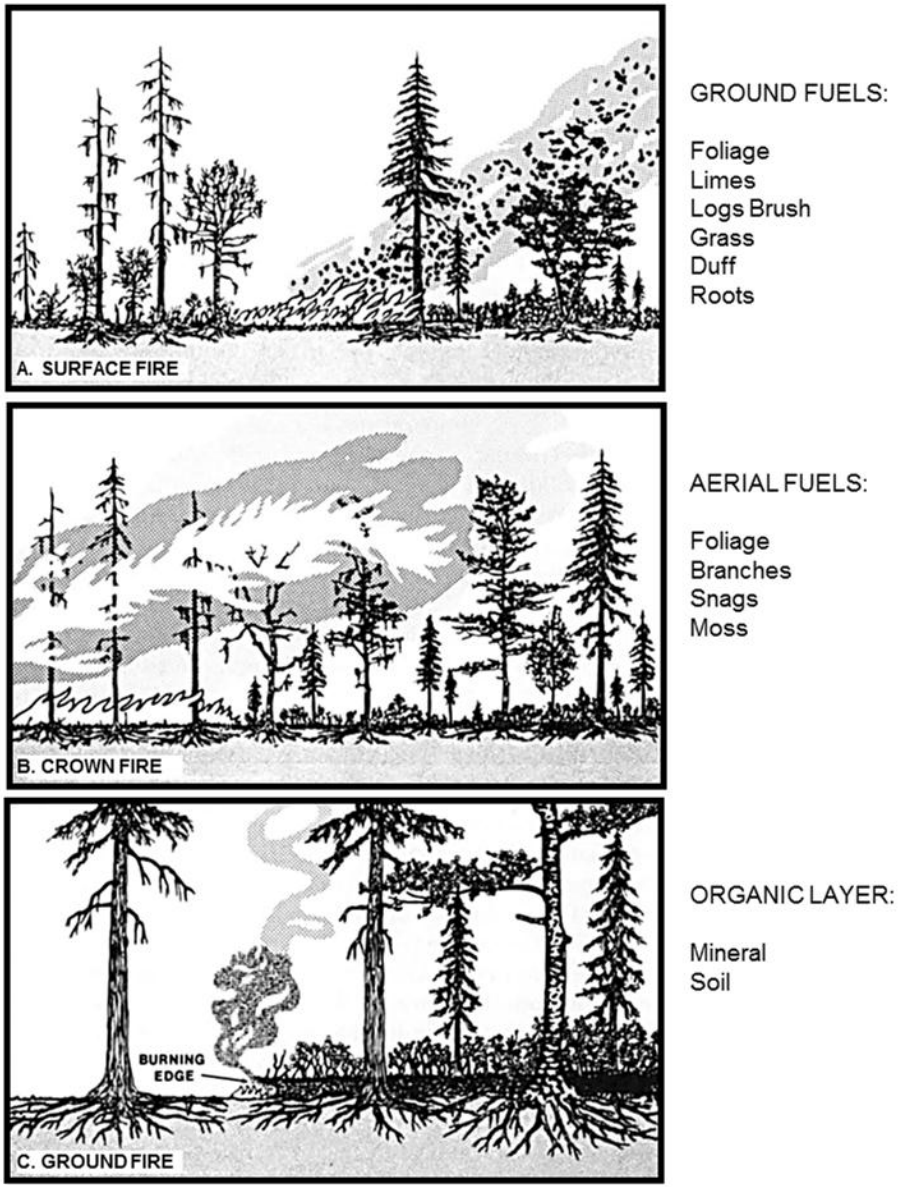

Figure II.9: Types of wildfires and sources of fuel (Modified from Scott, 1989)

Although a destructive process, fire is part of past and modern agriculture and economy. Indeed, it is a crucial agent for conversion of biomass and soil organic matter to CO_2 (IPCC 2007) and it is often used for agriculture and grazing to enrich the soils in nutrients. In preserved environments, fires are also part of the re-cycling of some ecosystems and plays an essential role in the ecological chains (Certini 2005). However, natural fires can have catastrophic impacts on the ecology, economy, and human health of a region (IPCC 2007). The used of prescribed fires

(burning of naturally accumulated forest floor or slash following tree harvest) is a standard practice that has been developed to reduce fuel levels, with the intention of minimizing the extent and severity of wildfires or facilitating germination and growth of desired forest species (Neary et al. 1999; Certini 2005). Natural fire variability and original vegetation may have been totally modified by anthropogenic practices, with the striking example of aboriginal populations in Australia who used to spread fires and burn the land systematically for farming purposes (Preece 2002).

II.3.2. Today's fires

II.3.2.1. Fire regimes

The development of natural fire is highly dependent on climatic and ecological conditions and varies in cycles of wetting and drying: it must first be wet enough to grow combustibles and consecutively dry enough to get them ready to burn (Pyne 2001). Therefore, wet forests normally burn during dry spells and savannas after rains. Those characteristics will define the "fire regime" of an area. Fire regime (from the Latin "regere" and French "régime", to direct, to manage or to rule) describes variations in characteristics regularly occurring in time and space, which are typical of meteorological and climatic variables such as precipitation and temperature (Krebs et al. 2010). Three general types of fire regimes can be differentiated: i) frequent, low-severity surface fires that are nonlethal to most plants; ii) infrequent, stand-replacing (high-severity) crown fires; and iii) mixed-severity regimes that experience both low and high-severity fires (Turner et al. 2007). All kind of fire regimes will affect the ecosystem through vegetation change (Bond et al. 2005), nutrient cycling (Turner et al. 2007), hydrology and erosion (DeBano et al. 1998). Some of these processes are critical to species that inhabit the ecosystem and to reproduce. For example, fires maintain grasslands that would otherwise convert to shrub or woodlands, and thus provide habitat for grazers (Brown and Smith 2000). On the contrary, in tropical forests, fires occur in

exceptional weather conditions and can be highly destructive with many negative impacts (IPCC 2007).

II.3.2.2. Repartition and variability

Fires are usually absent at latitudes poleward of 70N and 70S; they progressively increase towards the tropics and drastically drop at the equator. Essentially, fires occurrence is determined by two parameters: i) the availability of vegetation to burn depending on growth rates and precipitations, and ii) the inputs of sufficient energy to dry vegetation, ignite and sustain the fire. Consequently, fires mostly occur in two types of terrains: energy-limited areas (boreal forests, rainforests) and moisture-limited areas (savannas) (Flannigan et al. 2009).

In the tropics, the vegetation primarily consists of broad leaf evergreen rainforest (~13% of land surface) and wooded grassland savannas (~19% of land surface), Table 1. The combination of sufficient primary production and hot and dry periods make the savannas (located, e.g., in central Africa and northern Australia) the biome of highest risk of fire (Mouillot and Field 2005). The steppe-type grasslands covering Central Asia are also extremely fire prone, as a consequence of strong summer droughts and extensive grazing. In the Middle East, the steppe-biome is also present but is drier and sparser and thus experiences a very low fire occurrence. On the contrary, fires in the boreal forests are mostly dominated by climate variability and less influenced by humans, notably in Canada and Russia. This is not the case in the temperate zones, including Europe, the USA, SE Asia and parts of South America and Australia, where fire regime has been considerably modified by human activities. In those areas, the factors dominating fires are population density, landscape pattern and fire prevention policies (Mouillot and Field 2005).

Over the two hemispheres, no distinct or common fire season exists (Flannigan et al. 2009) and there is always fire activity somewhere on the planet (Carmona-Moreno et al. 2005). Fire activity in savanna areas such as central Africa and northern Australia can be strongly linked with precipitation, following the dry season throughout the year (Carmona-Moreno et al. 2005). Fires in these areas also depend on previous seasons/year rainfall and subsequent vegetation growth

(Russell-Smith et al. 2007). Thus, maximum burning tends to occur from December to February in the Sahel, India, and Central America, during October and November on the Saharan margin, and during July through September in southern Europe and North America (Harrison et al. 2010). In the southern hemisphere, peak burning in the tropics and subtropics of southern Africa, Australia and South America occurs during July through September, while December through February marks the peak fire season in the southern mid-latitude regions (Harrison et al. 2010). Overall, Mouillot and Field (2005) estimate that ~600 million hectares are burned each year, from which ~86% occur in the tropical savannas and grasslands (55.7% in Africa, 15.5% in South America, and 9.5% in Australia, and 6.2% in South Asia for the 1990s), Table 1. Forest fires represent only 11% of the yearly burned area (9% in the tropics, 1% in the boreal forest, and 0.9% in the temperate forest) but involve more biomass.

		S	S%	B	S%	FRI
Boreal forest		1689	11.7	6.5	1.1	260
	N. America	601	4.2	2.8	0.5	215
	Russia	1088	7.5	3.7	0.6	295
Temperate forest		789	5.5	5.7	0.9	138
	Europe	265	1.8	0.5	0.1	542
	N. America	485	3.4	3.6	0.6	134
	E. Asia	187	1.3	1.0	0.2	180
	Australia	117	0.8	1.1	0.2	109
Temperate grasslands		1699	11.8	19.4	3.2	88
	Middle East	792	5.5	0.5	0.1	1524
	Central Asia	709	4.9	15.5	2.6	46
	S. America	198	1.4	3.4	0.6	59
Savanna/Grassland		2589	17.9	520.1	85.9	5
	South Asia	284	2.0	37.7	6.2	8
	Africa	1184	8.2	332.6	54.9	4
	South America	666	4.6	91.9	15.2	7
	Australia	455	3.2	57.8	9.6	8
Tropical forest		1820	12.7	54.1	8.9	34
	Africa	520	3.6	0.6	0.1	939
	S. America	991	6.9	24.3	4.0	41
	SE. Asia	321	2.2	19.2	4.8	11

Never burned areas		5850	40.5	0	0	na
	Tundra	950	6.6	0	0	na
	Wetlands	350	2.4	0	0	na
	Desert	4550	31.5	0	0	na
TOTAL		14448	100.0	605.7	100.0	na

Table II.1: Surface (S) and percentage (S%) cover of regions and sub-regions considered here, as well as corresponding average burning area (B, Mha yr^{-1}) and the percentage it represents within the global burned area (B%), FRI indicates the Fire Return Interval (in years) (Adapted from Mouillot & Field 2005).

II.3.2.3. Observation and detection of fires

The large spatial and temporal variability of fires (Duncan et al. 2003) make their direct observation challenging, and several methods of direct and indirect detection have been recently developed in particular with the use of satellites. Light sensors in the visible and infrared spectrums allow the detection of temperature anomalies, the presence of flames, and smoke clouds. Commonly used satellite sensors are Along-Track Scanning Radiometer (ATSR, Arino and Plummer, 2001) and Moderate Resolution Imaging Spectroradiometer (MODIS, Justice et al. 2002), which have been providing since the last decade a quasi-global coverage of fire observation at a resolution of 1 km (Mieville et al. 2010). The most recent generation of fire emission inventories (Ito and Penner 2004; Schultz et al. 2008; Liousse et al. 2010; Mieville et al. 2010) are based on a combined approach of using burned area and active fire counts from satellites, accompanied by biogeochemical modeling of the available fuel load (Langmann et al. 2009).

However, even if these inventories have improved considerably in recent years, large uncertainties remain in the temporally and spatially highly variable emissions from vegetation fire (Mieville et al. 2010). In addition, the datasets have rather limited temporal coverage (few decades at the most). Thus, historical and dendrochronological records (i.e. fire-scar and stand-age data) are used to examine fire (related events and processes on time scales of days to centuries and on spatial scales from forest stands to the globe) (e.g. Mouillot and Field 2005; Marlon et al. 2008). Historical records usually span decades, whereas dendrochronological data

can span seasons to centuries. Other techniques, such as charcoal inventories, peat deposits, sediment cores and ice core records are used for paleo-records (cf. section II.2.3.).

II.3.3. Fire emissions to the atmosphere

Fires, from natural causes or human activities, release to the atmosphere considerable amounts of radiatively and photochemically active trace gases and aerosols. Those species contribute to atmospheric pollution and influence climate.

II.3.3.1. Gaseous emissions

The dominant product of any combustion process involving water and carbonaceous material (i.e. biomass) is carbon dioxide (CO_2). With carbon monoxide (CO), a product of incomplete combustion, those two gases account for 95% of carbon emissions from biomass burning (Langmann et al. 2009). Other trace gases emitted during fires are methane (CH_4) and higher non methane hydrocarbons (alkanes and alkenes), CH_3OH and higher alcohols, HCHO and other aldehydes, and organic acids (Andreae and Merlet 2001). This mixture of gaseous species emitted contributes to the formation of tropospheric ozone (O_3) in relatively high proportions specially in the tropics where fires contribute to 38% of tropospheric O_3 (Andreae and Merlet 2001). In addition, nitrogen containing compounds (e.g. NOx, N_2O, HCN) and halogen-containing compounds (e.g. CH_3Cl, CH_3Br) are also released in substantial amounts. Acetonitrile (CH_3CN) is used as a tracer of vegetation emissions, because of its long atmospheric residence time (Fraser and Lakshmanan 2000). On the contrary, fires represent only 3% of anthropogenic emission of sulfur-containing compounds (e.g. SO_2), and only 1.3% of total atmospheric sulfur (Andreae and Merlet 2001).

II.3.3.2. Aerosol emissions

Particles emitted during fires consist mainly of carbonaceous material being dominated by organic carbon and rBC up to 10 to 15% (Reid et al. 2005; Langmann et al. 2009). Inorganic compounds such as potassium, chloride, and calcium make up only a small fraction of the aerosol mass. Particulate trace organic compounds such as levoglucosan, manosan, and galactosan are also used as markers for biomass fire emissions, because of their long atmospheric residence time and the large contribution of biomass combustion to their atmospheric budgets (Fraser and Lakshmanan 2000). However, aerosol residence time is in general shorter than gaseous emissions and their repartition in the atmosphere is heterogeneous and decreases rapidly away from the source. Indeed and as mentioned earlier (section II.1.2.), the majority of rBC emitted will be deposited within a week of transport, mostly through wet deposition. Thus, only the smallest particles (<1µm) can eventually reach the poles, although they are not likely do not cross the Inter-Tropical Convergence Zone (ITCZ), due to their short residence time in the atmosphere.

II.3.4. Fires and climate interactions

The interactions of fires with climate are illustrated in Figure II.10, which reports the effect of fires on climate and the effect of climate on fires, and the associated feedbacks.

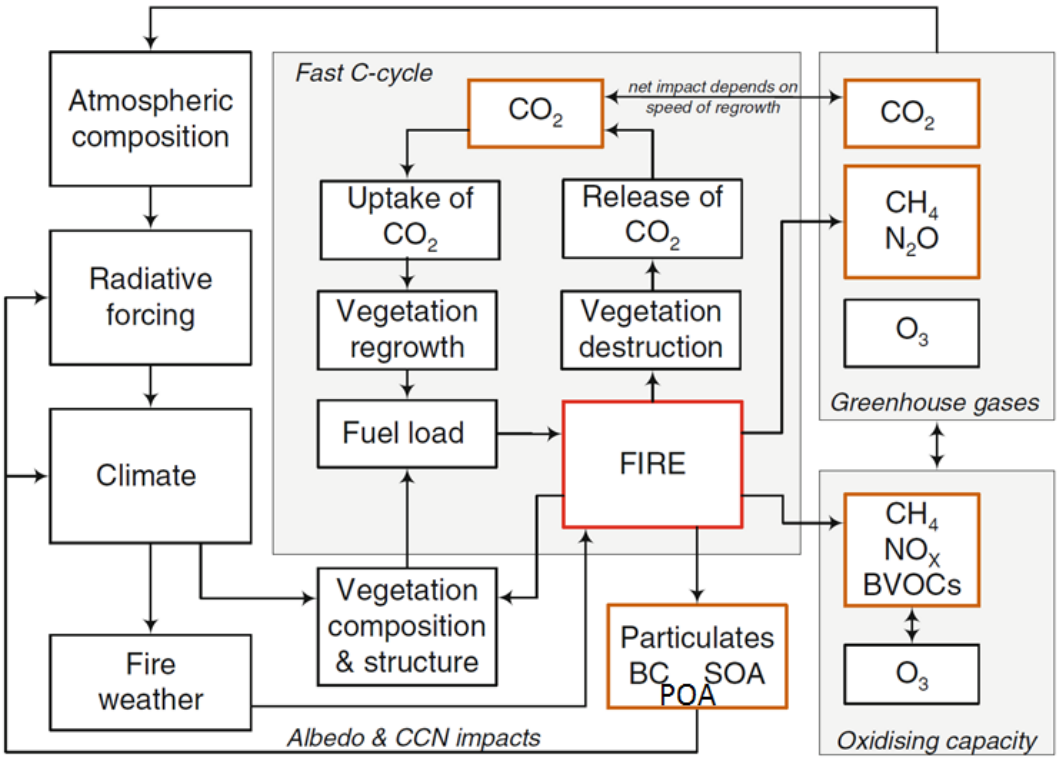

Figure II.10:Schematic showing carbon-cycle, atmospheric-chemistry and biogeophysical feedbacks from fire to the climate system (adapted from Harrison et al. 2010)

II.3.4.1. Influence of fire on climate

How fires influence the Earth climate is manifold, has many uncertainties and is still the object of ongoing research. The occurrence of fires modifies vegetation cover and thus influences local surface albedo and surface evaporation resulting in complex interactions within the climate system (Govaerts et al. 2002). Indeed, reduction of cloud cover due to the rise in air temperature such as previously observed over the Amazon (Koren et al. 2004; Feingold et al. 2005) and Mediterranean basins (Pace et al. 2005), increases heating by aerosols (see section II.1.3.1) and enhances the stability of air masses, generating a positive climatic feedback.

Emission of aerosols by fires *(Figure II.10).* In addition to rBC emissions, fire are a strong source of brown carbon which is light absorbing (in the UV notably) organic carbon (Lewis et al. 2008). On the other hand, aerosols particles in clouds can act as nuclei and increase the number

of small droplets, increasing the cloud's lifetime and their efficiency to reflect solar radiation (Reid et al. 2005; Lohmann et al. 2009). Aerosol particles may also enhance the availability of liquid water at the freezing level, and lead to more vigorous convective clouds (Andreae et al. 2004). In Indonesia, Podgorny et al. (2003) showed that the smoke released during the strong El Niño event of 1997, reduced the seasonal average solar radiation absorbed by equatorial Indian Ocean by 30-40 $W.m^{-2}$ during few months. Moreover, the deposition of absorbing aerosols such as rBC on snow surface also affects the radiative budget of the surface by decreasing albedo and induces positive feedbacks (Hansen and Nazarenko 2004), as discussed previously in section II.1.3. Overall, the global radiative forcing linked to aerosol particles emitted by fires is highly uncertain and is estimated about 0.03±0.12 $W.m^{-2}$ according to the IPCC 2007 report (IPCC 2007).

Gaseous emissions from fires. *(Figure II.10).* Biomass burning for deforestation is estimated to have contributed to ~19% of the atmospheric CO_2 increase since pre-industrial times (Bowman et al. 2009; Harrison et al. 2010). Large fires in Indonesia occurring during a strong El Niño period in 1997-1998, contributed alone to the largest annual increase in CO_2 since records began in 1957 (Harrison et al. 2010). The other main atmospheric gases emitted during fires are methane (CH_4) -which is 25 times more efficient than CO_2 as a greenhouse gas but has a shorter atmospheric lifetime- followed by nitrogen oxides (NO_x) and ozone (O_3) through secondary chemical reactions (Harrison et al. 2010). Bowman et al. (2009) estimated that biomass burning from deforestation fires currently contributes about 4% to the current total radiative forcing of CH_4 and 17% to forcing due to tropospheric O_3.

Change in surface albedo. Fires affect land-surface albedo by altering vegetation cover, but small-scale changes in land-surface albedo have very little effect on the global radiative budget compared to surface darkening due to rBC deposition (Figure II.10). Moreover, the impacts of these changes only persist a short time until the ecosystems starts to recover (Harrison et al. 2010). Other feedbacks, however, can be linked to changes in energy absorbed by the land, such as in tropical rainforests where deforestation fires initiate positive feedback cycle, creating canopy

openings, leading to reduced fuel moisture and low relative humidity which hence increases the risk of fires (Harrison et al. 2010).

II.3.4.2. Influence of climate on fire

Satellite observations have shown that in the tropics, wildfire variability is in part linked to the El Niño-Southern Oscillation (ENSO), which induces episodes of droughts in equatorial and tropical regions, and therefore, increases fire activity in these regions (Mieville et al. 2010). During the 1997-1998 El Niño episode, intense fires were observed in Indonesia, more particularly in peatland areas, leading to strong emissions of chemical species (van der Werf et al. 2006). Conversely, during La Niña phase of ENSO, an increase in fire activity is seen in the southern United States and Patagonia in Argentina (van der Werf et al. 2008). In boreal regions, high interannual variability is observed as well, correlated with the Arctic Oscillation and corresponding temperature anomalies (Balzter et al. 2007). Climate change may also affect fire activity by shifting spatial and temporal precipitation patterns and associated vegetation (Flannigan et al. 2009). In particular, increased ignition risk and extension of fire season is expected (e.g. Moriondo et al. 2006; Nitschke and Innes 2008; Kochtubajda et al. 2009), and may have already started in some areas notably in the western USA and Eurasia (Kasischke et al. 1995; Gillett et al. 2004; Westerling et al. 2006). In those areas, earlier snowmelt was observed to lead to earlier droughts. On the contrary, Williams et al. (2001) estimated that the fire season length may also decrease in some regions of Australia, with a shift in the peak maximum. Overall, it is estimated that if fire frequency and fire extent increase with a changing climate, a net increase in CO_2 emissions is expected during this fire regime shift (IPCC 2007; Flannigan et al. 2009).

II.3.5. Past forest fires –records and modeling

The interactions between climate, vegetation and fire regimes described in previous section are complex, and can be difficult to disentangle under modern conditions when fire regimes are influenced by human activities. However, a better understanding of these interactions is crucial

for accurate simulations of future climate. Global coupled climate-chemistry models (GCMs) aiming to predict future climate change must be evaluated against past climate records to adequately underpin policy decisions. Accurate reconstructions of recent fire history with high spatial and temporal resolutions are thus crucial, e.g. to test emission scenarios of gaseous species used to constrain GCMs when evaluated over the past recent decades. Furthermore, longer reconstructions of fire histories are also required to better assess the feedbacks between atmospheric chemistry and climate, notably during major climatic changes (e.g., the Last Glacial Maximum, LGM).

The use of fire-archives has largely increased during the last 20 years (Whitlock and Tinner 2010), in the attempt to reconstruct fire history in link with climate variability. Tree-rings, sediments records or charcoal, and more recently ice core records, are the most common fire archives used and sometimes combined. Figure II.11 shows the various proxy used for paleo-fire reconstructions as a function their respective spatial and temporal coverage.

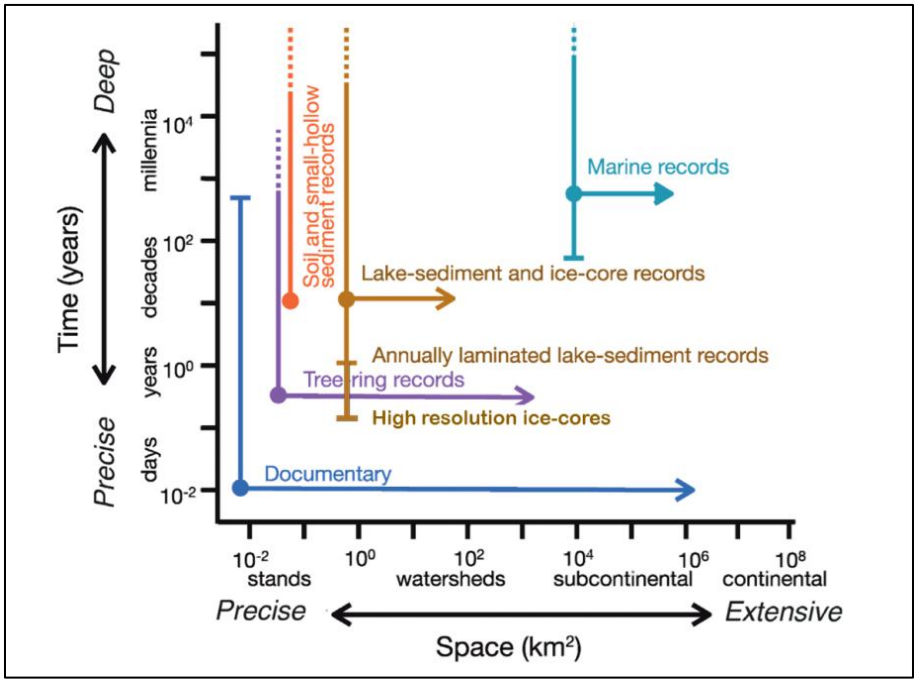

Figure II.11: Overview of paleo-fire archives, recording fire occurrences at different scales and resolution (adapted from Whitlock and Tinner, 2010)

II.3.5.1. Soils and sediment records

On long time scales, records of charcoal abundance in sediments from lakes, peat bogs and soils have showed a strong link between climate and fire activity, with reduced fire in cold intervals and increased fire in warm intervals, regardless of human populations presence (Bowman et al. 2009). Likewise, charcoal found in sediments dated from the Cretaceous-Tertiary boundary (65 million years BP) indicate massive and widespread wildfires emitting enormous amounts of particles in the atmosphere which may have contributed to the cooling of the Earth's climate and to the vast wildlife extinction (Wolbach et al. 1985). Recently, inventories of charcoal deposition (Whitlock and Larsen 2002; Marlon et al. 2008) and networks of tree-rings/fire scars records (Kitzberger et al. 2007), have been used to reconstruct worldwide fire occurrence over the last millenniums. However, those reconstructions from charcoal usually present low temporal resolution and reflect changes in environmental conditions at a decadal to centennial time scale only (Marlon et al. 2008). In fact, the long process of accumulation of charcoal particles in lakes and soils, in addition to surface layer mixing by benthic activity, generally prevent annual to seasonal scale resolution. Similarly, the difficult determination of the sources of charcoal particles results in spatial uncertainties (Gavin et al. 2007). In general, a distinction is made based on the particles size that are assumed to reflect local fire activity (few kilometers away from fire site) with diameters >100 µm, and to reflect more regional fires when particles are <100 µm (Clark and Royall 1995; Whitlock and Bartlein 2003). In order to improve the determination of the origin of those particles and to apportion between different types of ecosystems, other indicators can thus be used such as pollen, carbon isotopes, PAHs, or organic acids (notably in ice cores).

II.3.5.2. Ice core records

The last 200 years cover the pre-industrialization and the modern eras, and are thus of particular interest to evaluate coupled climate-chemistry model. However, only a few studies based on land-use practices, qualitative reports or tree rings analysis, attempted to reconstruct global fire history

over this time period (Houghton 2003; Mouillot and Field 2005). The recent evolution (1800-2000) of fires and subsequent emissions is thus poorly constrained. Contrary to soil and sediment archives, ice cores may offer high temporal resolution records of particular interest in this context.

A study from McConnell and others (2007) demonstrated the interest of rBC as a combustion proxy recorded in ice core, and was detailed previously in section II.2.1. Chemistry of ice cores has also been investigated as a proxy of past fire: high-resolution ammonium and formate profiles were used by Savarino and Legrand (1998) to reconstruct the frequency and the intensity of high-latitude biomass burning inputs having reached central Greenland between 1193 and 1980.

More recently, fire reconstructions have been extracted from gas records contained in ice cores. From an Antarctica ice core, Ferretti et al. (2005) obtained evidence of long-term fire trends from the ^{13}C content of atmospheric methane, which appeared to be disproportionately influenced by changes in the frequency and extent of fires over the past 2000 years. Using a methane source partitioning model, these authors concluded that biomass burning emissions were high from 0 to 1000 A.D. but reduced by almost 40% over the next 700 years. By measuring in Antarctica ice a direct proxy of fire emission, carbon monoxide and its two stable isotopes (C^{13} and O^{18}), Wang et al. (2010) were able to confirm and better estimate this large variation in southern biomass burning during the last 650 years. These authors demonstrated that total biomass burning during recent decades has been lower than at any time during the past 650 years. Such approach based on gas reconstructions from ice cores is promising and will need to be applied further in the past, notably to investigate how changes in fires occurrence and characteristics may have impacted chemistry-climate interactions during major climatic changes (e.g., LGM).

II.4. OBJECTIVES OF THE DISSERTATION

The objectives of this dissertation were to investigate records of rBC nanoparticles preserved in ice and sediment archives, including the transfer functions of rBC from the atmosphere to theses archives. The aim of this approach was to reconstruct past fire and anthropogenic driven combustion events. Specifically, the research focused on ice core records from Antarctica and on

a lacustrine sediment record (Lake Tahoe, CA, USA). The impetus for the research was a new analytical method specific to rBC with very low detection limits down to the part per trillion (ppt). The potential of using rBC as a high-resolution proxy to reconstruct past fire history had been proven by analysis of previous ice cores retrieved from the Himalayas, the Alps and Greenland, but had never been investigated in Antarctica. Here, we investigated rBC ice records at eight Antarctica sites characterized by different snow accumulation rates (low or high). The influence on rBC deposition to snow surface of local deposition processes, long range atmospheric transport, and emissions variability differs among these sites. Inter-comparisons of the reconstructions were performed to reach an understanding of spatial and temporal variability in rBC deposition to the polar continent in association with southern hemisphere fire activity (natural and anthropogenic) and climate variability.

In the sediment core, the rBC record was also expected to be influenced by long-range atmospheric-transported combustion rather than purely local fire events (recorded by micro charcoal). However, no rBC records have been reported so far in lakes and other sediment reservoirs. Therefore, a preliminary estimation of rBC transfer processes from lake waters to sediments had to be investigated prior to sediment analysis, so as to assess eventual losses or perturbations.

II.5. DISSERTATION ORGANIZATION

This dissertation is a compilation of papers written over the course of the Ph.D. research and of yet unpublished results. Chapter II presented a general background and state of the art on 1) rBC nature and characteristics, 2) rBC uses as a proxy for fossil fuel combustion and biomass burning, and on 3) forest fires and their importance in climate science.

Chapter III presents the methods used during the course of this PhD research, specifically analytical methods dedicated to rBC measurements, ice-core analysis and ice core dating.

Chapter IV and V present results and interpretation of rBC records from Antarctica. Specifically, chapter IV focuses on two high resolution rBC records from both a coastal site and an inland site

of West-Antarctica, and covering the calendar year period 1850-2001. Results of data exploration through spectral analysis and comparison with climatic indexes are reported in a journal article entitled "Large scale changes in 20th century black carbon deposition to Antarctica" by M. M. Bisiaux, R. Edwards, J. R. McConnell, M. A. J. Curran, T. D. Van Ommen, A. M. Smith, T. A. Neumann, D. R. Pasteris, J. E. Penner and K. Taylor which was published on October 12th 2011 on *Atmospheric Physics and Chemistry-Discussions*.

Chapter V focuses on the exploration of ice core records from the East-Antarctic Plateau (Dronning Maud Land) over the same time period but at lower temporal resolution than in Chapter 4. The results of annual snow accumulation calculations are presented as a journal article entitled "Variation of accumulation rates over the last eight centuries on the East Antarctic Plateau derived from volcanic signals in ice cores" by H. Anschütz, A. Sinisalo, E. Isaksson, J. R. McConnell, S.-E. Hamran, M. M. Bisiaux, D. Pasteris, T. A. Neumann and J.-G. Winther, published in October 2011 in the *Journal of Geophysical Research*. In the second part of the chapter, the findings of this article are applied to rBC ice core records to calculate annual flux deposition to the East Antarctic Plateau. Temporal and spatial variability of rBC concentrations and fluxes in the East Antarctic low-accumulation ice cores are investigated for the period 1800-2000 and results are presented in a journal article entitled "Black carbon deposition to the East-Antarctic plateau, 1800-2000" by M. M. Bisiaux, R. Edwards, J. R. McConnell, M. R. Albert, H. Anschütz, T. A. Neumann, E. Isaksson and J. E. Penner, published in *Atmospheric Physics and Chemistry-Discussions* in November 2011.

On the other hand, Chapter VI concerns rBC fate and occurrence in freshwater environments and evaluates the possibility of using rBC as a combustion proxy in lake sediments. Part of the findings of this study was published in *Environmental Sciences and Technology* in February 2011 as an article entitled "Stormwater and Fire as Sources of Black Carbon Nanoparticles to Lake Tahoe", by M. M. Bisiaux, R. Edwards, A. C. Heyvaert, J. M. Thomas, B. Fitzgerald, R. B. Susfalk, S. G. Schladow, and M. Thaw. Results obtained for the Tahoe study are compared to measurements performed in parallel in other oligotrophic lakes, and interpreted in terms of

transfer to the sediments. Finally, in Chapter VII, we apply those findings to the measurements of rBC concentrations in a sediment core from Lake Tahoe, and interpret the record in terms of a combustion record.

Lastly, chapter VIII concludes and suggests perspectives for future investigation of rBC nanoparticles in paleo-records as a combustion proxy.

Chapter III. Methods

III.1. BLACK CARBON MEASUREMENTS

III.1.1. The single particle soot photometer

Black carbon measurements presented in this dissertation manuscript have all been conducted on liquid phase samples with a single particle soot photometer (SP2, Droplet Measurements Technologies, Boulder, CO). This instrument provides exceptionally high resolution rBC detection particle per particle based on laser-induced incandescence. Originally designed as an atmospheric instrument for rBC measurements, the SP2 has been recently adapted for liquid water samples (McConnell et al. 2007; McConnell 2010; Bisiaux et al. 2011; Kaspari et al. 2011). However, the measurements of rBC in water samples with a SP2 implies the following assumptions on BC nanoparticles nature and properties:

-When they are produced, rBC particles are non-polar and hydrophobic, but few hours after emission to the atmosphere, adsorption of polar compounds on rBC surfaces makes them hydrophilic and available for collection by hydrometeors.

-The size mode of rBC transported in the atmosphere is under a µm and covered by the SP2 detection range after resuspension of the aerosols (c.f. next section).

Adaptation of SP2 to water samples analysis. The analysis of rBC in water samples with a SP2 requires the necessary step of sample aerosolization and flow injection analysis (FIA). This is accomplished with an ultrasonic nebulizer (USN, CETAC UT5000), where trickling water is pumped against a vibrating membrane of quartz (piezometer) and pulverized into a fine aerosol. Small water droplets are then conducted through an air flow to a drying system constituted of a heating and cooling part. Aerosols exhausting the USN and transferred to the SP2 are thus assumed to be dry, Figure III.1&2.

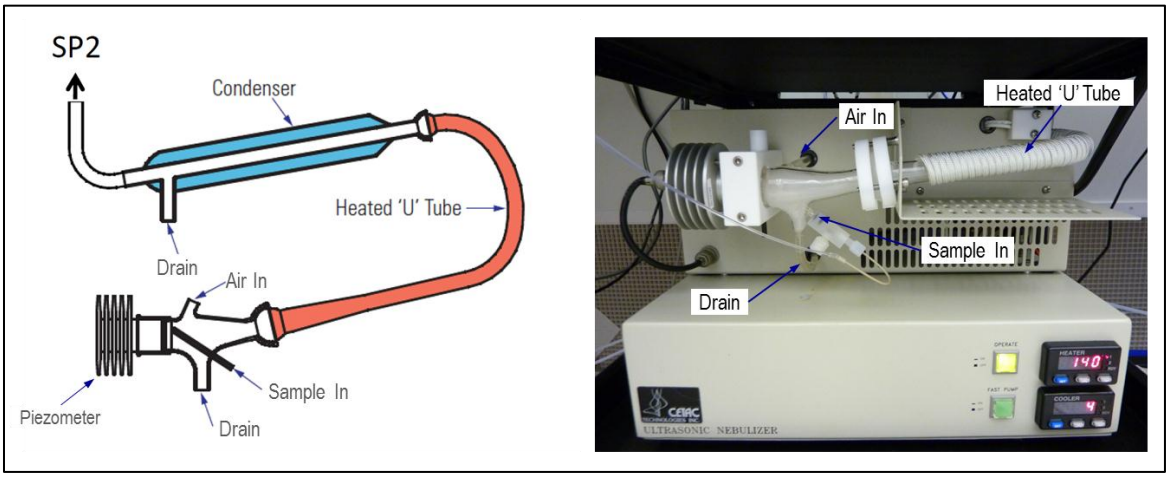

Figure III.1: Schematic of a USN CETAC UT5000 (left) and picture of this USN in operation (right). The white cloud in the aerosol chamber (glass) is visible and shows the aerosolization of the water sample.

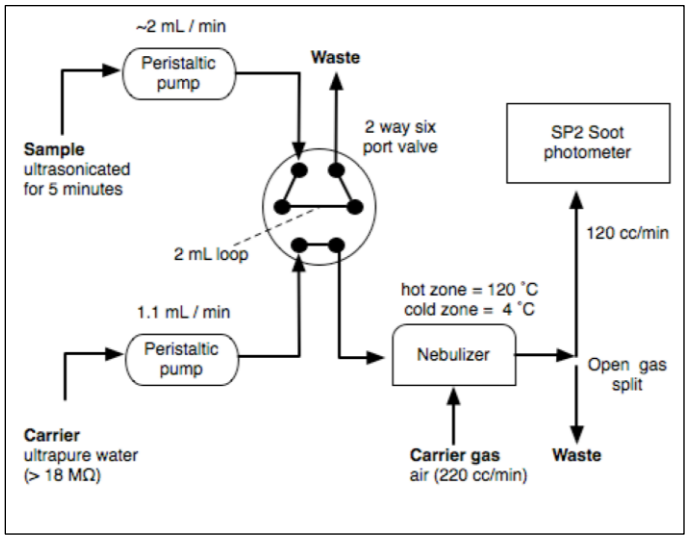

Figure III.2: Schematic of the coupled SP2-FIA analytical system.

Principle of the SP2. The SP2 has been described in detail by Schwarz et al. (2006) and compared with other instrument methods for BC analysis (Slowik et al. 2007; Seinfeld 2008). The principle of the instrument is based on the absorption by rBC particles of laser light until their incandescence. The instrument passes an air stream (from the USN in case of water samples) through an air sheathed jet inside in an intra-cavity ND-YAG laser (1024nm), Figure III.3. Owing

to their strong light-absorption properties notably in this wavelength band, rBC particles are rapidly heated to their boiling point where they incandesce at a wavelength proportional to their boiling temperature. The intensity of the individual particle incandescence events is proportional to the mass or rBC contained in the particle. The light emitted is detected by two avalanche photo-diodes orthogonal to the jet and transmitted to the computer through an electric signal. The detectors cover different part of the incandescence spectrum and thus different sensitivities. Particle count is visible in live on the software interface, while a factor based on rBC mass/incandescence ratio has to be applied to retrieve mass rBC content of the particle (see below).

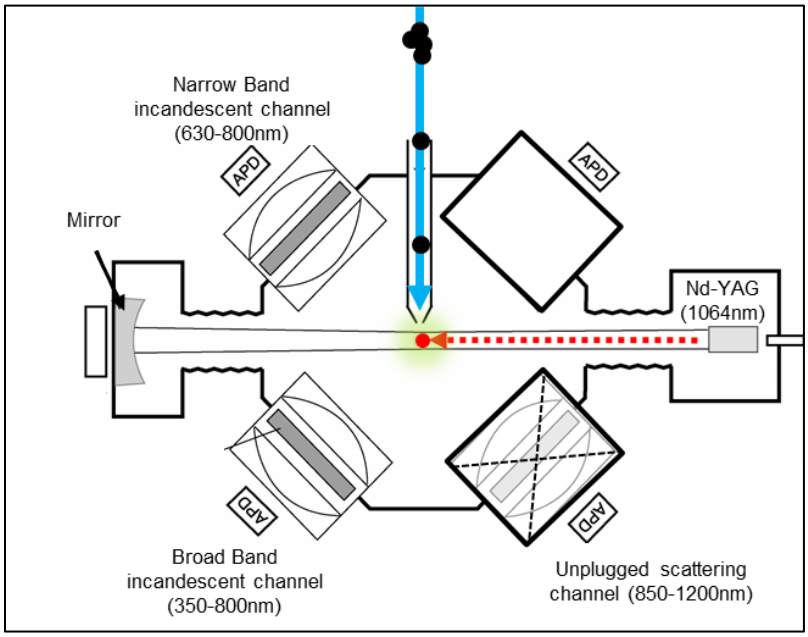

Figure III.3: Schematic of the SP2 (Droplet Measurement Technologies, Denver, CO) system used at DRI (adapted from Schwarz et al. 2006).

The SP2 also supports the use of scattering channels, specially adapted for the measurement of rBC particles fractal diameter in the air. In water or in melted ice, original coating that may have been deposited on the particle during formation or during atmospheric transport, are expected to have been modified (dissolved or chemically altered) thus the interest of particle coating for the liquid water samples is limited. Moreover, the process of sample nebulization and drying is suspected to modify eventual coating size and even to create non-original coating (e.g. with

salts). In the instrument used at DRI, the scattering channel was therefore unplugged to avoid useless acquisition of enormous data volume.

Interferences. In contrast to existing bulk optical and thermal/chemical based methods, which can be sensitive to positive interferences from a variety of organic species such as humic acids and melanoids, interferences are almost physically impossible with the SP2. Indeed, since the SP2 is based on a fundamental property of rBC (its boiling point temperature from ~3700 to 4300 K) it is not possible for organic substances to act as a positive interference in this method. For this to occur, they would have to form refractory nanoparticles with a boiling temperature also in the 3700 to 4300 K range. Particles which incandesce at temperature cooler and hotter than rBC include pure silicon and nickel (at ~ 3500 K), diamond (4500 K) and pure tungsten (5828 K) (Moteki and Kondo 2007). On the other hand, the effect of ultrasonic nebulization of water samples on positive interference was investigated by Schwarz et al. (2006). They aerosolized a variety of organic compounds on the SP2, including tocopherol, olive oil, sucrose, and humis material and detected no incandescence from those organic compounds.

Salt. Although not considered as interference, high salinity water samples were suspected to generate too much salt aerosol during the aerosolization process in the USN. Indeed, we found that salty water (salinity >3) was significantly decreasing the power of the YAG laser, with increased power drop with higher concentrations, and potentially affecting the optics. However, this was not a concern for the measurements presented in this dissertation, since sample salinity was always lower than 1.

III.1.2. Calibration of the instrument and protocol

III.1.2.1. Calibration of the SP2

The measurements described in this dissertation required both internal and external calibrations of the SP2.

Internal calibration. Calibration of the incandescence intensity was performed by Droplet Measurement Technologies (Boulder, CO) by introducing size selected graphite particles of known density into the SP2 using a differential mobility analyzer (DMA) (Slowik et al. 2007). This calibration was performed at least every year or every time the instrument was moved out of the clean lab. Previous studies have found that the SP2 response is independent of rBC particle morphology or organic coatings (Cross et al. 2010) and that the DMA calibration using graphitic rBC is applicable to rBC nanoparticles emitted by combustion (Schwarz et al. 2010).

External calibration. External calibrations of the nebulizer/SP2 interface were performed daily using 10 standards of rBC calibrations ranging from 0.03 to 80.00 µg/l. These standards were prepared freshly every 3 weeks using pure, commercial rBC dispersions (Tokai Carbon, Aquablack 162) showing a surface chemistry similar to that of hydrophilic rBC aerosols found in the atmosphere (Moosmüller et al. 2009). The instrumental response of these standards was compared with a hydrophilic rBC dispersion produced by an inverted diffusion flame and ozonation (Kirchstetter and Novakov 2007) and was found to give a comparable response.

rBC concentrations were quantified by first calculating individual rBC masses using the DMA incandescence internal calibration, and then summing the rBC masses over three second intervals (3sec). The FIA peaks in the resulting 3sec mass time series were integrated, and the peak areas were used to construct the external linear calibration, which was subsequently applied to quantify the sample peak areas, Figure III.4. Standard deviation of identical samples ran several times on the instrument was lower than 10% for concentrations above 0.1 µg/l and about 20% for lower concentrations. Since we observed a non-linear response for concentrations above 20 to 30 µg/l suggesting that some particles were missed, samples with concentrations exceeding 30 µg/l were diluted with ultrapure water to less than 20 µg/l.

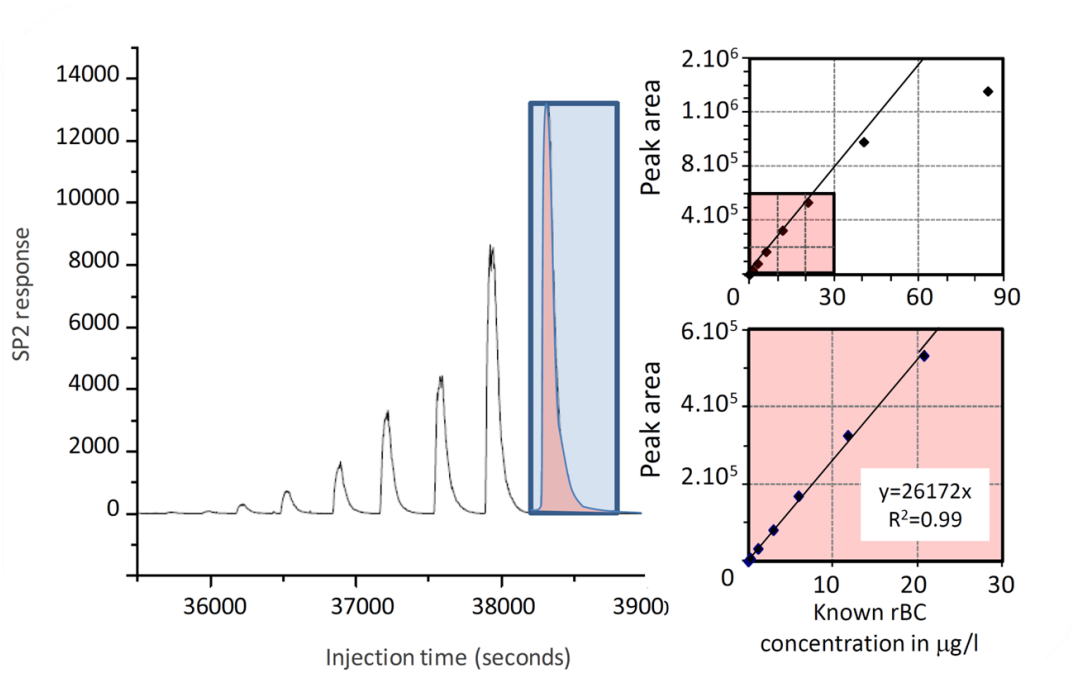

Figure III.4: A typical SP2 daily calibration at DRI. Peak areas of each standard (blue square) are reported on the graphs on the right as a function of known rBC concentrations. The top-right hand corner displays the bending of the calibration curve after ~20-30 µg/l. A zoom of the linear part is shown in the bottom graph.

Blanks. The lack of positive interferences allows very low blanks for the FIA-SP2 method. Moreover, the use of a class 100 clean-room for sampling equipment, sample preparation and analysis, resulted in rBC concentrations lower than the detection limit (<0.01 µg/l, 3σ) in blanks (ultrapure water >18MΩ) and matrix blanks (filtered with 0.02 µm Anopore filter).

III.1.2.2. Protocol of analysis for discrete measurements

Containers. We found that rBC concentrations in glass containers were decreasing faster in time than in plastic bottles, and attributed this effect to adhesion to the wall of rBC particles. The preferred container for water samples was thus chosen to be HDPE vials or bottles. Only standards were contained in glass jars, although not ultrasonicated. Quality control from day to day did not indicated significant rBC loss for not-ultrasonicated standard over less than 3 weeks (probably linked to enhanced stability of standard material compared to natural samples). We avoided any Teflon bottles or tubing, as it was observed to shut down abruptly the aerosolization

process. The vials and bottles were cleaned in the clean-room with ultrapure water (>18MΩ) and stored full. Non clean-room cleaned bottles were exceptionally used for concentrated samples (e.g. runoff water). For snow sampling, we used clean sampling equipment and Whirl pack® bags, which were found to contain rBC in very small quantities (0.01 µg/l) after ultra-sonication of ultra-pure water. Water samples were stored at a temperature close to 4°C and snow samples were stored frozen.

Sample injection. Prior to introduction to the USN, samples were always ultra-sonicated for ~5-10 minutes. Longer ultra-sonication was found to perforate thin HDPE bottles. Within the next 30 to 45 minutes, samples were then introduced to the USN using a 2ml loop and an ultrapure water carrier (>18MΩ) to ensure reproducibility of sample volume injected into the system. We used a peristaltic pump and non-teflon lines for injection. The liquid flow was set at 1.1 ml/min with an air flow (regular breathing air) of 125 ccm. In these conditions, the USN efficiency was stable and about 10% of liquid sample was nebulized. A sample typically required ~4 min to be run through the instrument and was always followed by a 1min blank or until baseline for highly concentrated samples. The commercial rBC (Tokai Carbon, Aquablack 162) was used to prepare quality control standards, which were run after every 10 samples. A method blank prepared from ultrapure water, and a sample replicate were also analyzed every ten samples.

III.2. CONTINUOUS FLOW ANALYSIS

III.2.1. Ice core analysis at the Desert Research Institute

All ice cores analyzed for this dissertation were measured at the snow and ice chemistry facilities of the Desert Research Institute consisting of a class-100 clean room, a cold laboratory (maintained at -20°C), and a wet chemistry laboratory described by McConnell et al. (2002; 2007), Figure III.5. Briefly, ice cores are cut at a ~3cm x 3cm square cross section and are melted vertically on a temperature controlled melter head. The ice sticks are maintained longitudinally in place and protected from air movement by a plastic stand (LDPE). The melter head is split into

three regions by squared 0.5-cm-deep engraved ridges, each pierced and connected to tubing and peristaltic pumps draining of the melted ice to the various instruments. Since eventual contamination is decreasing from the sides toward the center of the ice core (except at core breaks), the most inner ring of the melter head is considered as the cleanest part of the stick and used for ultra-trace measurements in the clean room (HR-ICP-MS, SP2). The outer ring is considered as waste (or sometimes kept for analysis such as ^{10}Be) and the medium ring melted ice is kept collected for less sensitive measurements (e.g. soluble ions such as NH_4^+, Ca^{2+}, NO_3^{2-}, Cl^-, conductivity, H_2O_2, pH).

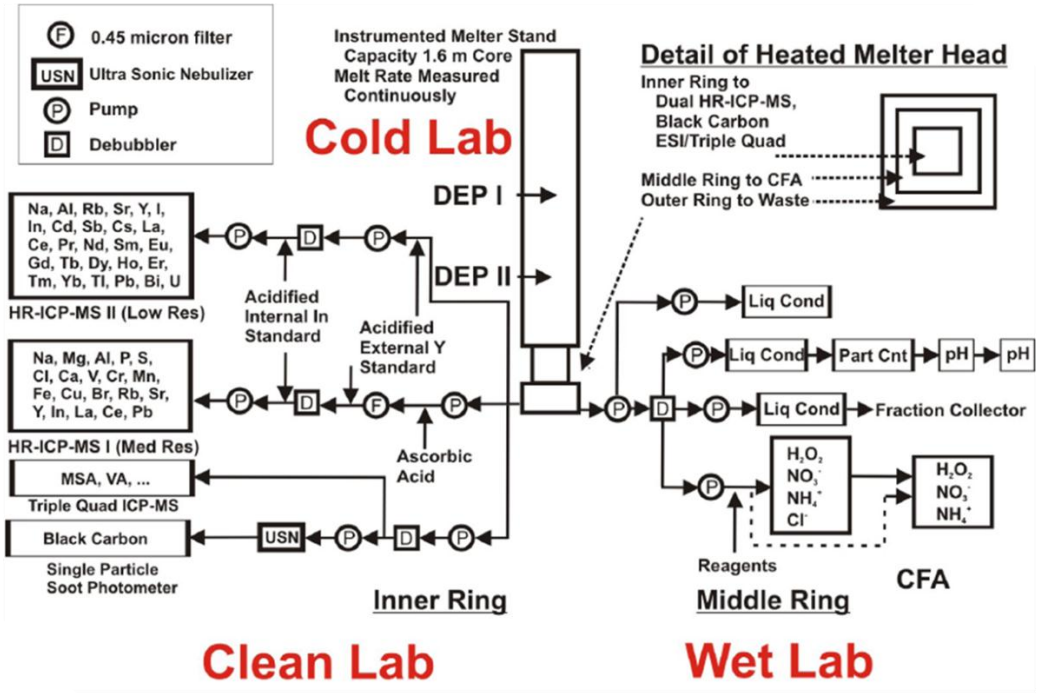

Figure III.5: Schematic of the snow and ice chemistry facilities system used at DRI, including the CFA-side and trace element measurements (courtesy of Joe McConnell).

Continuous coupling of ice melting and trace element analysis allow to measure at very low detections limits (part per trillion, ppt) of a broad spectrum of elemental and chemical species in exact depth co-registration and subsequently in very high depth resolution. Specifically, for rBC a single analysis is conducted with ~0.01 m water equivalent, and about 15-21 samples can be

obtained per year for high-accumulation ice core sites (WAIS-Law Dome sites) and 7-15 samples per year for low-accumulation sites (Antarctic Plateau) for the period considered in this dissertation (1800-2000).

III.2.2. Protocol of analysis

III.2.2.1. Ice core preparation and blanks

Ice cores were in general shipped to the National Ice Core laboratory (NICL), Denver, CO, where they were cut, packed into polythene lay-flat bags and shipped to the DRI in insulated boxes. Both the NICL and DRI facilities maintained a constant ambient temperature of -20°C or below while storing the ice cores prior to laboratory analysis. Within 30 min prior to melting, ice sticks were removed from their polythene bags and scraped with ceramic blades at each core break on ~0.2 mm, to remove eventual contaminated ice. External and internal calibrations of all instruments, including the SP2, were performed daily before melting. A replicate ice stick was run every time the instruments were turned on (once a day in general). Blanks (frozen ultrapure water) and quality control standards were run every 1h30-2h of melting.

III.2.2.2. Black carbon and ions measurements

Melted ice from the inner ring of the melter head was directed to the SP2 in continuous flow. A debubbler was used to degas any air contained in the lines. The instrument calibration and flows set points were identical in CFA (continuous flow analysis) and discrete samples modes.

Soluble ions were measured using the CFA system by absorption spectroscopy for Nitrate and Chlorine (NO_3^{2-}, Cl^-). Ammonium (NH4+) was measured by fluorometric spectroscopy and soluble sulfur, sodium and calcium by ICP-MS.

ICPMS measurements were carried out by two Thermo Finnigan Element-2, high-resolution inductively coupled plasma –mass spectrometers (HR-ICP-MS). In total, ~20 elements or species were measured. The meltwater stream was combined with both external and internal acidified

standards to prevent precipitation and chemi-adsorption of dissolved species onto the tubing walls, to monitor flow through the system, and to correct for matrix effects in the HRICP- MS nebulizers. A certified Standard Reference Material (SRM) from the National Institute of Standards and Technology (NIST # 1640) was used in conjunction with routine check standards and blanks to monitor baselines, response times, and the stability of the calibration during the analyses (McConnell et al. 2002; McConnell et al. 2005).

III.3. ICE CORE DATING

Five different methods can be applied and eventually combined, for ice core dating: i) annual layers counting, ii) identification of remarkable horizons, iii) cross-comparison with other ice core records, iv) modeling of ice thinning and ice flow and v) comparison with cyclic orbital parameters.

III.3.1. Annual layer counting

The seasonal variability of snow chemistry signature between summer and winter allow for dating of ice cores by annual layers counting. This approach is specifically accurate for ice cores covering the last centuries or collected at high-accumulation sites, but becomes difficult when depth increases due to ice thinning. Alpine glaciers, “coastal” Antarctic sites and top layers of the Antarctic plateau and Greenland are adapted for this technique which was first used to date an ice core drilled at Dye 3 (Greenland) (Hammer et al. 1986). Because of the temporal variability in snow accumulation (which can differ by 50% depending on the site (Anklin et al. 1998)), consistent layer identification is best accomplished when robust seasonal indicators are combined with multiple annually varying parameters to resolve eventual ambiguities (e.g. Banta and McConnell 2007; McConnell et al. 2007; Banta et al. 2008; Thomas et al. 2008), Figure III.6. Examples of robust seasonal indicators are the midwinter H_2O_2 concentration minima or the summer non–sea salt sulfur (nssS) concentration maxima, both principally driven by the variability in insolation. Dating from annual layer counting is widely used for recent ice cores but has been

applied as well for dating ice cores up to 40,000 years BP at GISP2 (Greenland) with uncertainty of 2% until 11,600 years BP, increasing to 10% around 40,000yr BP (Alley et al. 1993; Meese et al. 1994). More recently, this technique was applied to date an ice core from NorthGRIP up to 60,000 years BP (Andersen et al. 2006; Svensson et al. 2006; Vinther et al. 2006; Svensson et al. 2008).

Annual thicknesses are then converted to water equivalents, based on the ice core density and corrected for ice thinning using a simple Nye model (Fountain et al. 2004) that assumes a linear vertical strain rate through the total depth of the core.

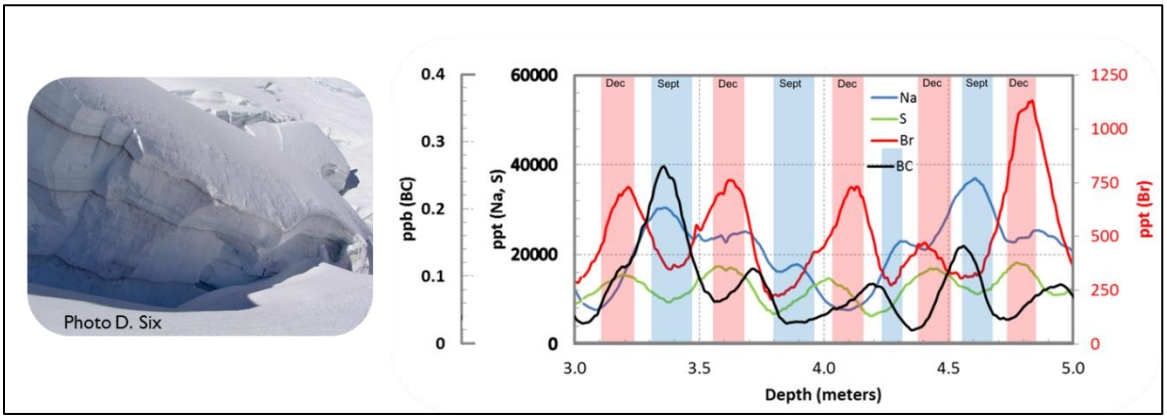

Figure III.6: (Left) Example of annual layers visible on an ice fall (Alpine glacier); brown layers mark summer layers. (Right) Illustration of the use of annual cycles for WAIS core: maximas and minimas correspond to specific periods of the year, depending on the proxy used (blue bands indicate winter-spring periods centered over September, red bands indicate summer periods centered over December)

III.3.2. Identification of remarkable horizons

Occasional deposition of atmospheric tracers in large quantities and over wide areas form remarkable horizons, which can help ice core dating and tie various records together (Figure III.7). Three typical horizons are mostly used for this purpose: radioactive layers due to nuclear weapons tests, volcanic eruptions and events involving radiogenic isotopes (e.g. ^{10}Be). While radioactive layers are only used for recent ice cores (atmospheric tests occurred principally between 1950 and 1966 (Jouzel et al. 1979), volcanic eruptions can be observed on older ice records (up to ~2000yr BP) specifically with high SO_4^{2-} and NO_3^- concentrations, presence of

Tephra, or peaks in conductivity. Finally, the formation of radiogenic isotope ^{10}Be which is sensitive to changes in the amount of cosmic rays getting to the stratosphere is a proxy of major modulation of the Earth's magnetic field or solar activity. It is thus used for ice core dating at very long time scales, revealing e.g. the Laschamp event 40,700 years BP (Singer et al. 2009) or the Brunhes-Matuyama magnetic inversion 780,000 years BP (Raisbeck et al. 2006).

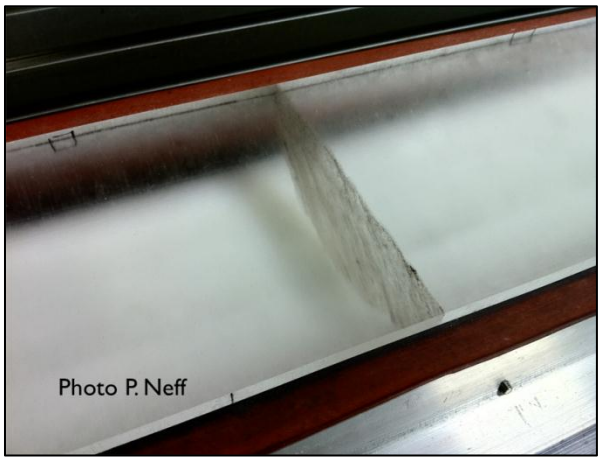

Figure III.7: A visible layer in a WAIS divide ice core (depth ~2500m) of unknown nature yet (likely Tephra or dust). Courtesy of Peter Neff from the NiCL facility.

III.3.3. Cross-comparisons with other ice core records

Absolute dating of ice cores is not always possible and correlations between various records (ice and sediment cores) are widely used. This dating method is called "relative dating" and is particularly useful when annual counting is not possible. The comparison of isotopic composition of speleothem calcite precisely dated (with U/Th ratio) and isotopic composition in the ice is one of the cross-comparison approach (Parrenin et al. 2007).

III.3.4. Utilization of ice thinning and ice flow modeling

When annual dating is not possible, ice flow and ice thinning modeling at and around drilling sites offers an opportunity to reconstruct age scales between remarkable horizons. These models include fluid mechanics laws and estimation of snow accumulation variability. Uncertainty resides

in the estimations of surface climatic conditions, bedrock topography, and physic properties of ice such as thermal conductivity and crystal size (e.g. Buiron 2010).

Chapter IV. High resolution rBC records from low elevation sites of Antarctica, cal. yr. 1850-2001

Article Title:

Large scale changes in 20th Century black carbon deposition to Antarctica

Journal Article published on October 12th 2011 in Atmospheric Physics and Chemistry Discussions, reproduced by permission of Copernicus Publications.

Authors:

Marion M. Bisiaux[1]*, Ross Edwards[2,1], Joseph R. McConnell1, Mark A. J. Curran[3,4], Tas D. Van Ommen[3,4], Andrew M. Smith[5], Thomas A. Neumann[6], Daniel R. Pasteris[1], Joyce E. Penner[7] and Kendrick Taylor[1]

*Corresponding author:

M. M. Bisiaux (marion.bisiaux@dri.edu);

[1] Desert Research Institute, Reno, NV, United States,

[2] Curtin University, Perth, WA, Australia

[3] Australian Antarctic Division, Kingston, TAS, Australia,

[4] Antarctic Climate and Environment CRC, University of Tasmania, Hobart, TAS, Australia,

[5] Australian Nuclear Science and Technology Organisation, Lucas Heights, NSW, Australia,

[6] Goddard Space Flight Center, NASA, Greenbelt, MD USA,

[7] University Michigan, Ann Arbor, MI, United states

Credits:

For this article, I was involved in data acquisition and took the lead on data interpretation and manuscript redaction.

ABSTRACT

Refractory black carbon aerosols (rBC) emitted by biomass burning (fires) and fossil fuel combustion, affect global climate and atmospheric chemistry. In the Southern Hemisphere (SH), rBC is transported in the atmosphere from low latitudes to Antarctica and deposited to the polar ice sheet preserving a history of emissions and atmospheric transport. Here, we present two high-resolution Antarctic rBC ice core records drilled from the West Antarctic Ice Sheet divide and Law Dome on the periphery of the East Antarctic ice sheet. Separated by ~ 3500 km, the records span calendar years 1850-2001 and reflect the rBC distribution over the Indian and Pacific ocean sectors of the Southern Ocean. Highly correlated over the past 60 years, the records show that coherent large-scale changes in SH rBC occurred at decadal to inter-annual time scales, notably in ENSO-like periodicities. Decadal trends in the records are similar to inventories of SH rBC emissions from grass fires and biofuels. The combined records suggest a large-scale reduction in rBC from 1950 to 1990 over the remote southern hemisphere.

IV.1. INTRODUCTION

Refractory black carbon (rBC, soot) aerosols are present in the Antarctic atmosphere, snow and ice (Chýlek et al. 1987; Warren and Clarke 1990; Chýlek et al. 1992; Grenfell et al. 1994). These aerosols are the result of long-range transport of biomass burning and fossil-fuel emissions across the Southern Ocean (Seiler and Crutzen 1980; Crutzen and Andreae 1990; Andreae et al. 2005). Ubiquitous in the troposphere, rBC aerosols are the primary absorber of visible light impacting the Earth's radiation budget and climate (Bond and Bergstrom 2006). Recent estimates of the globally averaged radiative forcing for rBC are as high as 1.2 W/m2 (direct + indirect effects), the second highest radiative forcing after carbon dioxide (Ramanathan and Carmichael 2008). However, the climate forcing from rBC in the atmosphere differs from that of greenhouse gases, which are well mixed and warm the Earth's surface. In contrast, rBC aerosols display large spatial and temporal gradients and heat the atmosphere while cooling the surface (Ramanathan

and Carmichael 2008). The highest atmospheric concentrations of rBC are found in the tropical belt resulting from the combustion of biomass and biofuels. In the Southern Hemisphere (SH), atmospheric concentrations are highly seasonal with emissions primarily from dry-season biomass burning in Australia, southern Africa and South America (Mouillot and Field 2005). In contrast to fossil-fuel emissions, which are highest in the northern hemisphere, biomass burning emissions are sensitive to changes in climate as well as to human activity such as tropical deforestation, land clearing, and fire suppression (Mouillot and Field 2005). While the effects of rBC in the modern atmosphere are numerous, little is known regarding its past variability and sensitivity to climate change and human activity.

Ice core records preserve a history of rBC variability in the atmosphere with sufficient temporal-resolution to resolve seasonal changes in emission strength and atmospheric transport. Combined with general circulation modeling and rBC emission inventories, these records can provide constraints on the paleo-rBC atmospheric distribution, past biomass burning emissions and climate feedbacks (Lamarque et al. 2010; McConnell 2010). Recent, high-temporal resolution ice core records of rBC from Greenland show that northern hemispheric rBC concentrations peaked during the early 20th Century from fossil fuel combustion (McConnell et al. 2007; McConnell 2010) perturbing the Earth's radiation budget. While a number of paleo-biomass burning records have shown centennial scale variability in SH biomass burning (Marlon et al. 2008; Falk et al. 2010; Wang et al. 2010; Whitlock and Tinner 2010), high temporal resolution rBC records have not been reported.

IV.2. ICE CORE LOCATIONS AND METHODS

Ice core sites. The ice cores used in the study included WDC06A from West Antarctica and DSSW19K from Law Dome in East Antarctica, Table IV.1. The WDC06A ice core was drilled from 2007 to 2011 to a depth of ~3330 m near the West Antarctic ice sheet divide (WAIS Divide, located ~550 km inland). The record shown here covers the top 50.3 m of the ice core, which was drilled using an electromechanical drill in a dry bore. The DSSW19K ice core site was

electromechanically drilled (dry bore) 19 km to the west of the Law Dome DSS drill site (4.7 km SSW of summit, ~ 100 km inland) to a depth of 120 m in 2004. The record shown here spans the top 37 m of the ice core. Average ice accumulation rates at the sites were similar: ~20 ± 3.4 cm/a for WDC06A, (Banta et al. 2008) and ~15 ± 3.1 cm/a for DSSW19K. However, physical processes at DSSW19K including the formation of sastrugi (dips and ridges formed by wind erosion) limit the temporal resolution at the site to ~1 year while the WDC06A record was found to preserve sub-annual variability (Banta et al. 2008).

rBC ice core analysis. Longitudinal sections of the WDC06A and DSSW19K ice core were analyzed for rBC using an ice-core melter system coupled to an ultrasonic nebulization/desolvation system (CETAC UT5000) (Bisiaux et al. 2011) and single particle intracavity laser induced incandescence photometer (SP2, droplet Measurements Technologies, Boulder, Colorado). This analytical method is described by previous studies (McConnell et al. 2007) and is described in section III.1. of this manuscript. Using this method, rBC was determined in the ice core at a depth resolution of ~ 1cm corresponding to ~25 to 35 data points per year at WAIS and ~10 to 15 at Law Dome.

Dating. Depth-age relationships for the records were developed using glaciochemistry and annual cycle counting for a suite of trace elements including sodium (Na), chloride (Cl), bromine (Br) and sulfur (S) (described in SI cf. section IV.5). Known volcanic eruptions (Tambora, Krakatoa, Agung) were also used as absolute time markers to confirm the annual layer counting. Although, extremely well preserved in the WAIS WDC06A record, annual cycles were generally less discernable in the Law Dome DSSW19K record because the net snow accumulation rate approximately equal to the height of the local surface roughness (Figure. IV.1 and in SI, Figure IV.5).

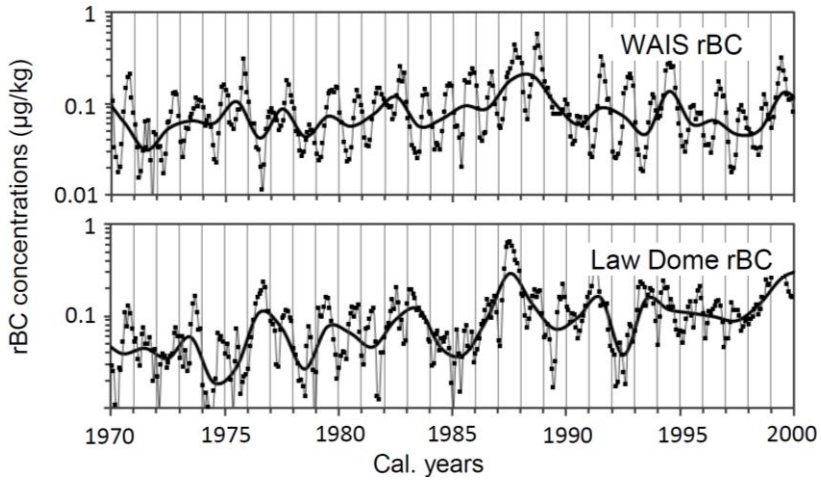

Figure IV.1: 1970-2000 monthly (dots) and annual smoothing (line) for rBC at WAIS and Law Dome.

Cross comparisons of high resolution, continuous sulfur and sea salt measurements in the Law Dome DSS0506 and DSSW19K ice cores were used to confirm the annual layer counting. The DSS0506 core, drilled near the Law Dome DSS site in 2005 in a much higher snow accumulation rate zone and analyzed in a similar fashion but not for rBC, contains distinct annual cycles in most of the elements and chemical species we measured so dating in that core is unambiguous. While the dating uncertainty for the DSSW19K record is relatively large in comparison to WDC06A, it is sufficiently accurate to allow the calculation of net snow accumulation and rBC fluxes for both records, especially when averaged over multi-annual to decadal time scales.

IV.3. RESULTS AND DISCUSSION

IV.3.1. Concentrations and fluxes

Concentrations of rBC in both records were log-normally distributed (Figure in SI IV.6) with geometric means (geomean) of 0.8 µg/kg (n = 4860) and 0.9 µg/kg (n = 2883) for WDC06A and DSSW19K, respectively. In the WDC06A core, sub-annual rBC concentrations were highly seasonal (Figure IV.1), with consistent low austral summer/fall concentrations averaging 0.04 µg/kg and high winter/spring concentrations averaging 0.15 µg/kg. The DSSW19K rBC concentrations were less variable with annual minima and maxima of 0.08 and 0.12 µg/kg,

respectively. In contrast, DSSW19K rBC concentrations were more variable than WDC06A but had a comparable annual geometric mean of ~ 0.08 µg/kg (Table IV.1).

		Location	Lat/long	Elevation (ASL)	Age of sample (in Cal.yr or as specified)	Annual concentrations (µg/kg)		Method
						Range[a]	Average[a]	
This study	Antarctica	WAIS (WDC06A)	79.46 S, 112.08 W	1766m	1970-2000	0.03 to 0.30	0.08	SP2-FIA
"	"	"	"	"	1850-2000	0.03 to 0.30	0.08	
"	Antarctica	Law Dome (DSSW19K)	66.78 S, 112.37 E	1230m[b]	1970-2000	0.02 to 0.32	0.08	
"	"	"	"	"	1850-2000	0.01 to 0.55	0.09	
McConnell et *al*. 2007	Greenland	D4	71.4 N, 44.0 W	2710m	1952-2002	<1 to 10	2.3	
"	"	"	"	"	1851-1951	~1 to 20	4	
Chylek et *al.* 1995	Greenland	Summit/GISP2	72.36 N, 38.30 W	3200m	320-330	0.5 to 6.5	2.1	Transmittance on quartz fiber filter
"	"	"	"	"	recent snow	-	2	
Chylek et *al*. 1987	Greenland	Camp Century	78.85 N, 55.232 W	2000m	4 kyrBP	-	2.5	
"	"	"	"	"	6 kyrBP	-	1.1	
"	Antarctica	Siple Dome	81.66 S, 148.83 W	1050m	recent snow	-	2.5	
Chylek et *al*. 1992	Antarctica	Byrd station	80.02 S, 119.53 W	1550m	0.7 to 10 kyrBP	0.1 to 0.95	0.5	
"	"	"	"	"	10 to 14 kyrBP	0.1 to 0.4	0.2	
Warren and Clarke 1990	Antarctica	South Pole station	90 S, 0 W	2830m	recent snow	0.1 to 0.3	0.2	
Grenfell et *al*. 1994	Antarctica	"	"	"	recent snow	0.1 to 0.3	0.3	
Grenfell et *al*. 1994	Antarctica	Vostok	78.46 S, 106.83 W	3488m	recent snow	1 to 7	(Contamination)	

Table IV.1: Ranges and averages of annual rBC concentrations for this study and previous work in Greenland and Antarctica (snow and ice). Approximate location of WDC06A and DSSW19K sites are shown on the map on left hand corner. [a]: For this work only, annual concentrations are calculated from the log values of monthly data and the average is the geometric mean of those annual concentrations. For Law Dome, out-layer year 1910 has been excluded of range estimation. [b]: Altitude measured by Digital Elevation Model from (Bamber et al. 2009).

Concentrations determined in the records were comparable to the snow rBC concentrations reported by Warren and Clarke (1990), Grenfell et al. (1994) and derived from a GCM model (Flanner et al. 2007), but lower than concentrations measured in older Antarctic ice by Chýlek et al. (1992), Table IV.1. Differences in the reported concentration range likely reflect the different time periods encompassed by the measurement and spatial variability, as well as the analytical methods used (Bisiaux et al. 2011; Kaspari et al. 2011). Annual rBC fluxes, estimated from rBC concentrations and annual accumulation rate estimates were 16 ± 2.7µg/m^2/a at WDC06A and 13.5 ± 2.7µg/m^2/a at DSSW19K for the same time period. Integrated over the whole Antarctic continent, this corresponds to a total rBC deposition of ~150 tonnes/a (~0.01% of total rBC emission in SH estimated by Lamarque et al., (2010)).

Time series of rBC concentrations from 1850 to 2000 are shown in Figure IV.2. Both sites displayed significant annual to decadal scale variability prior to 1950. After 1950 rBC concentrations decreased until ~ 1980 and then rose to pre-1950 concentrations. The decline in rBC at WDC06A during this period was not related to changes in the snow accumulation rate,

which was extremely stable during this time (Banta et al. 2008). At DSSWK19, annual snow accumulation rates are less certain than WDC06A and were not used to estimate fluxes at for individual years. However, changes in the Law Dome accumulation rate have been found at the DSS ice core located 19km from the DSS19WK site (van Ommen and Morgan 2010). This is known to be a regionally coherent change with other records on Law Dome and in Eastern Wilkes Land showing similar patterns (Morgan et al. 1991). The DSS record shows an unusual increase in snow accumulation after 1975 is found associated with changes in zonal atmospheric circulation, but no significant correlation (R^2 = 0.07, p = 0.41 for annual records and R^2 = -0.14, p = 0.08 for 5yrs smoothed records) was found between the DSS snow accumulation record and DSSWK19 rBC and the two records appear to be unrelated.

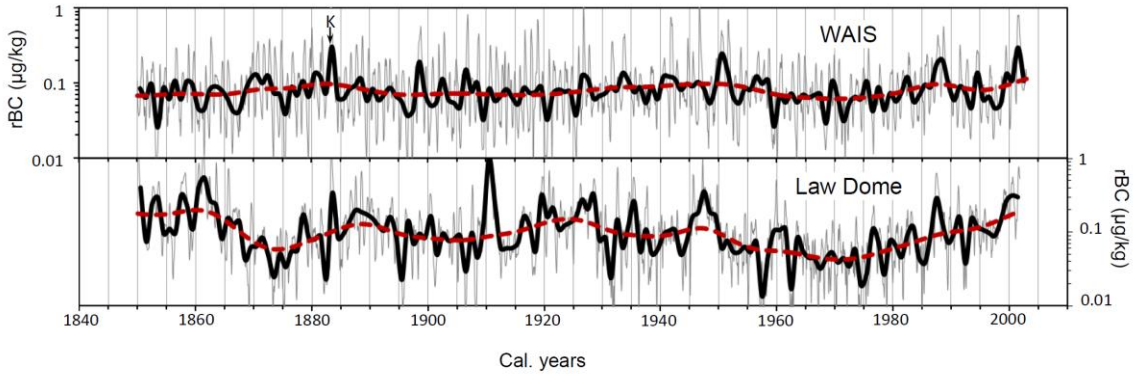

Figure IV.2: Smoothed rBC concentrations (thick) and decimal (thin) for WAIS (top) and Law Dome (bottom), re-sampled with a piece-wise linear interpolation integration. Red dash line is 21-yr smoothing with R implementation of Nadaraya-Watson kernel regression estimate. K marks the Krakatoa volcanic eruption used for dating.

To investigate the effect of local to regional changes in atmospheric circulation on the rBC records, the time series were compared with co-registered records of sodium (Na, a sea-salt proxy), which is modulated by both regional atmospheric transport and seasonal variability in salt emissions from the Southern Ocean by cyclonic activity and to a lesser extent from sea ice (Legrand and Mayewski 1997; Curran et al. 1998; Goodwin et al. 2004). The records of rBC and Na at both sites were found to be autocorrelated due to a strong annual cycle, in both species. However, Na was found to lead the rBC record, by ~ 3 months at WDC06A and ~2 months at DSSW19K (Figure IV.8 in SI for the 1970-2001 period) and no correlations were found between

Na records and rBC at the two sites except for the annual cycle (Figure IV.8b in SI). This suggests that rBC variability is not sensitive to atmospheric transport associated with cyclonic systems in the Southern Ocean, the principal source of Na in the ice core (Sneed et al. 2011). Variability of large-scale atmospheric transport (hemispheric) and source emissions at low latitudes are thus assumed to be the primary factors affecting rBC variability in the records.

Influence of ENSO. Spectral analysis of the rBC records over the 1850 to 2001 period revealed significant periodicities in the ~2 to 6yrs El Niño Southern Oscillation/Quasi-biennial oscillation band (ENSO/QBO, Figure IV.3a-b) suggesting that ENSO/QBO related climate variability modulates rBC in the records (Li et al. 2011). At WDC06A, significant periodicities in the ENSO/QBO band were found at 1.7yr (AR1 CI = 99%) and 5yr (AR1 CI = 90%) while at DSSW19K significant periodicities were found at 2.3yr (AR1 CI = 95%) and 6yr (AR1 CI = 95%).

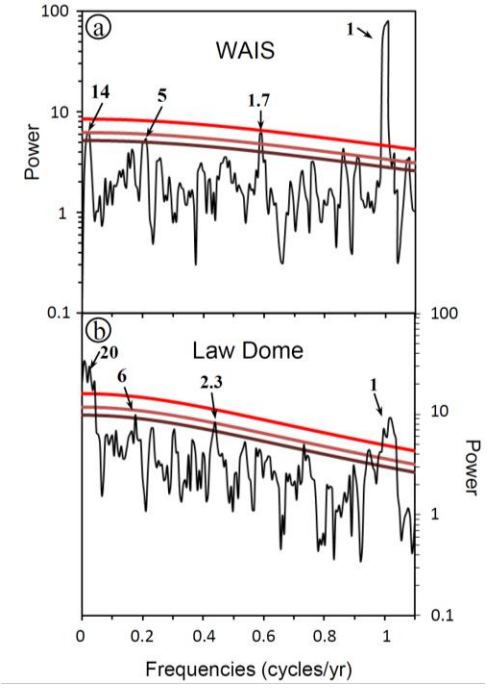

Figure IV.3: Spectrums obtained by Multi taper Method (MTM), for WAIS (a) and Law Dome (b) monthly rBC records for 1850-2001 period and confidence levels in red lines (90, 95, 99%). Significant periodicities (notably in ENSO and QBO band) an corresponding values in years are indicated as numbers on the graph.

These periodicities were coherent between the two sites over the 1970-2001 period (average coherence coefficient >0.38, Figure IV.9b in SI) suggesting a common modulation. No

ENSO/QBO periodicities were found in the WDC06A Na record (Figure IV.8a,b in SI) further suggesting that processes driving Na at WDC06A are distinct from the modulation of rBC. On the other hand, ENSO/QBO band periodicities were found in the DSSWK19 Na record, more influenced by the larger Na signal due to the more “maritime” characteristics of DSSW19K location (Morgan et al. 1997). However, the rBC signal was found to be systematically delayed from Na by 0.3 to 2.2yrs (Figure IV.8d. in SI).

IV.3.2. Decadal variability: Unprecedented period of low variance

On the decadal scale, the rBC records show similar features and variability, which appear to have no analogue in the ice core Na records or climatic indexes such as ENSO and the Southern Annular Mode (SAM). Notably, in the late 1950’s rBC concentrations decreased abruptly (Figure. IV.2 and IV.4) in parallel to the start of a low-variance period common to the two records, which persisted until ~1985 (Figure IV.10 in SI). This period of decreased concentration and variance is consistent with rBC emissions inventories (Figure IV.4) from Australia and South America grass fires (Lamarque et al. 2010) and Australia biofuel emissions (Ito and Penner 2005). This time period also coincides with the start of Australian rational fire prevention policies (prescribed fires instead of total fire suppression), which began in the 1950’s (Mouillot and Field 2005). Similar temporal variability does not occur in the emission inventory for SH forest fires (Mouillot and Field 2005). However, we note that recent estimates of SH rBC emissions (GFED 3, (van der Werf et al. 2010)) attribute ~41% of SH rBC to grass fires (61% if woodlands are included) with ~ 9% from forest fires and 26% from deforestation (primarily in South America). Thus, changes in the SH grassland (and woodland) fire regime from human activity and climate (hydroclimate) could have a significant impact on the SH rBC distribution.

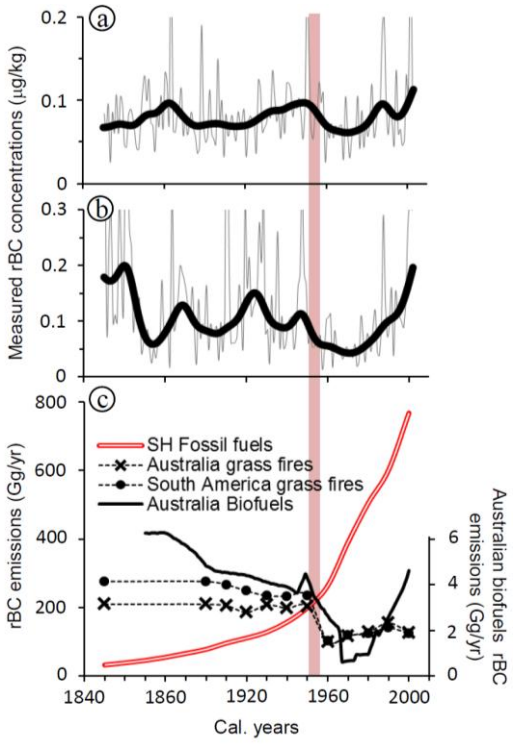

Figure IV.4: a,b: rBC records for WAIS and Law Dome. In gray, concentrations re-sampled to annual resolution with a piece-wise linear interpolation integration. Dark thick lines are 21-yr smoothing with R implementation of Nadaraya–Watson kernel regression estimate. c: comparison with reconstructed rBC emissions from SH fossil fuel anthropogenic use, Australian grass fires, South American grass fires (Lamarque et al. 2010) –left scale- and from Australian biofuels (Ito and Penner 2005) –right scale. The vertical bar highlights the beginning of fire prevention in Australia.

Emissions from SH deforestation, forest fires and fossil fuel combustion increased markedly after 1950 (Ito and Penner 2005; Lamarque et al. 2010), Figure IV.4, and may be reflected in increasing rBC concentrations observed in the last decades of the WDC06A and DSSW19K ice cores records. However, the time lag between the ice core record and rising emissions in the inventories suggest that these records may be insensitive to BC emissions transported across the Atlantic sector of the Southern Ocean.

IV.4. CONCLUSIONS

The high-resolution rBC ice core records in this study capture the variability of rBC deposition in two disparate regions of the Antarctic continent. These records appear to be influenced by variability similar to tropical Pacific climatic variability (ENSO) most likely due to the lagged response of grassland fuel loading to hydroclimate variability. Common variability in the records

from the 1950's to 1980's was also coincident with decadal variability in grassland and biofuel rBC emission inventories (Ito and Penner 2005; Lamarque et al. 2010). Thus, the records may be influenced by both climate variability and human activity. Further research combining general circulation model based rBC simulations with improved geospatial estimates of rBC emissions are required to deconvolve these factors. New ice core records are also required to investigate the spatial variability of rBC transport and deposition to Antarctica. In particular, development of ice core rBC records from Antarctic regions exposed to Atlantic air masses are needed to reconcile the temporal variability found in this study with increased emissions from South American deforestation and fossil-fuel combustion.

ACKNOWLEDGMENTS

This work was supported by NSF grants OPP 0739780, 0839496, 0538416, 0538427, the Australian Government's Cooperative Research Centres Programme through the Antarctic Climate and Ecosystems Cooperative Research Centre (ACE CRC) and the Desert Research Institute. We gratefully acknowledge Ken Taylor and the WAIS divide drilling team, the Law Dome drilling team and the DRI ice core team. The authors appreciate the support of the WAIS Divide Science Coordination Office at the Desert Research Institute of Reno Nevada for the collection and distribution of the WAIS Divide ice core and related tasks (Kendrick Taylor, NSF Grants 0440817 and 0230396). The NSF Office of Polar Programs also funds the Ice Drilling Program Office and Ice Drilling Design and Operations group for coring activities; Raytheon Polar Services for logistics support in Antarctica; and the 109th New York Air National Guard for airlift in Antarctica. The National Ice Core Laboratory, which archived the WAIS core and preformed core processing, is funded by the National Science Foundation. We thank Jean-Robert Petit for help and advice on spectral analysis as well as Jean-Francois Lamarque and Ito Akinory for help with emissions inventories.

SUPPORTING INFORMATION AVAILABLE IN THE FOLLOWING PAGE, SECTION IV.5.

IV.5. SUPPLEMENTARY INFORMATION TO CHAPTER IV

IV.5.1. Black carbon measurements

Continuous flow analysis was based on a steady sample flow and in-line detection of BC and other chemical substances as described in McConnell et al. (2007). In the cold room, previously cut one meter ice core sticks of 3x3cm, are melted continuously on a heated melter head specifically designed to eliminate contamination from the atmosphere or by the external parts of the ice. The melted ice from the most inner part of the ice stick is continuously pumped by a peristaltic pump and carried to a clean lab by Teflon lines. The recorded signal is continuous, integrating a sample volume of about 0.05 mL, for which the temporal resolution depends on the speed of melting, ice density and snow accumulation rate at the ice core drilling site. The two ice cores presented in this study have monthly to seasonal resolution over the time period that was examined.

Refractory black carbon (rBC) concentrations were determined using the same method as in (Bisiaux et al. 2011) and adapted to continuous flow measurements as described by (McConnell et al. 2007).

IV.5.2. Dating

The cores were dated by counting the annual cycles in trace chemistry notably in Sodium (Na), Chlorine (Cl), Sulfur (S) and Bromine (Br). Annual layer counting was evaluated using cross comparisons of peaks in S concentration in the DSS0506 collected from the high snow accumulation region at the top of Law Dome for specific volcanic horizons including Tambora (1815), and Krakatoa (1883) and Agung (1963).

For annual accumulation derived from the ice cores, we assumed ~3.1 cm water equivalent uncertainty in each year's accumulation from short scale spatial variability (glaciological noise) which was determined from measurements of annual accumulation in multiple parallel ice cores from the WAIS Divide ice core site (Banta et al. 2008).

IV.5.3. Fluxes

Annual rBC flux rates were calculated at WAIS by summing monthly flux rates (estimated by dividing the annual accumulation rate by 12 and multiplying by the monthly concentrations). A model estimate of the measured annual layer thinning due to ice flow proved to be very minimal in the most recent 150 years (measured layer thickness is ~1% less than the initial layer thickness) so no correction was made to the accumulation rates derived from the WDC06A ice core.

While the ice cores reflect sub-seasonal variations at both LD and WAIS, the measurements at LD lack unambiguous subannual markers that can be tied to specific calendar dates and for this reason only the annual averages in accumulation were derived from the record (mid-January to mid-January) (van Ommen and Morgan 2010).

IV.5.4. Spectral analysis

To investigate and extract the most prominent frequencies of our signal, we conducted spectral analysis on the rBC and Na records with Kspectra 3.0.2.software for multitaper method (Ghil et al. 2002) and with Analyseries 2.0.3 software (Paillard 1996) for Blackman-Tukey method (coherence and phasing) on Macintosh. We used different spectral analysis and compared them to confirm the robustness of our results.

Resampling, smoothing and spectral analysis was conducted on the log of the original values, and then changed back to normal.

IV.5.4.1. Multitaper method (MTM):

This method is independent of the spectral power, and even small amplitude oscillations may be considered as significant. This is not the case with a Blackman-Tukey method. The significance of each spectral peak is determined through a F-test (>0.90, >0.95, >0.99). We used monthly resolution record for this analysis. In our cases, with monthly resolution over 150 years, we use a

number of tapers of 3, and resolution = 2. For typical length instrumental climate records, this offers a good compromise between the required frequency resolution for resolving distinct climate signals (e.g., ENSO and decadal-scale variability) and the benefit of multiple spectral degrees of freedom (http://www.spectraworks.com/Help/).

We used in particular the high-resolution multitaper spectrum which is the weighted sum of the K eigenspectra, with a red noise significance (robust noise), reshaped at 95% with linear fit.

IV.5.4.2. Blackman-Tukey method (Figure IV.8 and IV.9)

This is the classical method for spectral analysis. In particular, we used it to determine the phase relationship between two data sets (between two sites or between rBC and Na), using two different filters to get the best spectral coherence for any given frequency. This coherence is a function of frequency with values between 0 and 1, and is a fraction of a common variance between two time series x and y through a linear relation. Coherence coefficients are given with 3 levels of confidence (high, medium levels -shown on graph- and low). Coherence is considered non-zero when coefficients reach for values > 0.38.

For this analysis we resampled (using piece-wise linear integration interpolation) the different datasets, using a time resolution 0.4 yrs, to keep the annual periodicity but remove any shorter-term variability. Phasing between the same periodicities was also determined through this method, and is given as a positive or negative value in radians as a function of delay between the two series.

IV.5.4.3. Variance estimation (Figure IV.10)

For variance calculation, we used this following equation:

$$\frac{\sum (x-\bar{x})^2}{n}$$

where x is the average of the data set (in log, thus the geometric mean) and n is the size of the data set. In order to represent the period of low variance (Fig. A6), we choose to apply a 21months running variance to the data set.

IV.5.5. Additional figures:

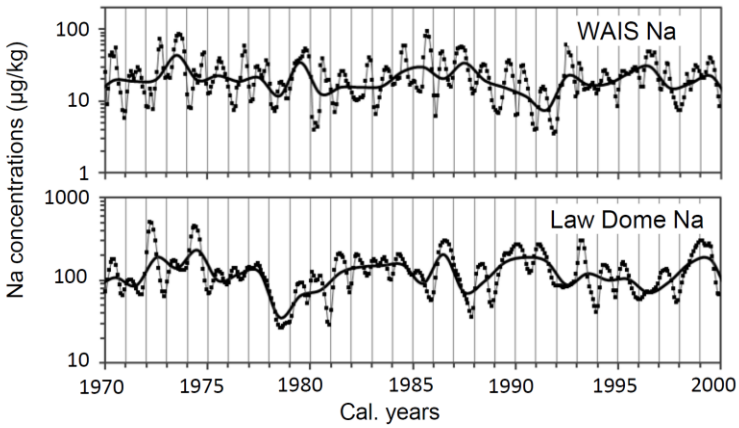

Figure IV.5: 1970-2000 monthly (dots) and annual smoothing (line) for Na at WAIS and Law Dome.

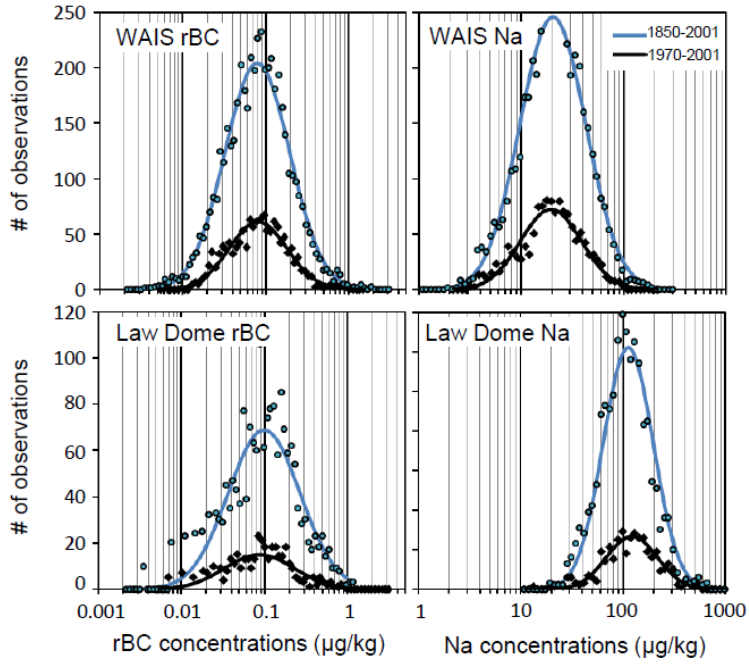

Figure IV.6: Distribution of rBC (left) and Na (right) data points at WAIS (top) and Law Dome (bottom)

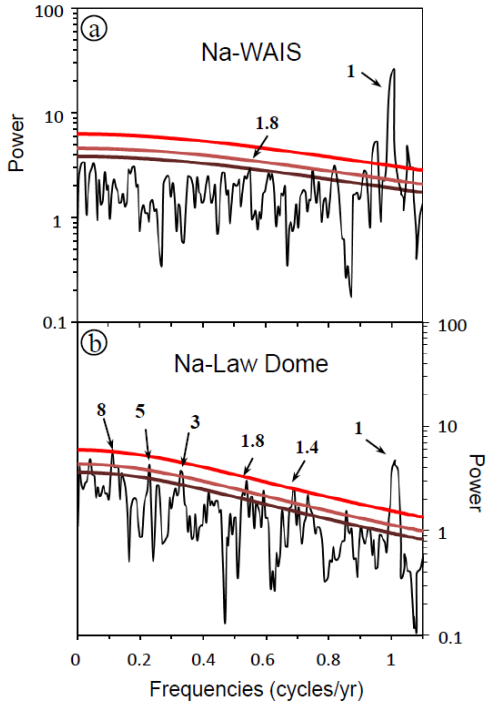

Figure IV.7: Top. Average (thick) and max-min (thin) coherence coefficients for 1970-2001 period between rBC and Na records for WAIS(a) and LD(c). Non zero coherence is > 0.38 and shaded. Time resolution is 0.4yr (Blackman Tukey spectrum using Bartlett window, band

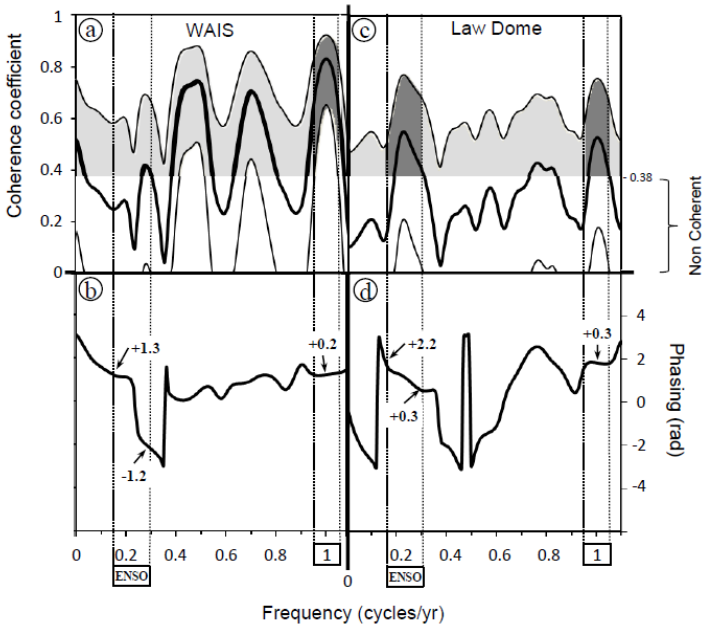

Figure IV.8: Spectrum obtained with Multi Taper Method for WAIS (a) and LD (b) monthly Na records for 1850-2001 period and confidence levels in red lines (90, 95, 99%). Numbers on graph indicate significant periodicities in years.

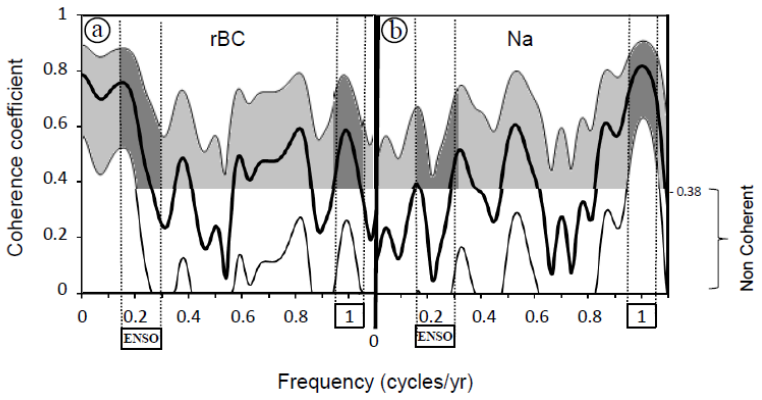

Figure IV.9: Average coherence (thick) and max/min (thin) between LD and WAIS periodicities for rBC (a) and Na (b) for the 1970-2001 period at a 0.4yr time resolution (Blackman Tukey spectrum using a Bartlett window, bandwidth 0.098, non-zero coherence >0.38). ENSO

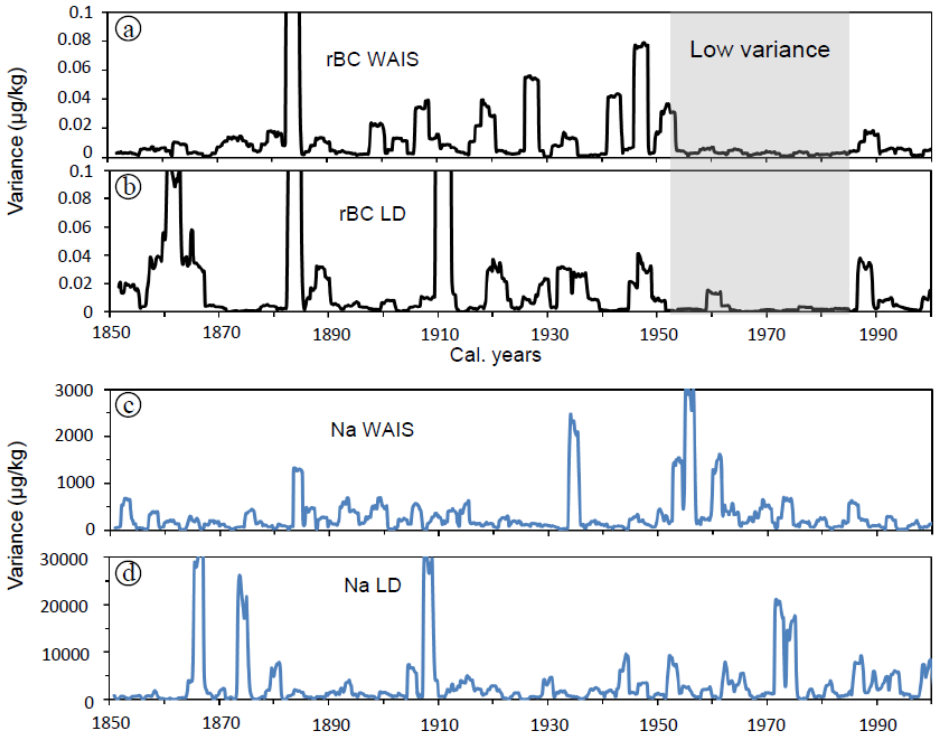

Figure IV.10: Moving variance (on log values) calculated for 21 months, from 1850 to 2000 at WAIS (a, c) and LD (b, d), for rBC (a, b) and Na (c, d). A period of low variance from 1955 to 1985 is common to the two sites, but only in rBC record.

Chapter V. rBC ice core records from the Eastern Antarctic Plateau, cal. yr 1800-2000

V.1. Article: Variation of accumulation rates over the last eight centuries on the East Antarctic Plateau derived from volcanic signals in ice cores

Paper published in the Journal of Geophysical Research in October 2011 and reproduced by permission of the American Geophysical Union.

Authors:

H. Anschütz,[1,6] A. Sinisalo,[2] E. Isaksson,[1] J.R. McConnell,[3] S.-E. Hamran,[2,4] M.M. Bisiaux,[3] D. Pasteris,[3] T.A. Neumann[5] and J.-G. Winther[1]

*Corresponding author:

H. Anschütz (helgard.anschuetz@npolar.no)

[1]Norwegian Polar Institute, Tromsø, Norway

[2]Department of Geosciences, University of Oslo, Norway

[3]Desert Research Institute, Division of Hydrologic Sciences, Reno, NV, USA

[4]Forsvarets Forskningsinstitutt, Lillestrøm, Norway

[5]NASA Goddard Space Flight Center, Greenbelt, MD, USA

[6]now at Norwegian Geotechnical Institute, Oslo, Norway

Credits:

For this journal article, I contributed to data acquisition during ice-core analysis at DRI and I helped reviewing the manuscript.

ABSTRACT

Volcanic signatures in ice-core records provide an excellent means to date the cores and obtain information about accumulation rates. From several ice cores it is thus possible to extract a spatio-temporal accumulation pattern. We show records of electrical conductivity and sulfur from 13 firn core from the Norwegian-USA scientific traverse during the International Polar Year 2007–2009 (IPY) through East Antarctica. Major volcanic eruptions are identified and used to assess century-scale accumulation changes. The largest changes seem to occur in the most recent decades with accumulation over the period 1963–2007/08 being up to 25 % different from the long-term record. There is no clear overall trend, some sites show an increase in accumulation over the period 1963 to present while others show a decrease. Almost all of the sites above 3200m above sea level (asl) suggest a decrease. These sites also show a significantly lower accumulation value than large-scale assessments both for the period 1963 to present and for the long-term mean at the respective drill sites. The spatial accumulation distribution is influenced mainly by elevation and distance to the ocean (continentality), as expected. Ground-penetrating radar data around the drill sites show a spatial variability within 10–20 % over several tens of kilometers, indicating that our drill sites are well representative for the area around them. Our results are important for large-scale assessments of Antarctic mass balance and model validation.

V.1.1. Introduction

The mass balance of the Antarctic ice sheet is a crucial parameter in climate 24 research (Alley et al. 2005; Vaughan 2005) and is constantly under debate (Vaughan et al. 1999; Giovinetto and Zwally 2000; Arthern et al. 2006; van de Berg et al. 2006; Horwath and Dietrich 2009) and a conclusive outcome is not yet reached, despite new and promising results and satellite techniques. For example, Davis et al. (2005) report growth of the Antarctic ice sheet over the time period 1992–2003. Recently, a study by Velicogna (2009) found a net mass loss over the time period 2002–2009 with an accelerating trend, based on data from the Gravity Recovery and

Climate Experiment (GRACE) satellite mission. Yet inter-annual variations are large as are the uncertainties and there is no conclusive trend for individual drainage basins (Horwath and Dietrich 2009). Rignot et al. (2008) use radar interferometry and a climate model to assess recent Antarctic mass changes and obtain also a total mass loss with increases during the most recent decade. In addition to gravity missions, altimetry data give information about mass changes, derived from elevation changes. However, analyses of repeat altimetry measurements and accumulation pattern showed that observed elevation changes are largely determined by accumulation variability (Davis et al. 2005), especially near the coast (Helsen et al. 2008), while little is known about the impact on a continent-wide scale. Especially the East Antarctic interior is to a large degree uncovered by ground-based measurements and in situ data are scarce. Turner et al. (2009) review recent results of Antarctic mass balance and find that East Antarctica seems to be mostly quiescent with local exceptions. The results reported by Turner et al. (2009) range from zero to slightly positive values for the mass balance of East Antarctica, but again the error bars are large and errors can be as high as the variability itself. Moreover, Turner et al. (2009) conclude that studies on Antarctic mass balance employing glaciological field data, e.g. Vaughan et al. (1999), give the most reliable results. Genthon and Krinner (2001) explain that especially the regions devoid of field observations introduce large errors in modeled assessments of a continent-wide accumulation pattern. Thus, it is important to obtain ground-truth for large scale estimates of Antarctic mass changes. The Norwegian-USA scientific IPY 2007–2009 traverse through East Antarctica aims to contribute a set of field data comprising among others firn-core records and ground-penetrating radar (GPR) data and thus help understanding the status of the East Antarctic ice sheet and its changes on scales of a few decades to more than one millennium. The traverse went from Norwegian Troll Station to South Pole in the austral summer 2007/08 and back on a different route via the Recovery Lakes area in 2008/09 (see Figure V.1). We will refer to the route taken in 2007/08 as the first leg and the route from 2008/09 as the second leg in this paper. Together the two consecutive traverse legs covered large parts of the interior of Dronning Maud Land. Along the route shallow (20–30 m) and intermediate-depth (80–

90 m) firn cores were drilled of which we present 13 records in total (9 shallow and 4 intermediate-depth). All the drill sites were linked by GPR data (Müller et al. 2010). Firn and ice cores are a valuable climate archive, allowing scientists to research climate variations as far back as 800000 years (Lambert et al. 2008). For the purpose of determining accumulation rates, mostly chemical species are used, often in conjunction with oxygen isotope data and electrical conductivity. Since all of these records tend to show an annual variation, they allow for identification of summer or winter peaks (depending on the species considered) and hence annual dating. However, in very low accumulation areas like the East Antarctic interior, an annual signal might not be preserved. Hence, identification of time markers is crucial in these areas for accumulation determination. Here, we focus on chemistry data (sulfur and sodium) and electrical conductivity to date the 13 firn cores by identifying known volcanic eruptions. This enables the calculation of accumulation rates and variability for the time periods between major eruptions.

V.1.2. Data and Methods

The firn cores NUS07-3, -4, -6, and -8 (Figure V.1) from the first leg were analyzed in the cold laboratory at Norwegian Polar Institute in Tromsø using the dielectric profiling (DEP) technique (Moore et al. 1991; Wilhelms et al. 1998). From the measured capacitance and conductance we derived dielectric permittivity and electrical conductivity. The records have been presented and discussed in Anschütz et al. (2009) where we also give some more details about the measuring technique. The firn cores NUS07-1, -2, -5 and -7 were analyzed for chemical composition (Figures V.2 and V.3) at the Desert Research Institute (DRI) in Reno, USA, using a sophisticated combination of continuous-flow analysis and mass spectrometry [McConnell et al., 2002]. The record of NUS07-1 has also been shown by Anschütz et al. (2009) where sulfur, sodium and electrolytical conductivity (i.e., the conductivity of the meltwater) are discussed for this core. Note that this core is named “site I” in Anschütz et al. (2009) due to a nomenclature of drill sites used during the expedition. The name has since been changed to “NUS07-1” for the sake of consistency and we therefore also refer to this core as NUS07-1 here. From the second leg the

firn cores NUS08-2, -3, -4, and -6 were analyzed using DEP (Figure V.4) and cores NUS08-4 and -5 for chemistry (Figure V.5).

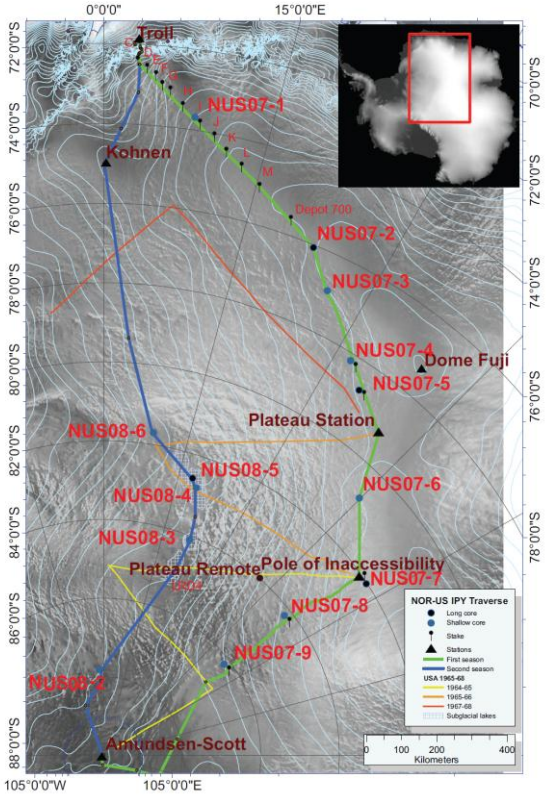

Figure V.1:Map of the traverse route 2007/2008 (green line) and 2008/2009 (blue line) with drill sites from both legs indicated (NUS07-X and NUS08-X). The South Pole Queen Maud Land Traverse routes [Picciotto et al., 1971] are indicate by the yellow-orange lines and relevant stations in the area of investigation are shown as well. Other dots indicate science stops along the traverse routes not relevant for this paper but shown for the sake of completeness. Elevation contour lines are in 100 m intervals. The map was compiled by K. Langley and S. Tronstad (Norwegian Polar Institute).

From the large amount of species measured by the device at DRI we use sulfur and sodium here. The sodium records were used to calculate non-sea-salt (nss) sulfur (see e.g. Traufetter et al. (2004)) which differs less than 10 % from the total sulfur at these inland sites. In the following we will refer to the nss-sulfur data as the “sulfur records” only. The DEP and sulfur records allow for 90 detections of volcanic peaks as shown by several studies on Antarctic and Greenland ices cores (Langway et al. 1995; Hofstede et al. 2004; Traufetter et al. 2004). We follow the criterion outlined by Cole-Dai et al. (1997) and other authors for identification of a volcanic peak: First, the

large peaks likely stemming from volcanic input were removed from the records. Second, the mean (background value) and standard deviation were calculated. For a peak to qualify as a volcanic eruption it has to fulfill two criteria: (1) the value has to be at or above two times the standard deviation and (2) has to stay at that level for at least two consecutive samples, in order to exclude outliers in the measurement. As the electrical conductivity increases with depth, we followed the method outlined by Karlöf et al. (2000) and other authors and normalized the DEP data by first detrending the conductivity records and then dividing by the standard deviation. Again, a peak has to be at or above two times the standard deviation for at least two samples. In order to derive accumulation rates from the dated horizons, information about density is needed. We measured the bulk density in the field and fitted a third order polynomial to these values (Ren et al. 2010) to obtain a smooth density distribution. Often the Looyenga-based density is used for accumulation calculation where DEP data are measured (Hofstede et al. 2004; Anschütz et al. 2009). However, we do not have DEP data available for the chemistry cores, therefore the bulk density was used here. A comparison between Looyenga-based density and bulk density for the DEP cores yields an average difference of 3–4 %, comparable to the values reported by Hofstede et al. (2004). Error estimation follows the discussion by Anschütz et al. (2009) and Müller et al. (2010): We assume an age uncertainty of three years between volcanic horizons (discussed below in more detail) (Hofstede et al. 2004; Traufetter et al. 2004), a depth error of two centimeters and a relative density error of 3.5 % of the respective density values (Hofstede et al. 2004).

From error propagation we derive an overall mean error of the calculated accumulation rates of 4.8 % for the time periods considered here. Errors are given as absolute values for the respective results in Table 3. The relative errors for the period 1815–2007/08 are comparable with results by Frezzotti et al. (Frezzotti et al. 2005; Frezzotti et al. 2007).

A reflection horizon at the corresponding depth of the Tambora layer (1815) was identified in the GPR data based on the dating of the firn cores. In order to evaluate the areal representativity of the firn core data, the layer was followed between two firn cores (Figure V.6). Uncertainties in the

GPR derived layer depth and conversion to accumulation rates originate from uncertainty in firn core dating, lateral density variability between the firn cores, digitization of the GPR data, and accuracy in layer picking. We estimate the combined effect of these error sources to be up to 8 % (Müller et al. 2010).

V.1.3. Results

The records of electrical conductivity and sulfur were used to identify volcanic horizons by comparison with well-dated records (Hofstede et al. 2004; Traufetter et al. 2004). Yet not all peaks could be assigned to known volcanic eruptions. Here, we focus on some prominent peaks, roughly one per century, in order to detect longer-term (century-scale) accumulation changes. The volcanoes and depths of the respective DEP or sulfur peaks in the different cores are given in Tables V-1 and V-2.

volcano	year	NUS07-1	NUS07-2	NUS07-3	NUS07-4	NUS07-5	NUS07-6	NUS07-7	NUS07-8
Agung	1963	6.44	3.49	3.00	2.37	2.72	-	3.39	3.22
Krakatau	1883	14.44	10.48	7.62	6.93	7.66	5.63	9.1	9.22
Tambora	1815	20.70	15.24	10.98	10.33	11.62	8.98	13.42	13.57
Unknown	1695	-	22.96	16.98	16.03	18.12	13.76	20.37	-
Deception Island	1641	-	26.02	20.34	16.92	20.10	17.03	23.21	-
Unknown	1622	-	27.27	22.49	20.39	-	20.32	-	-
Huaynaputina	1600	-	28.96	25.33	-	22.77	-	25.29	-
Kuwae	1453	-	36.19	-	-	29.36	-	32.55	-
El Chichon	1342	-	42.29	-	-	34.72	-	36.39	-
Unknown	1259	-	46.75	-	-	38.44	-	42.01	-

Table V.1: Snow depths of volcanic peaks in the cores from the first leg. All depth units are in meters and the date refers to the year of eruption as this is more certain than the year of deposition (see text).

volcano	year	NUS08-2	NUS08-3	NUS08-4	NUS08-5	NUS08-6
Agung	1963	7.19	5.51	4.92	4.76	7.33
Krakatau	1883	18.10	12.17	11.70	11.39	14.31
Tambora	1815	26.91	17.84	16.83	16.32	18.02
Unknown	1695	-	25.85	25.19	24.25	-
Deception Island	1641	-	29.27	28.43	27.61	-
Unknown	1622	-	-	29.71	28.86	-
Huaynaputina	1600	-	-	-	29.94	-
Kuwae	1453	-	-	-	38.05	-
El Chichon	1342	-	-	-	43.98	-
Unknown	1259	-	-	-	48.40	-

Table V.2: Snow depths of volcanic peaks in the cores from the second leg. All depth units are in meters and the date refers to the year of eruption.

The DEP-signal responds to both enhanced acidity due to large volcanic eruptions and enhanced sea-salt input (Moore et al. 1991). In order to distinguish between conductivity peaks from volcanic events and peaks from enhanced sea-salt content, we also looked at the sodium data for the deep chemistry core NUS07-2 from the first leg and compared sodium peaks with peaks in electrolytical conductivity. A direct comparison between electrical conductivity and sodium is not possible since we do not have DEP data for this core, therefore we use the electrolytical conductivity here.

core name	lat.	long.	elevation m a.s.l.	acc. 1963–2007/08 kg m^{-2} a^{-1}	acc. 1815–2007/08 kg m^{-2} a^{-1}	long-term acc. kg m^{-2} a^{-1}	acc. from *Arthern et al.* [2006] kg m^{-2} a^{-1}
NUS07-1	73°43' S	07°59' E	3174	55.9±3.9	52.0±2.0	-	58
NUS07-2	76°04' S	22°28' E	3582	28.0±2.0	33.0±0.7	33.3±1.2[1]	42
NUS07-3	77°00' S	26°03' E	3589	23.7±1.7	22.0±0.5	27.8±1.0[2]	40
NUS07-4	78°13' S	32°51' E	3595	17.5±1.2	19.0±0.5	20.9±0.8[3]	36
NUS07-5	78°39' S	35°38' E	3619	20.1±1.4	24.0±0.5	26.0±0.9[1]	37
NUS07-6	80°47' S	44°51' E	3672	-	16.0±0.4	21.1±0.7[2]	32
NUS07-7	82°04' S	54°53' E	3725	26.1±1.9	29.4±0.6	29.5±1.0[1]	30
NUS07-8	84°11' S	53°32' E	3452	30.0±2.1	32.0±1.2	-	40
NUS08-2	87°51' S	01°48' W	2583	63.4±4.2	67.4±2.6	-	65
NUS08-3	84°08' S	21°54' E	2625	45.3±3.1	40.1±1.0	38.8±1.4[4]	43
NUS08-4	82°49' S	18°54' E	2552	36.1±2.1	36.7±0.9	37.2±1.3[3]	34
NUS08-5	82°38' S	17°52' E	2544	37.6±2.3	35.0±0.8	35.5±0.8[1]	34
NUS08-6	81°42' S	08°34' E	2447	49.2±3.4	39.2±1.5	-	41

[1] 1259–2007/08

[2] 1600–2007/08

[3] 1622–2007/08

[4] 1641–2007/08

Table V.3: Accumulation over the most recent decades, 200-year mean and long-term mean in the NUS cores, compared with the results by Arthern et al. [2006]. The 200-year values for sites NUS07-1, -3, -4 and -6 have been taken from Anschütz et al. [2009].

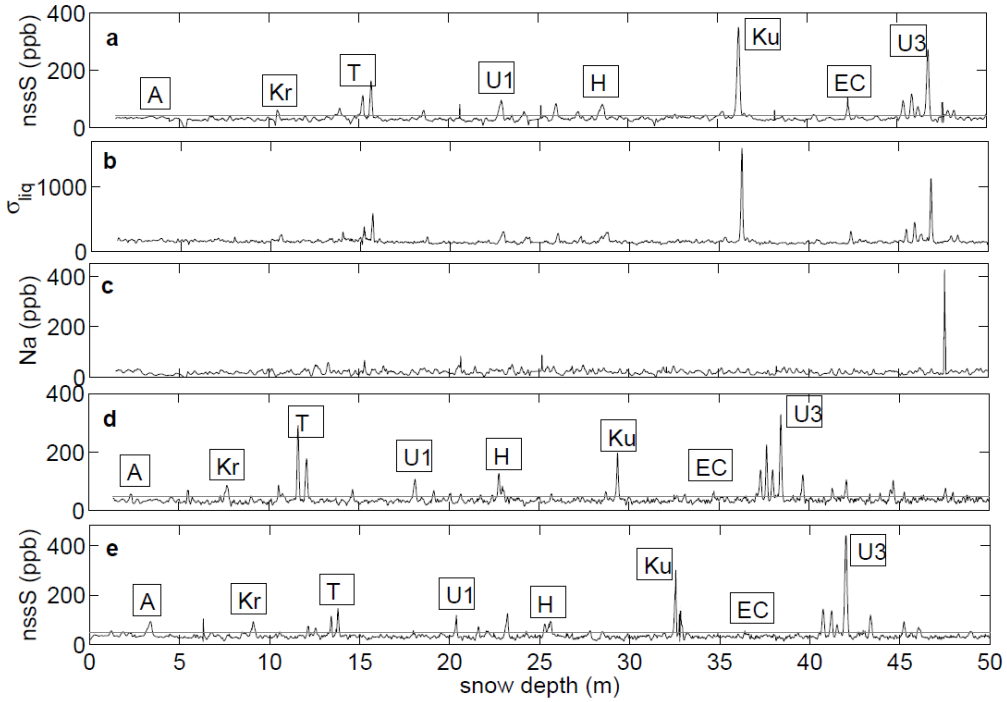

Figure V.2: Records of chemistry data for the cores NUS07-2 (a: nss-sulfur, b: electrolytical conductivity, c: sodium), NUS07-5 (d: nss-sulfur) and NUS07-7 (e: nss-sulfur). The two-fold standard deviation is indicated by the grey line in the sulfur records. A: Agung 1963, Kr: Krakatau 1883, T: Tambora 1815, U1: Unknown 1695, H: Huaynaputina 1600, Ku: Kuwae 1453, EC: El Chichón 1342, U3: Unknown 1259. Note that only the top 50 m are shown here as they fully cover the time period we are concerned with here.

Figure V.2 shows that some peaks in the electrolytical conductivity record indeed seem to coincide with enhanced sodium. However, the peaks discussed here are not linked to enhanced sea salts, at least not for this core. Furthermore, Figure V.2 shows that peaks in sulfur and electrolytical conductivity coincide very well, strengthening also the dating of the DEP records by comparison with the sulfur records. The most prominent peaks served as time markers, like the double peak Tambora (Indonesia) 1815/Unknown 1809 that has been observed widely in Antarctic ice cores (Legrand and Delmas 1987; Langway et al. 1995; Cole-Dai et al. 2000; Karlöf et al. 2000; Hofstede et al. 2004, among others). Thus, we used this double peak as an absolute time marker to date the other peaks in respect to the Tambora peak. Generally, a time lag of about one year between eruption and deposition is assumed by most studies, however, deposition dates are usually less certain than eruption dates, therefore all volcanic dates mentioned in this paper are eruption dates. Traufetter et al. (2004) report an uncertainty in

deposition dates between ±1 year and ±5 years back to AD 1200. As has been already mentioned in the error discussion, we thus assume an average age uncertainty of ±3 years here, in accordance with Anschütz et al. (2009) and Hofstede et al. (2004). One of the more recent peaks that is observed well in Antarctic ice cores corresponds to the eruption of Agung (Lesser Sunda Islands, Indonesia, 1963) (Delmas et al. 1985). Although the signal is not very large in most of our cores, we use this as the most recent time marker. The eruption of Pinatubo (1991), which would provide an even more recent time marker, is not unambigously detected in our firn-core records. Krakatau (Indonesia) erupted in 1883 and has been detected in several ice cores around the continent (Karlöf et al. 2000; Hofstede et al. 2004; Traufetter et al. 2004). The unknown peak from 1695 is reported by several authors, with slightly different dates, varying from 1693–1697 (Cole-Dai et al. 2000; Budner and Cole-Dai 2003). Here we use 1985 as the eruption date in accordance with (Hofstede et al. 2004; Anschütz et al. 2009). The subantarctic volcano of Deception Island erupted in 1641(Aristarain and Delmas 1998; Hofstede et al. 2004; Ren et al. 2010), however, some authors ascribe a signal at that time to the eruption of Awu (Sangihe Islands, Indonesia) (Karlöf et al. 2000; Stenni et al. 2002) or Mount Parker (Philippines) (Cole-Dai et al. 2000; Traufetter et al. 2004). Most likely, the signal is an overlap of several eruptions. Since Deception Island is the closest one to the Antarctic continent, we attribute the 1641 peak to this volcano. Another unknown eruption occurred in 1622 (Hofstede et al. 2004), and in 1600 Huaynaputina (Peru) erupted, being also visible in several ice cores (Cole-Dai et al. 2000; Karlöf et al. 2000; Budner and Cole-Dai 2003). Here, we use the Huaynaputina peak where it is detectable and Deception Island or Unknown 1622 for cores that do not quite reach back to 1600. Before 1600 dating is less certain due to the sparsity of historic documentation of volcanic eruptions (Traufetter et al. 2004). However, some prominent peaks have been dated in deeper ice cores and allow us to assume reliable dating for several of our observed peaks as well. The eruption of Kuwae (Vanuatu, southwest Pacific) in 1453 is easily identified in ice cores from both hemispheres (Langway et al. 1995; Karlöf et al. 2000; Oerter et al. 2000; Ren et al. 2010) and in some studies it provided the largest peak in the entire record (Palmer et al. 2001; Gao et al.

2006). The eruption of El Chichón (Mexico) in 1342 is seen less often than the one of Kuwae, but some authors report prominent peaks for this eruption as well (Cole-Dai et al. 2000; Karlöf et al. 2000; Budner and Cole-Dai 2003; Hofstede et al. 2004). Here, it is 180 not as large as the Kuwae signal, but visible in all of the deeper cores.

The “1200-sequence” of several peaks in the late 13th century is another obvious time marker. This sequence has been detected in deeper cores from the Antarctic plateau (Cole-Dai et al. 2000; Karlöf et al. 2000), as well as some Greenland cores (Langway et al. 1995; Hofstede et al. 2004; Ren et al. 2010). We picked the oldest and - in most cores - the largest one of these four peaks for our discussion. It is believed to have occurred in 1259 where some authors attribute it to El Chichón in Mexico and some prefer to call it an unknown volcano. Since there has not been a conclusive attribution to El Chichón, we stay with the term “Unknown” here.

V.1.4. Discussion

V.1.4.1. Temporal variability

In light of sea-level change it is important to assess the mass budget of the Antarctic ice sheet and determine accumulation rates and possible spatial and temporal changes. Anschütz et al. (Anschütz et al. 2009) discuss temporal accumulation variability for some of the sites from the first leg (NUS07-3, -4, -6 and -8). They find a decreased accumulation averaged over the time period 1815–2007 in relation to the value for 1641–1815. They also give a comprehensive discussion of temporal variability in other cores from East Antarctica. Here, we present new results from the chemistry cores of the first leg (NUS07-2, -5 and -7, Figures V.2 and V.3) and the DEP (Figure V.4) and sulfur records (Figure V.5) of most of the cores from the second leg (NUS08-2, -3, -4, -5 and -6).

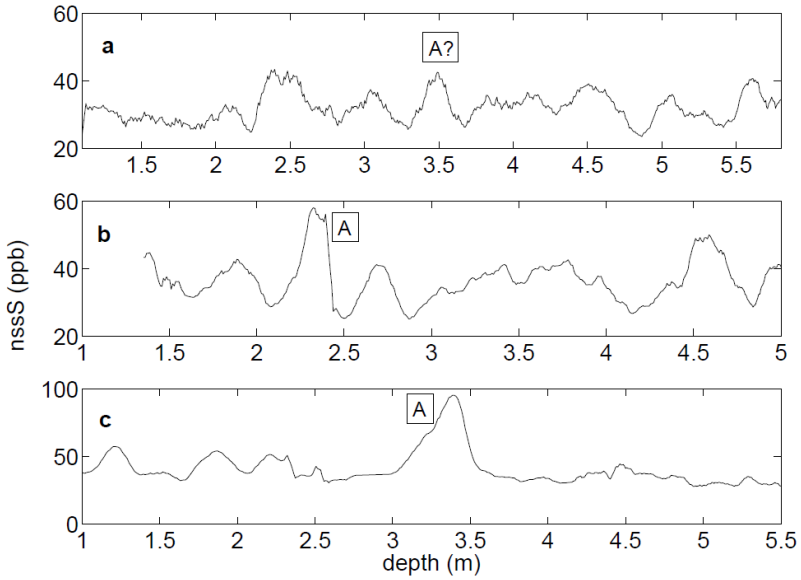

Figure V.3: The Agung eruption in the deep cores from the first leg. a) NUS07-2, b) NUS07-5, c) NUS07-7. Since the peak in NUS07-2 is just at the two-fold standard deviation (see Figure V.2) and also less clear than in the other cores, it is displayed with a question mark here.

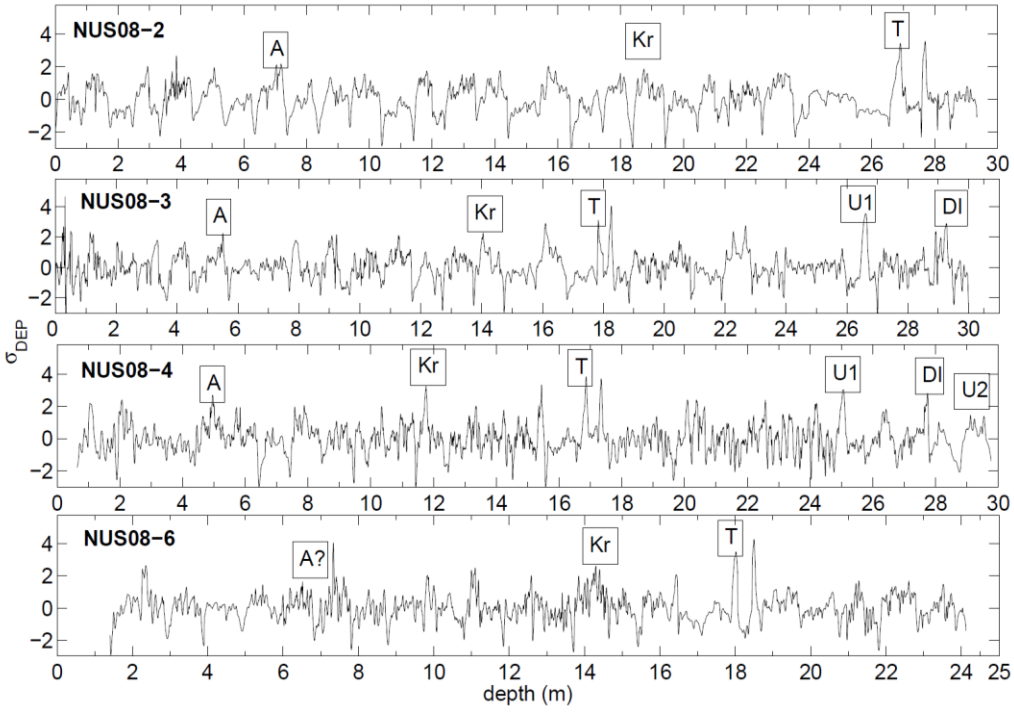

Figure V.4: Normalized DEP-based conductivity for the cores NUS08-2, -3, -4 and -6 from the second leg. The volcanoes discussed in the text are indicated. DI: Deception Island 1641, U2: Unknown 1622; other abbreviations see Figure V.2. The negative spikes in parts of the records are due to varying core quality and slightly differing diameter and are not eliminated here completely as full elimination would induce data gaps.

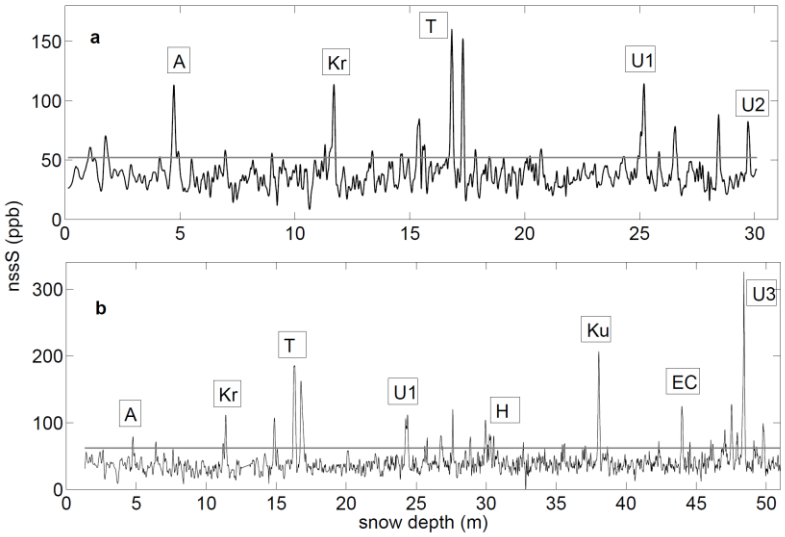

Figure V.5: Sulfur data for the cores NUS08-4 (a) and NUS08-5 (b) from the second leg. The two-fold standard deviation is indicated by the grey line. Same abbreviations as in Figure V.2. Note that only the top 50 m of NUS08-5 are displayed here, covering the period back to about 1250 AD that we are concerned with in this paper.

We identified the eruption of Agung (1963) in all of the cores but NUS07-6 which enables us to address the question of recent accumulation changes. Arguably the Agung eruption is not always very clear in the DEP profiles as they are generally more noisy than the sulfur data. However, intercomparison of the records allows for a reliable identification also in most of the DEP cores. Where identification is somewhat questionable due to noisy 201 data or small peaks, a question marked is depicted in the respective figures. In the chemistry cores from the first leg the Agung peak is much smaller than the very prominent earlier peaks like Tambora and Kuwae. Thus, due to the scaling of the full record the Agung peak does not depict very well and therefore we show in addition a figure of the top meters of these records where Agung is visible (Figure V.3). The accumulation rates averaged over the time periods between the respective volcanic horizons are depicted in Figures V.7 and V.8.

All the data from the first leg exhibit a slight decrease in accumulation since 1963, with the exception of the northernmost site NUS07-1 (Figure V.7). NUS07-3 shows a very slight increase over the period 1963–2007 in comparison with 1883–1963, however, this increase is within the range of uncertainty. For the majority of the sites (NUS07-2, -4, -5, -7 and -8) the accumulation

between 1963–2007 is the lowest in comparison to the other time periods considered in the respective record. NUS07-6 (depicted in Anschütz et al. (2009)) does not show the eruption of Agung due to lower core quality in the top meters, therefore only the period 1883–2007 is considered, which again reveals the lowest accumulation in the entire record from this site (Figure V.7). These results show that virtually all of the highest elevation sites (above 3200 m) reveal a decreasing trend of accumulation over the last decades. This is in accordance with the findings of Isaksson et al. (1999) who report accumulation values from firn cores along a traverse line from the grounded coastal area up to the Amundsenisen plateau in Dronning Maud Land. They find that accumulation has been decreasing over the time period 1965–1996 for sites above 3250 m and mostly increasing below. Hence, they conclude that an accumulation increase as reported for instance by Mosley-Thompson et al. (1999); Hofstede et al. (2004); Oerter et al. (2000) is not necessarily valid for the whole plateau area of Dronning Maud Land.

In the 17th century accumulation at the three sites NUS07-3, -4 and -6 seems to be considerably higher than during the 20th century, whereas sites NUS07-2, -5 and -7 exhibit no such changes (Figure V.7). This shows that temporal accumulation changes are site-dependent and can vary significantly between sites spaced several hundreds of kilometers apart. The largest changes in the long-term records from sites NUS07-2, -5 and -7 occur largely in the most recent decades, as the accumulation rates over the period 1963–2007 are mostly lower than during the other time periods considered here. This contrasts with results from some other studies on the East Antarctic plateau that found a recent increase in accumulation, for instance Mosley-Thompson et al. (1999); Frezzotti et al. (2005); Stenni et al. (2002); Hofstede et al. (2004). However, distances between individual study sites are large and observational time periods between the studies differ, rendering it difficult to compare changes in more detail. The sites from the second leg are all located more westerly and at lower elevations compared to the ones from the first leg and the temporal accumulation pattern is quite different. Sites NUS08-2 and -4 show a decrease and sites NUS08-3, -5 and -6 an increase over 1963–2008. At sites NUS08-3 and -6 the recent accumulation (1963–2008) is in fact the highest in the entire record for the time periods

considered here (Figure V.8). Sites NUS08-4 and -5 are only spaced 55 km apart, yet the temporal accumulation pattern is rather different for the recent decades. NUS08-5 shows a slow, but continuous decrease of accumulation since 1600 with the exception of the most recent period (1963–2008). NUS08-4 shows a similar decrease since 1622, but here the decrease continues also over 1963–2008. The changes between the periods 1883–1963 and 1963–2007/08 vary between +26 % at site NUS08-3 to -22 % at site NUS07-2. When compared with the long-term record for the respective core, the changes range from +17 % to -25 % (Table V.3 and Figures V.7 and V.8). Even though the Agung peak is not as certain in some of our DEP cores as for example 247 the Tambora peak, the overall picture as discussed above remains valid, where accumulation seems to have mostly decreased for the sites of the first leg and mostly increased for the second leg. Ren et al. (2004) report accumulation values from snow pits along a traverse line from Zhongshan Station to Dome A. They find that higher-elevation sites (above 3400 m) show a decrease in accumulation for the recent decades whereas sites below that elevation show an increase. This fits well with our findings from both traverse legs.

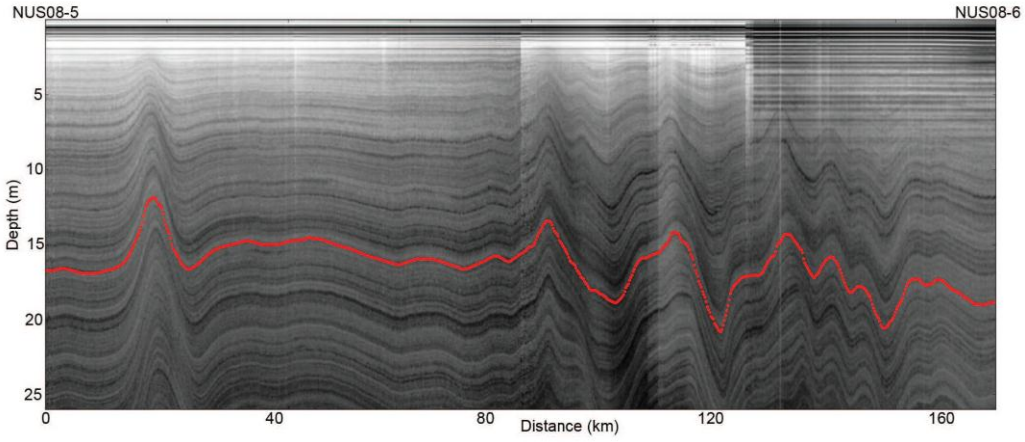

Figure V.6: Radargram of the stretch between NUS08-5 and -6. The Tambora layer is highlighted by the red dashed line.

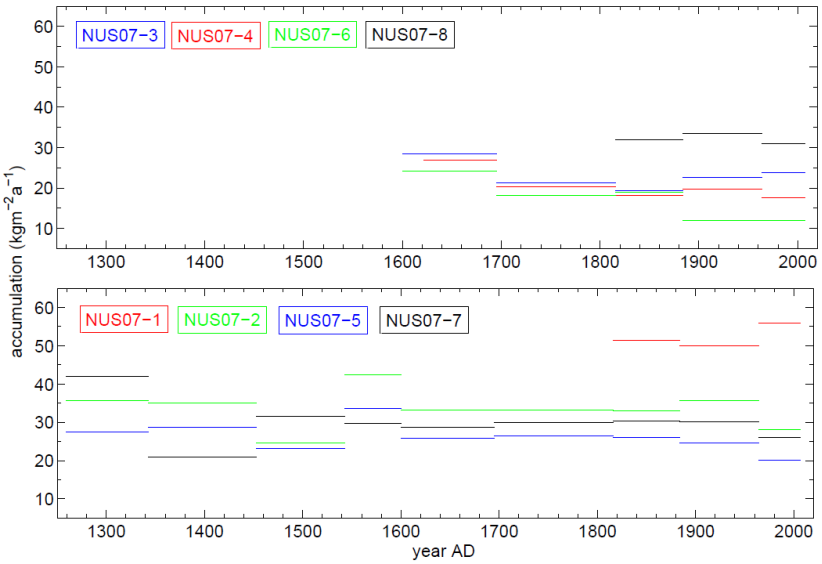

Figure V.7: Temporal variability of accumulation rate in the cores from the first leg. Top: DEP cores; bottom: chemistry cores.

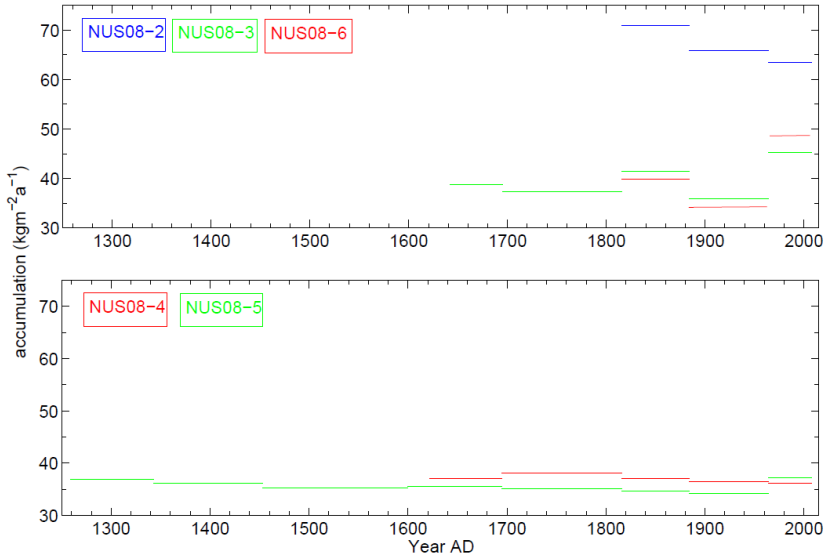

Figure V.8: Temporal variability of accumulation rate in the cores from the second leg. Top: DEP cores; bottom: chemistry cores.

In summary, there is no consistent trend over the area of the two traverse legs and different sites show a different temporal pattern. Yet for some of the sites the most recent changes seem to be the largest. This might implicate that recent changes are in fact occurring over different parts of the East Antarctic plateau, even though the direction of changes (decreasing or increasing) does not exhibit the same trend for all sites. As for the earlier time periods, there is no evidence of the Little Ice Age in our deeper cores: the accumulation averaged over the period 1453–1815, i.e.,

between the eruptions of Kuwae and Tambora, results as 32.6 kg/m^2/a at site NUS07-2, 25.7 kg/m^2/a at site NUS07-5, 29.2 kg/m^2/a at site NUS07-7 and for the second leg 35.5 kg/m^2/a at NUS08-5. All these values differ only insignificantly from the long-term accumulation rates and the values over the period 1815 to present at the respective sites (Table V.3). Li et al. (2009) report sharply reduced accumulation rates for the period 1450–1850 from a drill site to the east of our investigation area in Princess Elizabeth Land (core DT263 at 76°32.5'S, 77°01.5'E and 2800 m asl). A comparison with their results stresses that a different temporal accumulation pattern over different parts of the East Antarctic plateau persisted also for earlier time periods and evidence of the Little Ice Age is not necessarily found in all cores around the continent.

V.1.4.2. Spatial variability

The South-Pole Queen Maud Land Traverses (SPQMLT) went through large parts of Dronning Maud Land in the 1960s (Picciotto et al. 1971) and some of their sampling sites are relatively close to our drill sites (see Figure V.1). They determined accumulation rates from snow-pit stratigraphy and at selected sites additionally from measurements of radioactivity, discovering fallout from nuclear tests in the 1950s and 1960s. Anschütz et al. (2009) compare accumulation values from the first leg with SPQMLT data and find that accumulation in this area is lower than reported by SPQMLT. For sites close to the area visited during the second leg of the traverse, Picciotto et al. (1971) report an accumulation value of 38 kg/m^2/a for their site SPQMLT 2-12 which is 31 km from our site NUS08-5 and 33 km from NUS08-4. The value of 37.6 kg/m^2/a at site NUS08-5 thus is in good agreement, whereas NUS08-4 shows a slightly lower value of 36.1 kg/m^2/a. For their site SPQMLT-2-16, 22 km from our site NUS08-6, Picciotto et al. (1971) obtain 35 kg/m^2/a. Here, our results are higher with 49.2 kg/m^2/a, yet this is one of the sites where a recent accumulation increase occurs. The 200-year mean of 39.2 kg/m^2/a is in better agreement with the results of Picciotto et al. (1971). However, one should bear in mind that comparison is limited due to large spatial distances and different time periods. Moreover, Magand et al. (2007) demonstrate that older data sets, like some of the SPQMLT data, are often biased and tend to

overestimate accumulation on the polar plateau. In general, the spatial representativity of point measurements such as firn-core records can be assessed by GPR data. For the first leg, Anschütz et al. (2009) show 5.3 GHz-GPR data around the sites NUS07-4 and -6 and find a general variability of about 10–20 % over several tens of kilometers for the Tambora layer. Müller et al. (2010) follow GPR layers over an 860 km long profile of the first leg and find a mean accumulation of 23.7 kg/m^2/a over the period 1815–2007 with a standard deviation of 4.7 kg/m^2/a 292 or 20 % over the entire GPR profile. Figure V.6 shows a radargram between NUS08-5 and -6 with the Tambora layer highlighted. The system used is an ultra-wideband FMCW-radar with a center frequency of 1.75 GHz and a bandwidth of 2.5 GHz. System parameters and processing steps are discussed in detail by Müller et al. (Submitted). The layering over some parts of this stretch is very smooth. Yet especially in the northern part (towards NUS08-6) the amplitude of layer variation is larger (Figure V.6). The average accumulation over the time period 1815–2008 over this 170 km long stretch is 36.8 kg/m^2/a with a standard deviation of 3.6 kg/m^2/a or 10 %. This is on the lower edge of the values reported by Anschütz et al. (2009) and Müller et al. (2010) for parts of the first leg. Our results of spatial variability of GPR layers are in good agreement with the findings from Richardson and Holmlund (1997). Even though the core sites are thus representative for the area around them, comparison between individual sites is still limited by large spatial distances and spatial variability between them. However, a general pattern is obvious, as accumulation decreases with increasing elevation and distance to the coast (continentality). This has been reported in various studies (Isaksson et al. 1999; Vaughan et al. 1999; van de Berg et al. 2006; Müller et al. 2010) and is confirmed by our results as well. Table V.3 shows accumulation values for the most recent decades, averaged over the period 1963 to present, based on the detection of the eruption of Agung. For comparison, we also give the 200-year mean values, based on the eruption of Tambora in 1815 and the respective long-term mean for the individual cores. As explained above, the Tambora eruption was used as an absolute time marker, and the 200-year mean should give a sufficiently long time interval to obtain a stable accumulation result where possible decadal variations are smoothed out. Accumulation is mostly

higher for sites on the second leg than on the first. 314 This is clearly related to elevation differences (Table V.3). The accumulation over parts of the Recovery Lakes area (NUS08-4 and -5) is in the range of the higher values of the first leg. In general, accumulation is very low on the high East Antarctic plateau, for parts of the first leg even lower than expected (Anschütz et al. 2009) which fits the results from some other studies as well, e.g. Genthon et al. (2009).

Several large-scale assessments have been carried out in order to derive a spatial pattern of accumulation for the entire Antarctic ice sheet, e.g. by Vaughan et al. (Vaughan et al. 1999); Giovinetto et al. (2000); Arthern et al. (2006); Monaghan et al. (2006); and van de Berg et al. (2006). Even though a detailed comparison is limited due to the resolution of these studies (typically around 50–100 km or more), it is interesting to compare values for the area around our drill sites based on the large-scale assessments. Anschütz et al. (2009) discuss accumulation at sites NUS07-3, -4, -6 and -8 for the period 1815–2007 in comparison to the results by Monaghan et al. (2006) and Arthern et al. (2006). They find lower in-situ values than these two studies. Müller et al. (2010) derive accumulation averaged over the time period 1815–2007 along an 860 km GPR profile for the first leg and likewise find lower values compared to the studies by Monaghan et al. (2006), Arthern et al. (2006) and van de Berg et al. (2006). They conclude that this might support the suggestion that accumulation has been increasing for much of the East Antarctic plateau over the last 50 years, as the studies by Arthern et al. (2006) and Monaghan et al. (2006) represent largely this time period. This finding is not supported by our firn-core data from the first leg, highlighting again the complexity of the temporal accumulation behavior and the difficulties to draw conclusions for a large area from single drill sites.

Furthermore it is important to be aware that the values reported by Anschütz et al. (2009) and Müller et al. (2010) are point measurements and two dimensional profiles, respectively, and are averaged over a 200-year period, whereas the other studies give areal averages and look at more recent time periods of a few decades. In Table 3 we compare our accumulation values over the period 1963 to present with the results by Arthern et al. (2006). It is evident that the drill sites of the first leg show a much lower accumulation (up to 50% lower) compared to the study by

Arthern et al. (2006), whereas the results from the second leg mostly fit well, with deviations between 2–12 %. The differences might be due to scarcity of in-situ observations available for the compilation by Arthern et al. (2006) as well as the reasons mentioned above, namely different time periods and resolution of this large-scale assessment. Monaghan et al. (2006) and van de Berg et al. (2006) both report values of 20–50 kg/m^2/a for our area of investigation with the exception of the area around South Pole where accumulation reaches 50–100 kg/m^2/a in both compilations. Thus, our in-situ values are largely on the lower edge or even below their assessments, especially for the sites of the first leg.

Our results show that some parts of the plateau with elevations above 3200 m exhibit less accumulation than obtained by large-scale assessments which has important implications for the determination of the overall mass balance of the Antarctic ice sheet.

V.1.5. Conclusions

In total 13 shallow and intermediate-depth firn cores from the East Antarctic plateau have been analyzed for electrical conductivity and sulfur to establish a volcanic chronology and assess accumulation rates. The spatial accumulation distribution is influenced by elevation and continentality, fitting the expected pattern well. Spatial variability derived from GPR data is in the range of 10–20 % over several tens of kilometers which is in accordance with other studies from the interior of East Antarctica (Richardson et al. 1997; Frezzotti et al. 2005). The accumulation results for the high elevation sites above 3200 m are lower than values by the large-scale assessment of Arthern et al. (2006), yet the sites at lower elevations are in reasonably good agreement.

The temporal pattern does not show an overall clear trend, however, most of the sites of the first leg, i.e., the more easterly and higher elevation sites, reveal a decrease in accumulation over the period 1963–2007. For the second leg (the more westerly sites at comparatively lower elevations), there are some sites that show an increase over this time period in accordance with other results from East Antarctica (Mosley-Thompson et al. 1999; Hofstede et al. 2004; Frezzotti

et al. 2005). The largest changes seem to have occurred in the most recent decades, with the longer-time pattern being mostly rather stable. Recent changes deviate from the long-term mean of the respective core by up to 25 %. No clear indication of the Little Ice Age could be found in our data.

Our study shows that temporal variability differs strongly between different sites, rendering difficulties to obtain a conclusive outcome for Antarctic mass changes based on individual ice374 core studies. Hence, our results can serve, together with similar studies, as a valuable input for large-scale models and obtaining ground truth for satellite-based estimates of the mass balance of East Antarctica.

ACKNOWLEDGMENTS

This work has been carried out under the umbrella of TASTE-IDEA within the framework of IPY project no. 152 funded by Norwegian Polar Institute, the Research Council of Norway and the National Science Foundation of the USA. This work is also a contribution to ITASE. The help of several people in the lab is gratefully acknowledged. Special thanks to the traverse teams. K. Langley and S. Tronstad (Norwegian Polar Institute) helped with Figure V.1.

V.2. ARTICLE: VARIABILITY OF BLACK CARBON DEPOSITION TO THE EAST ANTARCTIC PLATEAU, A.D. 1800-2000

Article published on November 22nd in Atmospheric Physics and Chemistry-Discussions

Authors:

Marion M. Bisiaux[1]*, Ross Edwards[1,2], Joseph R. McConnell[1], Mary. R. Albert[3], Helgard Anschütz[4,5], Thomas A. Neumann[6], Elisabeth Isaksson[4] and Joyce E. Penner[7]

Corresponding author:

M.M. Bisiaux (marion.bisiaux@dri.edu)

[1] Desert Research Institute, Division of Hydrologic Sciences, Reno, NV, USA

[2] Curtin University, Imaging and Applied Physics, Perth, WA, Australia

[3] Thayer School of Engineering, Dartmouth College, Hanover, NH 03755-8000, USA

[4] Norwegian Polar Institute, Tromsø, Norway

[5] now at Norwegian Geotechnical Institute, Oslo, Norway

[6] NASA Goddard Space Flight Center, Greenbelt, MD, USA

[7] University Michigan, Ann Arbor, MI, United states

Credits:

For this study, I took part in data acquisition and took the lead of data interpretation and manuscript redaction.

ABSTRACT

Refractory black carbon aerosols (rBC) from biomass burning and fossil fuel combustion are deposited to the Antarctic ice sheet and preserve a history of emissions and long-range transport from low latitudes. Antarctic ice core rBC records may thus provide information with respect to past combustion aerosol emissions and atmospheric circulation. Here, we present six East Antarctic ice core records of rBC concentrations and fluxes covering the last two centuries with approximately annual resolution (cal. yr. 1800 to 2000). The ice cores were drilled in disparate regions of the high East Antarctic ice sheet, at different elevations and net snow accumulation rates. Annual rBC concentrations were log-normally distributed and geometric means of annual concentrations ranged from 0.10 to 0.18µg/kg. Average rBC fluxes were determined over the time periods 1800 to 2000 and 1963 to 2000 and ranged from 3.4 to 15.5 µg/kg/m^2/a and 3.6 to 21.8 µg/kg/m^2/a respectively. Geometric-mean concentrations spanning 1800 to 2000 increased linearly with elevation at a rate of 0.025 µg/kg/500m. Spectral analysis of the records revealed significant decadal scale variability, which at several sites was comparable to decadal ENSO variability.

V.2.1. Introduction

Nanoparticles of refractory black carbon (rBC, soot) aerosols are emitted to the atmosphere during fires and fossil fuel combustion and transported over long distances at the hemisphere scale (Seiler and Crutzen 1980; Crutzen and Andreae 1990; Andreae et al. 2005). Because of their low albedo light absorption properties, rBC nanoparticles alter air temperature, snow albedo and impact climate (Jacobson 2001; Ramanathan et al. 2001; Penner et al. 2002; Flanner et al. 2007; Ramanathan and Carmichael 2008; Moosmüller et al. 2009). The prediction of future rBC emissions is therefore a key parameter for global climate modellers (Ramanathan and Carmichael 2008).

However, even if surveys of rBC atmospheric concentrations and fire occurrence are being built for the last few decades thanks to the development of new satellite tools (Ito and Penner 2004;

Chung et al. 2005), the history of rBC fire emissions over last two centuries is incomplete (Mouillot and Field 2005). Indeed, detailed fire history over periods covering the pre-industrial time to the modern era is lacking, notably because common fire proxies such as charcoal deposits or gas emissions reconstructions from ice cores can't reconstruct large spatial variability at inter-annual time scales (Marlon et al. 2008; Wang et al. 2010). Nonetheless, fire regimes are likely to have been modified by anthropogenic activities such as tropical deforestation, land-clearing practices or through natural changes in precipitation and temperature patterns with the changing climate (Nitschke and Innes 2008; Bowman et al. 2009; Dube 2009).

Recently several studies have directly used rBC from ice cores to reconstruct records of past combustion spanning the transition from the preindustrial to the modern era. In the northern hemisphere, ice cores from Greenland and the Himalayas, have shown the impact of coal combustion on rBC snow concentrations (McConnell et al. 2007; McConnell 2010; Kaspari et al. 2011). In the southern hemisphere (SH), two high resolution rBC records from Antarctica have recently been used to investigate the evolution of forest and grass fires (Bisiaux et al. 2011). The records, from the West Antarctic Ice Sheet (WAIS) and Law Dome, spanned the time period 1850-2001 and showed large-scale changes in rBC deposition linked to climatic oscillations such as El Niño Southern Oscillation (ENSO) and the anthropogenic modification of fire regimes.

However, the contribution of each continent to Antarctic rBC deposition remains unknown, as well as the influence of atmospheric transport to sites located in the Atlantic sector of Antarctica. Ice core sites, located at high elevation on the East Antarctic Plateau in East Antarctica may record different variability than the sites previously studied on coastal East Antarctica and the West Antarctic Ice Sheet (Bisiaux et al. 2011). The present study uses rBC paleorecords from the Atlantic sector to investigate spatial and temporal variability of rBC deposition and the link with emissions sources. We use six ice core records from Dronning Maud Land (Figure V.9) and focus on the cal. yr. period 1800-2000, covering preindustrial and modern eras. These sites have low annual snow accumulation rates (20-60 $kg/m^2/yr$) compared to the sites investigated by Bisiaux et al. (2011) (150-200 $kg/m^2/yr$) and have a lower temporal resolution (annual to multi-annual). We

use accumulation calculations from Anschütz et al. (2011) to estimate rBC fluxes at these sites and the importance of precipitation on rBC concentrations. Periodic oscillations in the rBC records are investigated through spectral and multiple regression analysis and compared to Na records (measured simultaneously), to evaluate the influence of transport in the observed rBC variability.

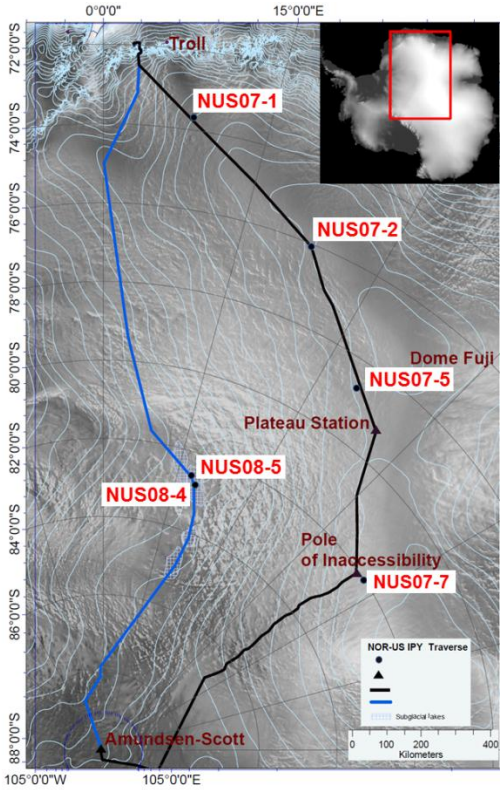

Figure V.9: Map of the traverse route 2007/2008 (black line) and 2008/2009 (blue line) with drill described in this study sites from both legs indicated (NUS07-X and NUS08-X). Relevant stations in the area of investigation are shown as well. Elevation contour lines are in 100 m intervals. The map was compiled by K. Langley and S. Tronstad (Norwegian Polar Institute) and adapted for this study, and adapted from Anschütz et al. (2011) for this study. Complete map can be found in section V.1.

V.2.2. Drilling sites and methods

V.2.2.1. Drilling site locations and characteristics

The sites are all located on the East Antarctic Plateau (elevation>2500m), in Dronning Maud Land (Figure V.9). The cores were drilled during two exploratory traverses by a Norwegian-

American team (NUS) in the summer of 2007 (cores "07-X") and in the summer of 2008 (cores "08-X'). Latitudes, longitudes and elevations are compiled in Table V.4. Cores NUS08-4 and NUS08-5 were drilled in adjacent locations and only ~17 km apart. All cores are firn cores of total length under 90 meters of which we present the top part, down to a depth corresponding to cal. yr. 1800 (Table V.4). However, the top dates are not common to all cores (due largely to fragile near-surface firn sections) and range from cal. yr. 1989 for NUS 07-5 to cal. yr. 2008 for NUS 07-7, Table V.4.

		This study						Bisiaux et al. 2011	
		NUS07-1	NUS07-2	NUS07-5	NUS07-7	NUS08-4	NUS08-5	WAIS (WDC06A)	Law Dome (DSSW19K)
	Lat - long	73°43'S - 07°59'E	76°04'S - 22°28'E	78°39'S - 35°38'E	82°04'S - 54°53'E	82°49'S - 18°54'E	82°38'S - 17°52'E	79°46'S - 112°08'W	66°73'S - 112°83'E
	Elevation (in m ASL)	3174	3582	3619	3725	2552	2544	1766	1390
	Depth of yr 1800 for this study /total core depth	22.2 / 30.5	16.4 / 90.4	12.6 / 89.5	14.6 / 90.6	18.05 / 30	17.5 / 92	-	-
	Period covered	1800-2006	1800-1993	1800-1989	1800-2008	1800-2004	1800-1993	1850-2001	1850-2001
	Number of data points	2154	1501	1111	1308	1672	1616	4860	2883
Annual rBC conc. (geometric mean) in µg/kg…	...since 1800	0.16	0.12	0.14	0.18	0.10	0.11	0.08	0.09
	…range (2σ)[a]	0.09 to 0.26	0.07 to 0.19	0.08 to 0.26	0.12 to 0.27	0.06 to 0.18	0.07 to 0.18	0.05 to 0.12	0.05 to 0.2
	…since 1963	0.14	0.14	0.18	0.19	0.15	0.12	0.08	0.07
	…range (2σ)[a]	0.08 to 0.27	0.08 to 0.24	0.14 to 0.24	0.13 to 0.29	0.08 to 0.26	0.08 to 0.20	0.05 to 0.12	0.04 to 0.15
Annual accumulationb in kg/m2/a…	...since 1815	52.0 ± 2.0	33.0 ± 0.7	24.0 ± 0.5	29.4 ± 0.6	36.7 ± 0.9	35.0 ± 0.8	200 ± 3.4	150 ± 3.1
	…since 1963	55.9 ± 3.9	28.0 ± 2.0	20.1 ± 1.4	26.1 ± 1.9	36.1 ± 2.1	37.6 ± 2.3	-	-
Annual rBC fluxes (geometric mean) in µg/m2/a…	...since 1800c	8.3	3.9	3.4	5.3	3.7	3.9	16	13.5
	…range (2σ)	4.6 to 14.2	2.5 to 6.2	1.8 to 6.3	3.5 to 8.0	2.1 to 6.9	2.2 to 6.5	9.8 to 24.4	7.3 to 30.6
	...since 1963	7.8	3.9	3.62	5	5.4	4.5	-	-
	…range (2σ)	4.0 to 15.8	2.4 to 7.3	2.6 to 5.2	3.1 to 8.0	2.7 to 10.0	2.7 to 8.0	-	-

Table V.4: Sites characteristics for NUS records, rBC concentrations, accumulation and fluxes. a: multiplicative standard deviation; b: from section V.1; c : we assume same accumulation rate for the 1800-1815 periods

V.2.2.2. Ice core analysis

Longitudinal sections of the NUS ice cores were analysed from 2008 to 2010 at the Desert Research Institute on an ice-core melter continuous flow analysis system with in-line rBC measurements. The inner $1cm^2$ of the sections were used for the rBC analysis according to the method previously used in McConnell et al. (2007) and McConnell (2010), and described in detail by Bisiaux et al. (2011). The rBC analysis consisted of an ultrasonic nebulizer/desolvation system (CETAC UT5000) coupled to a Single Particle Soot Photometer (SP2, Droplet Measurement Technologies, Boulder, Colorado). In this system, ice core meltwater was nebulized and de-

solvated to form a dry aerosol. The aerosol then passed into the SP2, where individual particles in the diameter range ~70-400nm were heated up to incandescence by an Nd-YAG laser (1064nm), and the emitted radiation measured by optical detectors (photomultiplier tubes). Individual particle masses were determined using calibration data generated from the introduction of rBC particles of known mass directly into the SP2. Additional calibrations of the SP2 coupled to the ultrasonic nebulizer (USN) were performed daily using rBC colloids. These calibrations were used to account for rBC losses in the USN. Depth resolution of the analytical system was estimated at 1 cm.

V.2.2.3. Ice core dating.

Dating was based on the identification and mapping between ice cores of a number of chemical markers corresponding to explosive volcanic eruptions. Specifically, we used continuous, high-depth-resolution measurements of non-sea-salt sodium (nssS) in the WAIS Divide (WDC06A) ice core to identify layers with significant volcanic sulphur concentrations. The years corresponding to these layers were determined from annual layer counting in the WAIS Divide ice core (Bisiaux et al. 2011). Using similar continuous, high-depth resolution measurements of nssS in the six East Antarctic cores (Table V.4), we mapped the years with significant volcanic sulphur from WAIS Divide to East Antarctica. Although well-known large volcanic events (e.g., Tambora, Krakatoa, Agung) were included in the mapping, we also used much smaller, less known volcanic events to fill in the depth-age relationships were possible. Dating between mapped volcanic horizons assumed uniform accumulation between horizons. Accumulation rate at each site (Table V.4) was based on this depth-age dating and the density profile measured on each core (Anschütz et al. 2011).

The number of rBC data points varied from 6 to 10 per year. However, the dating uncertainty on these data is likely on the order of several years due to the low annual snow accumulation rates and physical processes, such as the redistribution of snow by wind. Overall, the dating uncertainty may be as large as +/-5 years between the dating horizons. Site 07-1 was thought to

have a more robust dating, as it benefits from previously published accumulation rate data (Isaksson et al. 1999). Further refinement of the 08-5 and 08-4 depth-age relationship was performed by independently mapping the 07-1 timescale to the records using rBC trends, determined using single spectrum analysis (Kendall test for trends at 95% significance). The existing dating horizons were maintained, and the trend alignment was performed between them. This refinement resulted in coherent trends between the 08-4 and 08-5 records, which were drilled in the same region (separated by 17km).

V.2.2.4. Data analysis.

Period studied. The study focused on two time periods, including 1800 to 1990-2003 (time period depending on the ice core considered) and 1963 to 1990-2003. These time periods were selected to coincide with the snow accumulation calculations by Anschütz et al. (2011). For the purpose of this study, the snow accumulation rate from the time period 1809 to 1815 was assumed to extend to 1800.

Concentrations. Concentrations of rBC were re-sampled to annual concentrations by a piecewise linear-interpolation (Paillard 1996). Average concentrations presented are geometric means. Standard deviations are multiplicative standard deviations described by (Limpert et al. 2001) and cover 68.3% of the variability, corresponding to: σmin_{conc} = geometric mean*geometric standard deviation; and σmax_{conc} = geometric mean / geometric standard deviation. For 21-yr smoothing, the annual value is smoothed using an R-implementation of Nadaraya-Watson kernel regression. Monotonic trend analysis was performed using the non-parametric Mann-Kendall test (Mann 1945; Önöz and Bayazit 2003). Non-linear trends were calculated with singular spectrum analysis using Kspectra software (Ghil et al. 2002) at a 95% Kendall level of confidence. Z-scores were used to standardize trends (by subtracting mean concentrations and dividing by the standard deviation). Resampling, smoothing, trend and spectral analysis were conducted on the log of measured rBC concentrations, and then back transformed to concentrations.

Fluxes. Flux calculations were based on longer term average accumulation estimates obtained by Anschütz et al. (2011) from a few well known volcanic horizons, and are therefore dependent on the ice core dating. Fluxes are estimated by multiplying annual concentrations and accumulation rates corresponding to the two time-periods chosen. Range of fluxes is estimated as: σminflux = σminconc*{accumulation – σminaccu); and σmaxflux = σmaxconc *(accumulation + σmaxaccu).

Spectral analysis. Spectral analysis was conducted using Analyseries software (Paillard 1996). Significant periodic oscillations in the rBC and Na ice core records and their spectral coherence were investigated using the Blackman Tukey method with a Barlett window. In this study we define coherence as the fraction of common variance between two time series x and y through a linear relation, and considered non-zero when coefficients reach values >0.38 (Paillard 1996). Here we use raw-data re-sampled to a 0.4yr step with piecewise linear interpolation to perform the calculations. Coherence coefficients are given with 3 levels of confidence (low, medium and high), of which we only present the medium level, and only for coefficients >0.38 in Figure V.14. Principal components #1 extracted from records are calculated with an embedding dimension of 20 and theory from Vautard and Ghil (1989).

V.2.3. Results and Discussion

V.2.3.1. Concentrations and fluxes

Concentrations of rBC were found to be log-normally distributed with geometric means of annual concentrations ranging from 0.10 to 0.18µg/kg since 1800 and from 0.12 to 0.19µg/kg since 1963, Table V.4. Overall, the NUS ice core geometric mean rBC concentrations were higher than the concentrations previously determined at lower elevation sites for the same time periods at WAIS (WDC06A) and Law Dome (DSSW19K) (Bisiaux et al. 2011). We attribute this difference to the very low annual snow accumulation rates on the Plateau (Table V.4) and thus to a low rBC dilution by snow, suggesting a significant fraction of dry versus wet deposited rBC. However,

annual rBC fluxes estimates since 1800 are still lower (3.4 to 8.3kg/m^2/a) than those determined for the WDC06A and DSSW19K (Table V.4).

The time series of annual and 21-yr smoothed rBC concentrations at all NUS sites are shown on Figure V.10. Significant monotonic trends, with superimposed decadal variability (from 1800 onwards, Mann-Kendall test double-sided p values <0.0001), were found in annual rBC concentrations at sites 07-5, 08-4 and 08-5. The linear trends at these sites represented an increase of ~0.02 ± 0.01µg/kg/100 years. Comparison of the records at annual resolution revealed no significant cross-correlations, including for sites 08-4 and 08-5, which were within 17km of each other. We conclude that surface processes (accumulation rate variability, sastrugi, blowing snow, and snow sublimation) limit the rBC signal to below noise ratio except on interannual to decadal scale (Pomeroy et al. 1999).

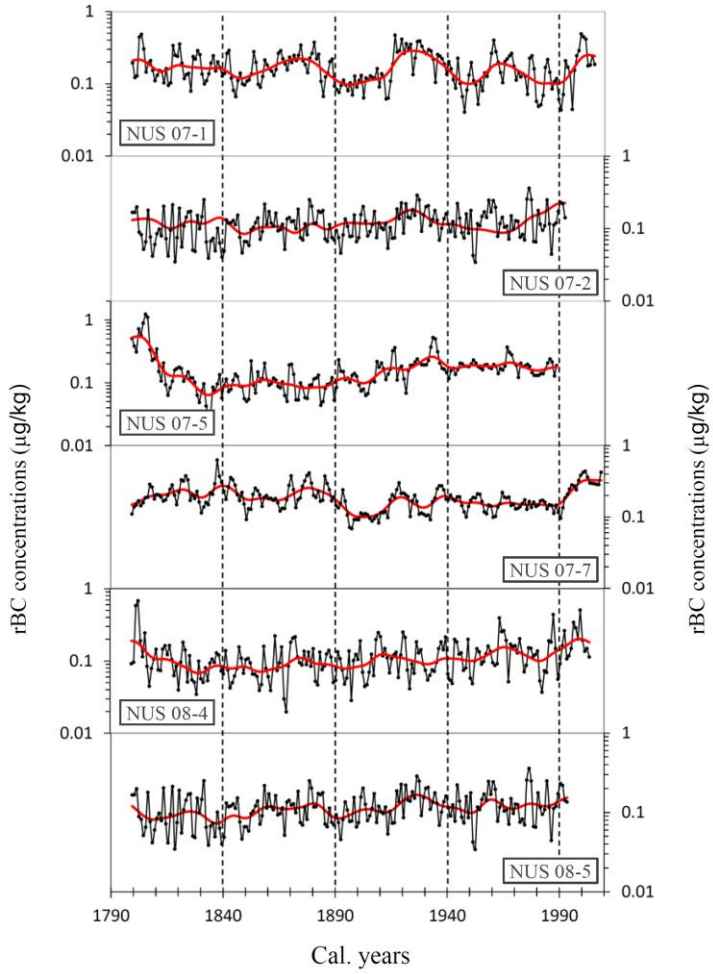

Figure V.10: Time series of rBC concentrations. Black line is annual (piece-wise linear integration interpolation of log raw data) and red line is 21 yr k-smooth on annual (calculated in log space).

Decadal scale variability was investigated using singular spectrum analysis non-linear trend reconstruction (Ghil et al. 2002). Significant non-linear trends ($p<0.05$, Mann-Kendall trend test) are shown in Figure V.11. Non-linear trends from sites 08-4 and 08-5 (which were independently mapped to the 07-1 timescale) were highly correlated ($r= 0.64$, $r2= 0.41$, $n=195$, $p<0.01$). Correlation coefficients for the other records were insignificant, but with some common features. Comparison of these non-linear trends (normalized by Z-scores), cf. Figure V.11, revealed a period of low-concentrations from cal. yr. 1890 to 1920, common to observations made at WAIS and Law Dome (Bisiaux et al. 2011). Here, however, this drop is followed by a period of relatively high concentrations until ~1940 and peaking locally in the 1930s. While this peak was detected in

the high resolution record from Law Dome (Bisiaux et al. 2011), it was absent from the WAIS record. With the exception of site 07-2 (Figure V.11), the NUS rBC records also lacked the period of low variance, from ~1940 to ~1980, found in the WAIS and Law Dome records. Finally, the last 20yrs (1980-2000) show an increasing trend for all cores recording this period, which was also noted by Bisiaux et al. (2011) for WAIS and Law Dome.

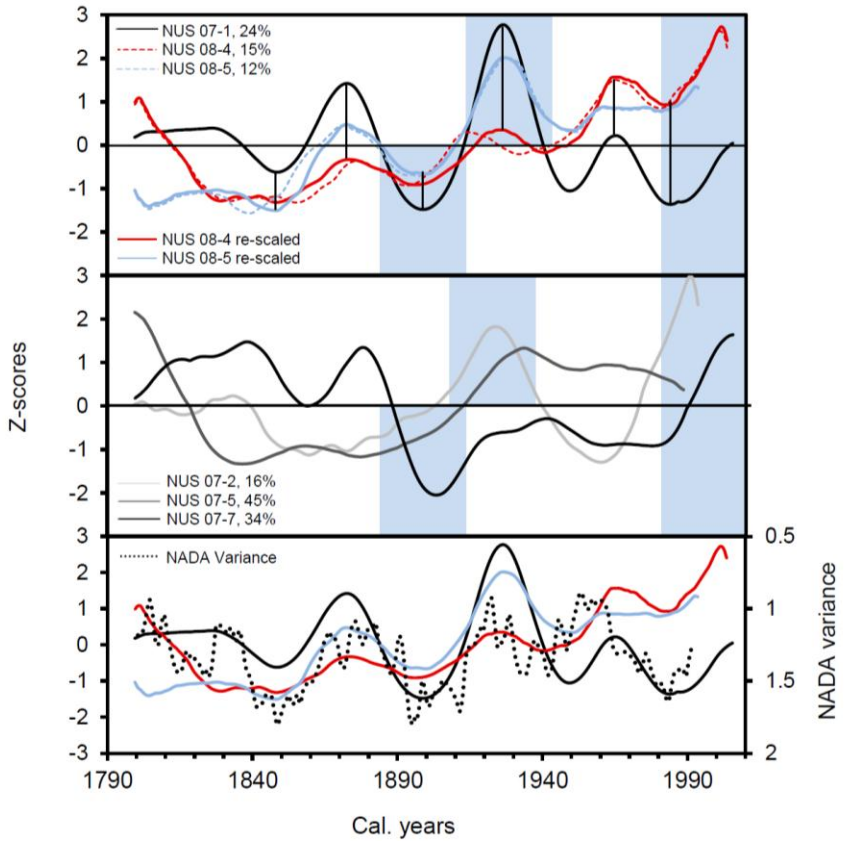

Figure V.11: Z-scores of non-linear trends (Kspectra software, Kendall significance =95%) for the six NUS rBC records, as a function of time. Corresponding fraction of record variability is indicated next to record name (%). Top: comparison of twin sites 08-4 and 08-5, re-scaled from 07-1 dating (plain curve). Original dating is shown as dotted line. Middle: other three records 07-2, 07-5 and 07-7. Shaded areas highlight specifically common features and/or trends. Bottom: comparison of Z-scores from sites 07-1, 08-4, 08-5 with NADA variance (dotted line, scale inverted).

V.2.3.2. Effect of elevation

The geometric average of the annual rBC concentrations at each site was found to increase linearly with elevation. Linear correlation coefficient (r) was 0.81 when concentrations were averaged since 1800 (r^2=0.67, n=8, p=0.01), and 0.92 when concentrations were averaged since

1963 (r^2=0.86, n=8, p<0.01), Figure V.12a. The slope of this linear regression corresponds to an increase of 0.015 and 0.025µg for an elevation gain of 500 m, respectively.

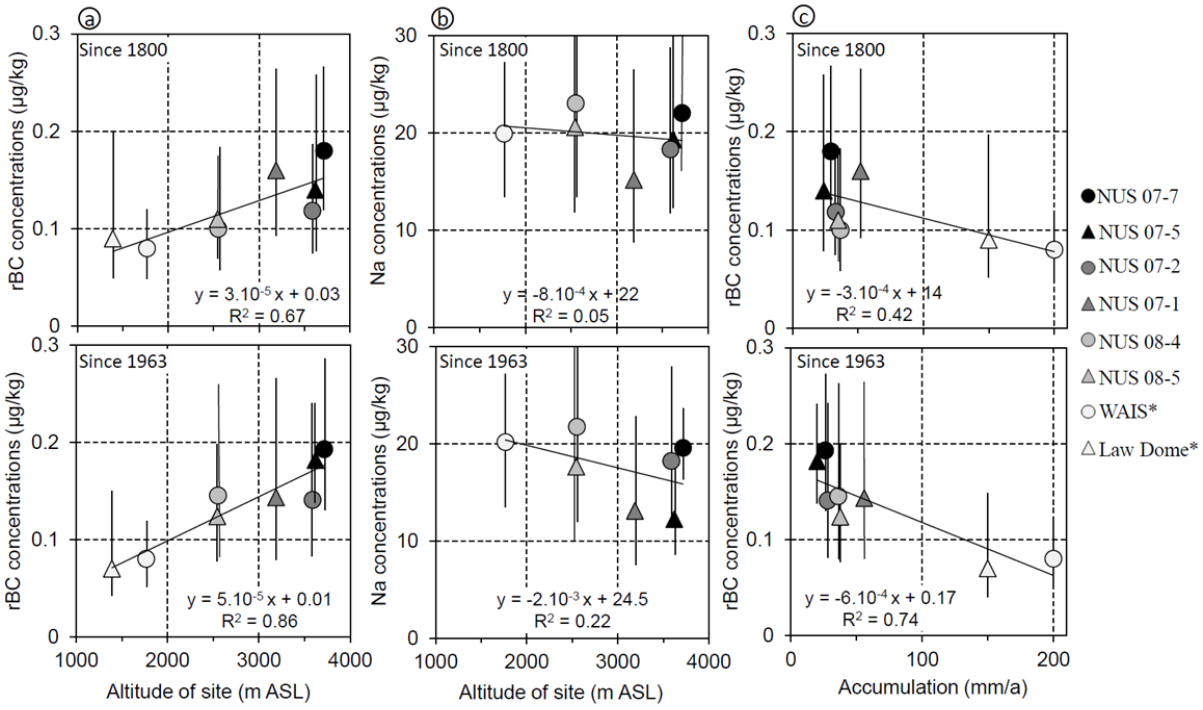

Figure V.12: Geometric mean rBC (a) and Na (b) concentrations ~since cal. yr. 1963 as a function of site altitude. For Na, regression line was calculated without the maritime site "Law Dome". (c) Geometric mean rBC concentrations as a function of accumulation after cal. yr.1963 (Anschütz et al. 2011). Uncertainty bars refer to table V.4. Regression lines and coefficients are based on geometric mean values. R^2 indicates the coefficient of determination. * Indicates values for Law Dome and WAIS from Bisiaux et al. (2011, accepted), Chapter IV.

The increase of rBC with elevation was previously observed in the southern latitude atmospheres by Schwarz et al. (2010) and modelled in for Arctic snow by Skeie et al. (2011). Stohl (2006) also modelled increased atmospheric loading in the southern latitudes and attributed this increase to rBC transport from lower latitudes towards the ice cap, along isentropic trajectories that may not reach the surface of the region lower than the Plateau and remain at higher elevation.

To investigate whether rBC transport to the Plateau is modulated by the intrusion of marine air masses, the variability of Na concentrations (geometric means) with elevation was also investigated. In this case, no significant relationship was found (r^2 = 0.05, n=7, p>0.05), confirming observations previously made by Bertler et al (2005) showing no relationship between elevation and Na concentrations for altitudes above 2000m, Figure V.12b. We hypothesize that

these absence of correlation with elevation for Na and presence of correlation for rBC are due both to a difference in the sources of Na and rBC aerosols and to a difference in atmospheric transport. Indeed, the main sources of Na are marine aerosols, which are transported to the East Antarctic Plateau by low pressure systems (Sneed et al. 2011). Transport processes associated with rBC, must therefore occur at a different altitude than that for Na transport. This suggests that rBC inputs to the atmosphere of the East Antarctic Plateau are not controlled by the intrusion of marine air masses and implies that transport in the upper troposphere may be important. Vertical profiles of rBC in the near-Antarctic atmosphere reported by Schwarz et al. (2010) found that rBC increased with altitude. Here, wet removal processes limit the lifetime of rBC near the boundary layer, while dry air in the upper atmosphere increases the rBC residence time.

Annual water accumulation, on the contrary, does show a significant inverse trend with rBC concentrations, but only from 1963 onwards (r^2= 0.72, r=0.85, n=8, p<0.01). However, this correlation is determined mainly by the WAIS and Law Dome data points, with NUS sites clustering around the same values (Figure V.12c). Uncertainties inherent in the net snow accumulation rate must also be considered. Acknowledging these caveats, the slope of the linear regression of 0.030µg in rBC for a 50mm decrease in accumulation can be compared with the increase of 0.025µg rBC estimated for every 500m in elevation, for the time period from 1800 to the present (Figure V.12a, top). For the two time periods shown in Figure V.12, the change in elevation explains ~80% of the difference in rBC geometric mean concentrations. Therefore, we suggest that the main process controlling the spatial differences in geometric rBC snow concentrations between the sites of the Antarctic Plateau, is the decrease in accumulation and corresponding increase in rBC dry deposition inducing less dilution of the particles. This relationship does not explain the monotonic trends found for some of the records (07-2, 08-4, 08-5), which do not exhibit a similar decrease in accumulation rate (Isaksson et al. 1999; Anschütz et al. 2011) from 1800 to 1963 (cf. Table V.4 for site elevation).

V.2.3.3. Influence of transport

For the sites 07-1, 08-4 and 08-5, cross-correlations of the annual rBC and Na suggest common high frequency variability between the rBC and Na species at each site without leads or lags (Figure V.13). This data suggest a transport component linked to some of the high frequency variability. Non-linear low frequency trends similar to those found in the rBC records (Figure V.13) were not found in the Na records. According to Sodemann and Stohl (2009), precipitation in this high-altitude region of the Eastern Antarctic originates from sources located much further north than for the coastal regions. The lack of a correlation between the annual rBC data at the remaining sites and the non-linear trends at 08-4, 08-5 and 07-1 suggests that the low frequency rBC variability may be linked to emission variability, or to upper level transport variability.

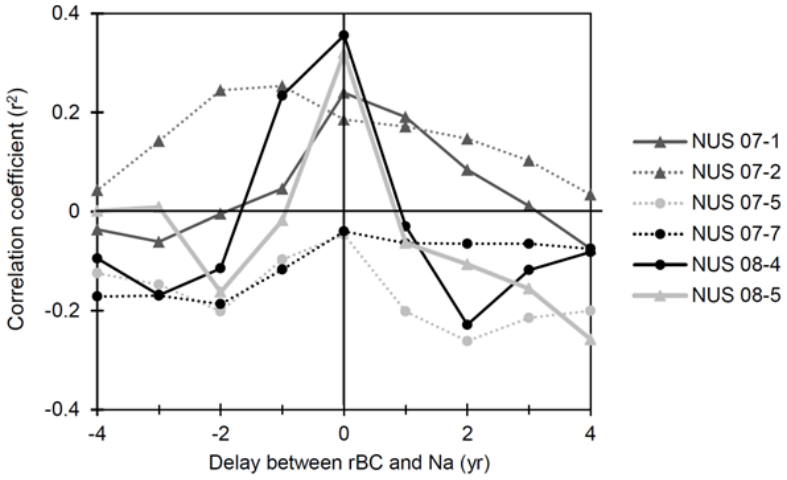

Figure V.13: Cross correlation coefficients between Na and rBC from the same record. Na leads rBC for delays >0 and rBC leads Na and for delay <0.

To test this hypothesis, the spectral coherence for Na and rBC was investigated (Figure V.14). This analysis determined the coherence between periodic signals in the rBC and Na time series. A high coefficient for a given frequency suggests that the two periodic signals have coherent variability. Sites 08-4 and 08-5 exhibit coherence coefficients higher than 0.38 (black line), for a large portion of the bandwidth. Notable exceptions are the El Niño Southern Oscillation (ENSO) from ~4 to 7 years and at lower decadal frequencies. For sites 07-2 and 07-7, coherence is much lower and often <0.38, confirming observations made on cross-correlations between Na and rBC

(Figure V.13). Coherence between Na and rBC for sites 07-1 and 07-5, were similar to 08-4 and 08-5 with less coherence at low frequencies (<0.2 cycles per year).

The spectral power of rBC time-series is shown as a red line in Figure V.14. Peaks of high power designate frequencies explaining some variability of the signal. If those power peaks do not correspond to a peak in coherence between Na and rBC (black line), they indicate an oscillation that is not likely linked to a common transport effect (NT). A periodicity of ~4.5 to 7 years (~0.17 to 0.2) is found common to sites 07-2, 07-5, 07-7, 08-4 and 08-5. This period window suggests the influence of the El Niño Southern Oscillation (ENSO). However, even if an ENSO "signature" is present, the direct comparison of rBC with ENSO index is not significant, and may be explained by two reasons. First, the records do not have the temporal resolution to adequately resolve the signal from noise. Second, ENSO has by nature, a dual effect on fire potential, by inducing drought on one side of the Pacific and floods on the other side, rendering a potential ENSO-fire signal very disparate (Krawchuk and Moritz 2011).

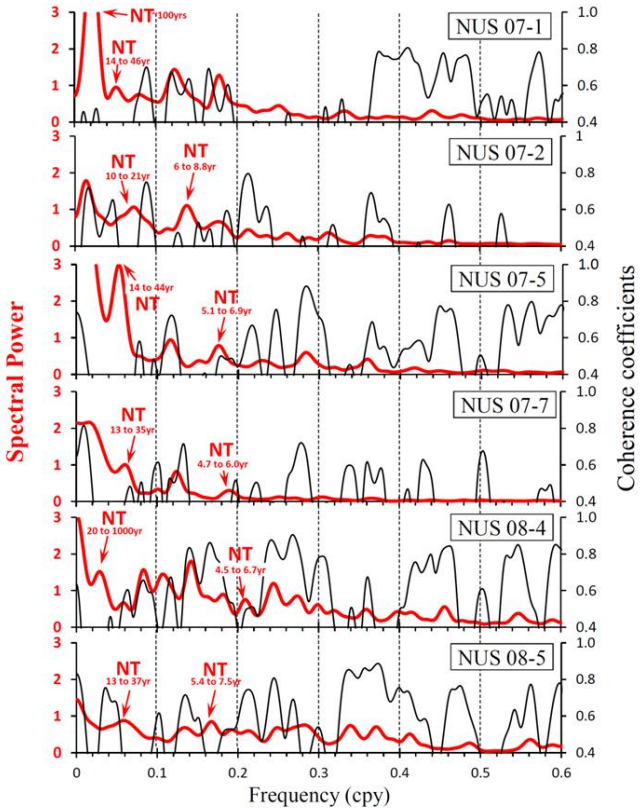

Figure V.14: Spectral power (red) of rBC NUS records and coherence coefficients (black) between rBC and Na investigated for the whole period (since 1800). Non-zero coherence is above 0.38. Letters "NT" stand for "Non Transport" and indicates periodic signal in the rBC record that is not coherent to Na (no black peak) and that is likely related to rBC emissions rather than regional to long-range atmospheric transport. The red numbers below "NT" show the corresponding periodicity (in years).

However, a NT periodic oscillation of ~15 to 40 years (0.05+/- 0.024 cycles per year) is found in records 07-1, 07-2, 07-5, 07-7 and 08-4, in Figure V.14. This long-term periodicity in rBC, which is not related to Na, suggests a link to upper level atmospheric transport, emission variability or both that may be linked to ENSO. Indeed, this periodicity is found to correspond to an ENSO reconstruction derived from the North American Drought Atlas (NADA) (Li et al. 2011), which is anti-correlated to the large-scale rBC variability observed in Figure V.11, bottom (scale inverted). Here, higher rBC concentrations are associated with low variance periods (La Niña, colder) and lower concentrations during high variance periods (El Niño, warmer). This suggests that increased rBC emissions from fire drive higher rBC loading of the Antarctic atmosphere during decadal time periods dominated by La Niña.

V.2.4. Conclusions

Concentrations of rBC found in the NUS ice cores reveal both spatial and temporal variability during the 1800-2000 time period. Spatial variability was primarily associated with changes in elevation and is likely linked to increase atmospheric loading in rBC and/or decrease accumulation with altitude. Relatively stable net snow accumulations rates at the NUS sites (Anschütz et al. 2011), suggest that decadal variability is related to changes in the rBC aerosol in the overlying air. On the other hand, the absence of strong correlations between the records indicates that local atmospheric transport and surface processes may be highly influencing rBC concentrations. This is confirmed by high correlation and coherence coefficients between Na and rBC for some of the sites. This observation is different from the results obtained at WAIS and Law Dome by Bisiaux at al. (2011). Indeed, at those low elevation sites, it was shown that most of the recorded rBC variability was independent from local atmospheric transport over the Pacific and Indian sectors and meteorology. On the Antarctic Plateau, rBC may on the contrary be linked to

Atlantic-sector cyclonic activity. However, spectral analysis revealed the existence of non-transport oscillatory signals common to almost all the records. Common features in the records' non-linear trends, showing relatively low concentrations from 1890 to 1910, high concentrations until 1930 and an increasing trend at the end of the 21st century, confirm the presence of a variability linked to rBC sources only. Nevertheless, while large-scale changes in rBC deposition at WAIS and Law Dome was found to correspond to a change in anthropogenic activities, measurements from the East Antarctic Plateau suggest a link with ENSO-long term emissions. In any case, global climate and aerosols models may enlighten the variability of rBC deposition to Antarctica, and the apportionment between the various continental sources.

ACKNOWLEDGMENTS

This research is based upon work supported by the National Science Foundation under Grant No.'s 0538185, 0538416, 0538595 and has been carried out under the umbrella of TASTE-IDEA within the framework of IPY project no. 152 jointly funded by the U.S. National Science Foundation, the Norwegian Polar Institute, and the Research Council of Norway. The project is part of the Trans-Antarctic Scientific Traverse Expeditions – Ice Divide of East Antarctica (TASTE-IDEA), and the International Partners in Ice Coring Sciences (IPICS) under the ISCU-WMO endorsement for the International Polar Year 2007-08 and 2008-09. We gratefully acknowledge the NUS traverse field teams, the National Science Foundation, the Norwegian Polar Institute, the DRI ice core analysis team. Logistic support in Antarctica was provided by Raytheon Polar Services in Antarctica; and the 109th New York Air National Guard. The National Ice Core Laboratory, which archived the ice cores and preformed core processing, is funded by the National Science Foundation.

Chapter VI. rBC sources to oligotrophic lakes and transfer processes to sediments

The recent development of the SP2-FIA method for ice cores samples finds another application in the measurements of very clear water samples from oligotrophic lakes. Indeed, those low-concentrated waters have not yet been widely studied for rBC due to the difficulties to measure very low rBC concentrations. Sources and fate of rBC in freshwater environments is thus, not well understood. In this chapter, we present a comprehensive study of rBC occurrence and sources to oligotrophic lakes with the SP2-FIA method to: i) assess local rBC sources in Lake Tahoe basin, ii) spatially compare rBC concentrations with four US oligotrophic lakes, and iii) investigate the transfer processes from sources to sediments.

VI.1. CONTEXT OF STUDY

Lake Tahoe is a large ultra-oligotrophic lake in the Central Sierra Nevada and lies at an elevation of ~1900 m. The volume of the lake is 156 km^3, and its surface area is 501 km^2, 38% of the total basin area of 1,313 km^2 (including the lake surface area). Mean annual precipitation ranges from over 140 cm/yr in watersheds on the west side of the basin to about 67 cm/yr near the lake on the east side of the basin (Daly et al. 1994). Most of the precipitation falls as snow between November and April, although rainstorms combined with rapid snowmelt account for the highest flows and occasional floods (Coats et al. 2008). There is a pronounced annual snowmelt runoff in late spring and early summer, with a timing varying from year to year and with locations in the basin (Coats et al. 2008).

We used the Lake Tahoe hydrologic basin as a large scale outdoor laboratory that represents a relatively pristine ecosystem, subject to both natural and anthropogenic activities in the watershed

and airshed that are responsible for the lake undergoing loss of clarity (Jassby et al. 1999). This study focused on rBC concentrations in water discharging into the Lake, including road runoff, residential runoffs and streams. Those values were compared with middle lake concentrations, close-to-shore concentrations and dry-deposition to the lake. The temporal variability of rBC concentrations in the middle lake was compared to the occurrence of a forest wildfire, to the type and length of precipitation events, and to urban and basin-snow melt.

VI.2. ARTICLE: STORMWATER AND FIRE AS SOURCES OF BLACK CARBON NANOPARTICLES TO LAKE TAHOE

Journal Article published on February 24, 2011 in Environmental Science and Technology and reproduced by permission of ACS Publications

Reference: (Bisiaux et al. 2011)

Authors:

Marion M. Bisiaux*[†], Ross Edwards[‡†], Alan C. Heyvaert[†], James M. Thomas[†], Brian Fitzgerald[†], Richard B. Susfalk[†], S. Geoffrey Schladow[§] and Melissa Thaw[†]

*Corresponding author:

M.M. Bisiaux (marion.bisiaux@dri.edu);

†Division of Hydrologic Sciences, Desert Research Institute, Reno, NV, 89512, USA.

‡Dept of Imaging & Applied Physics, Curtin University of Technology Bentley, Perth, Western Australia 6102.

§ Tahoe Environmental Research Center, University of California, Davis, 1 Shields Avenue, Davis, CA, 95616 USA.

Credits:

For this article, I conducted all data analysis with the help of Melissa Thaw and took the lead of data interpretation and manuscript redaction.

ABSTRACT

Emitted to the atmosphere through fire and fossil fuel combustion, refractory black carbon nanoparticles (rBC) impact human health, climate and the carbon cycle. Eventually these particles enter aquatic environments, where they may affect the fate of other pollutants. While ubiquitous, the particles are still poorly characterized in freshwater systems. Here we present the results of a study determining rBC in waters of the Lake Tahoe watershed in the western United States from 2007 to 2009. The study period spanned a large fire within the Tahoe basin, seasonal snow-melt and a number of storm events, which resulted in pulses of urban runoff into the lake with rBC concentrations up to four orders of magnitude higher than mid-lake concentrations. The results show that rBC pulses from both the fire and urban runoff were rapidly attenuated suggesting unexpected aggregation or degradation of the particles. We find that those processes prevent rBC concentrations from building up in the clear and oligotrophic Lake Tahoe. This rapid removal of rBC soon after entry into the lake has implications for the transport of rBC in the global aquatic environment and the flux of rBC from continents to the global ocean.

VI.2.1. Introduction

Black carbon is a component of the freshwater environment that has been poorly characterized (Masiello and Druffel 1998; Simpson and Hatcher 2004; Shrestha et al. 2010). Produced from the incomplete combustion of vegetation (fires), fossil fuels and petrogenic processes (mineral, graphite), black carbon comprises a spectrum of related materials ranging from charred vegetation to refractory graphitic nanoparticles (Masiello 2004). These materials are present throughout the Earth system, impacting climate (Jacobson 2001; Ramanathan et al. 2001; Ramanathan and Carmichael 2008), the carbon cycle (Kuhlbusch 1998; Masiello and Druffel 1998; Mitra et al. 2002; Forbes et al. 2006) and human health (Schneider et al. 2008; Suglia et al. 2008). Notably, several studies have shown that black carbon is a significant component (up to 20%) of sedimentary organic carbon in the remote ocean (Dickens et al. 2004) and could represent a significant carbon sink (Masiello and Druffel 1998). While particulate black carbon

(diameter >0.45 μm) have been determined in soils (Lehmann et al. 2008; Lohmann et al. 2009) and sediments (Masiello and Druffel 1998; Lohmann et al. 2009), the low concentrations of black carbon suspended in fresh water bodies and in the oceans have proven more difficult to analyze (Kim et al. 2004; Hockaday et al. 2007; Dittmar 2008). The abundance and sources of black carbon in freshwater and the fraction exported to the ocean are thus almost unknown, as well as its effect on aquatic chemistry (Mitra et al. 2002; Forbes et al. 2006).

In this paper, we focus our interest only on refractory black carbon nanoparticles (rBC) of diameters comprised between 60 and 400nm. Those particles can be produced from the fragmentation of charcoal or from the gas-phase condensation and subsequent carbonization of pyrolysis emissions (Moosmüller et al. 2009 and references therein). In this last case, rBC typically consists of fractal aggregate chains of spherules with diameters of ~ 30 to 40 nm (Zhang et al. 2008; Posfai and Buseck 2010) capable of long-range transport in the atmosphere and thus available as tracers for smoke emissions (McConnell et al. 2007). In both cases, the particles are very refractory (i.e., vaporizing only at very high temperature), have very large surface areas and are potent adsorbers of polycyclic aromatic hydrocarbons (PAHs) and persistent organic pollutants (POPs) (Gustafsson et al. 1997; Buckley et al. 2004; Moermond et al. 2005; Burkhard et al. 2008; Nguyen et al. 2010). Initially hydrophobic, partial surface oxidation or coating of the particles with organic species (Moosmüller et al. 2009) allow it to disperse in water forming hydrosols small enough to be ingested by biota.

The objective of this study was to gain a basic knowledge of rBC hydrosols in freshwater by investigating the concentrations, variability and likely sources of rBC in an oligotrophic lake. The study was performed in Lake Tahoe and its watershed (NV-CA, United States), famous for its water clarity and relatively pristine setting in the Sierra Nevada Mountains. However, small urban centers and roads encircle the lake, leading to inputs of urban runoff. Concentrations of rBC in urban runoff, streams, the lake's near-shore zone and mid-lake water column were examined between January 2007 and September 2009. This time period included a major fire (Angora fire), which occurred from June 26th to July 2nd, near the southwestern end of the lake. The fire allowed

the examination of an increase of rBC aerosols on the lake and its mobilization from the fire site to a nearby stream.

VI.2.2. Materials and Methods

VI.2.2.1. Water sample collection

Mid-lake. Water column samples were collected by the University of California-Davis as part of their mid-Lake Tahoe profile (MLTP) station time series. Each profile consisted of approximately 12 samples taken at lake depths ranging from 0 to 450 m, with a sample collection occurring almost every month from January 2007 through January 2009.

Urban runoff. Automated samplers collected untreated water discharging into Lake Tahoe from urban areas as part of a previously established regional stormwater monitoring program (Desert Research Institute and the University of California-Davis Tahoe Environmental Research Center (Coats et al. 2008)). Four storm events were sampled from October 2007 to January 2009 at stations located in Tahoe City, Kings Beach, Incline Village and South of Tahoe Airport. To study rBC in the fire affected Angora watershed, samples were collected from the upper Angora Creek (Figure VI.1A) during July 2007 and January 2009. This watershed suffered a large forest fire in summer 2007 from June 26th to July 2nd which destroyed more than 1200 hectares of forest and over 240 homes.

Free runoff. Water from free runoff (not from culverts) was also sampled (grab samples) from random locations at five sites in South Lake Tahoe during the spring of 2009 on four different days corresponding to four different weather conditions. Two of these sites were located 25 m from Highway 50 between the road and the beach (South Beach sites). The Bijou and Regan sites were also on the south shore but farther away (~350m) from Highway 50. The last site collected stormwater runoff released into the Upper Truckee River from nearby Highway 50 and 3 km upstream from where the stream discharges into Lake Tahoe (Figure VI.1C).

Near Shore Zone. Spatial and temporal variability of the rBC concentrations in the near shore zone (NSZ) of South Lake Tahoe was investigated. NSZ was defined as the water band starting at 1 m from the beach-water interface and extending into the lake up to 100 m or until the water depth reached 7.5 m. Lake water was sampled at four sites along the South Lake Tahoe shore (Figure VI.1C) with a centrifuge tube hand-dipped into lake water from a canoe. NSZ sample sites from west to east are: *Upper Truckee discharge, Regan, South Beach* and *Bijou,* corresponding to the "off shore" locations of onshore stormwater monitoring sites (Figure VI.1C). At the NSZ sites, samples were collected during three storm events and one clear day of spring 2009 and at distances of about 1, 10, 50 and 100 m from the shore.

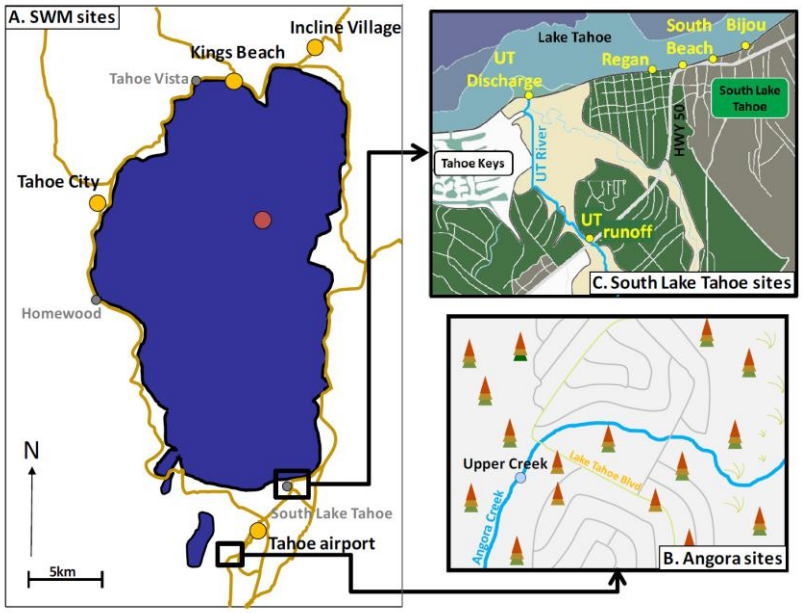

Figure VI.1: Map of sample locations around Lake Tahoe. A: In orange are the SWM sites and in red the MLTP station. The Figure B shows a drawing of the Angora neighborhood with the two sampling sites. The Figure C is a map of sampling sites at South Lake Tahoe, for stream sampling sites (Upper Truckee River (UT) sites) and near shore sampling sites (Regan, South Beach, Bijou).

VI.2.2.2. Flow injection-SP2 black carbon analysis

Concentrations of rBC were determined using a single particle intracavity laser induced incandescence photometer (SP2, Droplet Measurement Technologies, Boulder, Colorado)

coupled to a Flow Injection (FIA) system with ultrasonic nebulization/desolvation (CETAC UT5000), Figure VI.2.

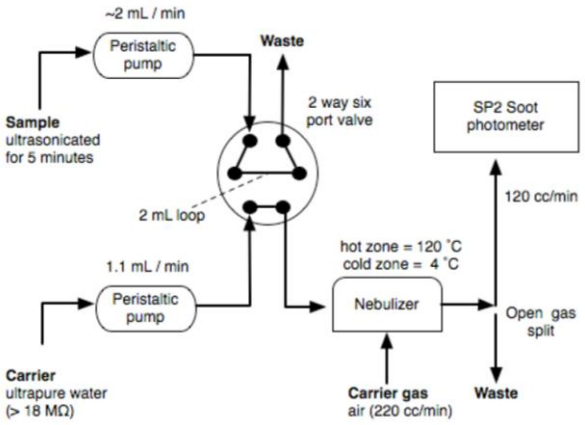

Figure VI.2: Schematic of the coupled SP2-FIA analytical system.

Analyses of rBC aerosols using the SP2 have been described in details in several papers (Stephens et al. 2003; Moteki and Kondo 2010; Schwarz et al. 2010) including inter-instrumental comparisons with other black carbon analytical methods (Slowik et al. 2007). The SP2 determines rBC from the wavelength resolved incandescent light emitted by individual rBC particles heated to their boiling point (3700 to 4300 K) inside an intracavity ND-YAG laser (1064nm). As a result of the unique boiling range of rBC (higher than pure silicon or nickel), the method is free of positive interferences from organic substances such as humic acids or PAHs, either as aerosol particles or coatings in rBC (Schwarz et al. 2006; Moteki and Kondo 2007). Furthermore, the method is insensitive to rBC particle morphology (Cross et al. 2010) but restricted to a particle size range of ~ 60 to 400 nm depending on particle density. This size range is smaller than typical charcoal fragments or mineral graphite particles (Dickens et al. 2004). In the FIA adaption of the method, 2ml samples are injected into an ultrapure water carrier, nebulized and desolvated before passing through the SP2. Concentrations of rBC are determined using a calibration of the incandescent light intensity to individual rBC particle mass combined with an external calibration of the FIA / nebulizer system using commercial pigments of known rBC concentration (Aquablack 162, Tokai Carbon, Tokyo) refer to section III.1.2. and Figure III.4.

External calibrations were performed daily for concentrations ranging from 0.03 to 80 µg/l with 10 standards. Procedural blanks were investigated using filtered lake and river water (< 20 nm, anopore filter) and were below the detection limit (~ 0.01 µg/l, 3σ). Instrumental blanks were prepared from ultrapure water (>18 MΩ) and were also below the detection limit. Replicate samples, a quality control standard and an instrumental blank were run every 10 samples with a standard deviation of less than 10% for concentrations above 0.1 µg/l and ~20% for lower concentrations. Samples with concentrations exceeding 30 µg/l were diluted with ultrapure water to concentrations lower than 20 µg/l.

VI.2.3. Results and Discussion

VI.2.3.1. rBC response to the Angora wildfire

Mid-lake concentrations. rBC concentrations in mid-lake samples displayed high variability with depth and time ranging from 0.02 to 0.45 µg/l with a geometric mean of 0.05 µg/l. For a lake volume of about 180 km^3, this represents a total rBC mass of ~9tons or 0.01 to 0.02% of the Dissolved Organic Carbon (DOC) pool, assuming fairly low DOC concentrations ranging from 300 to 400 µg/l (Stuart Goldberg, UCSD, personal communication). Orders of magnitude higher black carbon concentrations have been reported in sea water (~800 to 3700 µg/l in Gulf of Mexico (Dittmar 2008), ~90 to 280 µg/l in the Chesapeake Bay (Mannino and Harvey 2004)) and in river water (~100 to 400 µg/l in the Delaware river (Mannino and Harvey 2004)). However, these studies were based on the indirect measurement of black carbon decomposition products (hydrogen deficient molecules), not measured with the SP2 method (this paper). In contrast, black carbon measurements in the Gulf of Maine established concentrations in particulate organic carbon (large non dissolved black carbon particles of diameter > 700 nm) ranging from only 0.1 to 16 µg/l (Flores-Cervantes et al. 2009), overlapping the concentrations found in Lake Tahoe with the SP2 method, albeit a larger particle size range. In order to compare these various studies, the

relationship between black carbon decomposition products, particulate black carbon (> 700 nm) and rBC needs further investigation.

Seasonal variability. The seasonal variability of the total water column rBC is shown in Figure VI.3, as well as an insert illustrating two rBC profiles (concentration/depth) for May and August 2007. The total water column rBC time-series displays minima in May-June 2007, September 2007, and January-February 2008 and 2009 (< 20 g/m^2) and a maximum in July-August 2007 (55 and 100 g/m^2, respectively). The relatively high values of March and April 2007 (~45 g/m^2) correspond to the onset of snowmelt at lower urbanized elevations. In contrast, the low rBC values during the months of May and June are synchronous with broad basin runoff from higher elevation non-urbanized snowmelt, which brings large volume of water to the lake {, #760}{U.S., #760}{Survey, #760}{website, #760}. The two-to-four fold increase in rBC during July and August 2007 corresponds to the Angora fire, which occurred from June 26th to July 2nd 2007. After the fire, there was no rain over the watershed for the remainder of July and August. Therefore we assume that fire inputs of rBC should have contributed to lake concentration through dry deposition onto the lake surface. After this transient maximum, rBC concentrations in the lake decreased and stayed low until the end of sampling in August 2009.

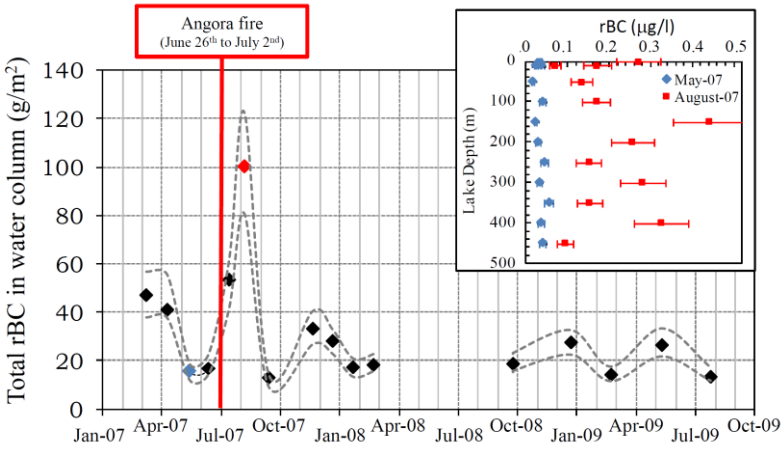

Figure VI.3: Total rBC in Lake Tahoe mid-lake site water column (in g /m^2) from February 2007 to January 2009. The red line shows the timing of the Angora fire, which damaged 12.5 km^2 of land in the Southern Lake Tahoe area. The gray dashed lines display the error envelope for total rBC data points. On the insert on the top right hand corner is shown two rBC mid-lake profiles for the specific months of May and August 2007 (in µg/l), illustrating the disturbance induced by the fire on rBC concentrations.

Angora site. Observations from the Angora Creek, within and immediately downstream of the fire area (Figure VI.1B), also suggests low rBC inputs from streams into the lake. Overall, from July 2007 to January 2009, rBC concentrations at the upper Angora Creek ranged from 0.3 to 1 µg/l. Three days after the fire (July 5th) and a year and a half later (January 23rd 2009) the upper Angora Creek site also exhibited low rBC concentrations with levels similar to the ones observed in the middle of the lake (0.3 µg/l). Assuming an average concentration of 0.5 µg/l, the rBC input to Lake Tahoe from Angora Creek was about ~1.6 kg for the winter 2009 (Table VI.1). Since the Creek represents about 1% of the watershed runoff inputs to Lake Tahoe, the stream was probably a negligible source of rBC to the lake during and after the fire, confirming the hypothesis that the increase in rBC lake concentrations synchronous to the fire was driven by atmospheric dry deposition processes. These results also imply that rBC deposited to soil is relatively immobile.

rBC concentrations (µg/l) per event per site				
	Winter 08	Winter 2009		
	jan-2008	oct-2008	nov-2008	jan-2009
Tahoe City	50.7	82.6	11.6	na
Kings Beach	126.3	157.0	56.9	96.4
Incline Village	174.9	334.8	99.2	138.6
Tahoe Airport	351.3	127.9	156.0	281.2
Angora Creek	na	na	0.1	0.5
Runoff Volume per event (m^3) per site				
Tahoe City	96	26	98	179
Kings Beach	25	1	12	26
Incline Village	3	1	4	6
Tahoe Airport	97	21	69	57
rBC input to lake per event (kg) per site				
Tahoe City	0.14	0.06	0.03	na
Kings Beach	0.09	>0.01	0.02	0.07
Incline Village	0.02	0.01	0.01	0.02
Tahoe Airport	0.96	0.07	0.30	0.46
Total runoff per winter (m^3) per site				
Tahoe City	87,382	114,212		
Kings Beach	2,226*	3,818		
Incline Village	3,721	2,744		
Tahoe Airport	11,582	18265*		
Angora Creek	2,293,664	3,426,338		
rBC inputs to the lake per winter (kg) per site				
Tahoe City	4.4	5.4		
Kings Beach*	0.3	0.4		
Incline Village	0.7	0.5		
Tahoe Airport	4.1	3.4		
Angora Creek	na	1.6		

Table VI.1: rBC concentrations and discharge data at the storm water monitoring stations for four storm events. *indicates a gap in data for total discharge estimations, thus, those numbers have to be used with caution and just as indications.

VI.2.3.2. rBC input to Lake Tahoe from urban stormwater runoff

Concentrations of rBC in urban stormwater runoff samples were systematically higher than in the mid-lake samples by a factor of 100 to 1000, supporting the existence of additional sources of rBC not related to forest fires. Runoff rBC concentrations were rarely less than 5 µg/l and were

often in the 30 to 100 µg/l range. rBC concentrations in highway stormwater runoff samples were typically between 100 to 400 µg/l and as high as 600 µg/l.

Storm water monitoring. Stormwater monitoring (SWM) samples provide an overview of rBC concentrations in runoff in relation to urbanization type. Table V.1 displays the rBC concentrations in composite samples representing the average concentration for an entire storm event. *South Tahoe Airport* (site exhibiting the larger commercial/industrial activities) and *Incline Village* (highest residential coverage) showing elevated rBC concentrations (from 100 to 350 µg/l). Lower rBC concentrations were observed for stormwater draining less populated and commercialized areas (from 10 to 150 µg/l at *Kings Beach* and *Tahoe City*). Those concentrations at each site were extrapolated to the total runoff volume of the events to estimate rBC inputs to the lake (Table V.1). At *South Tahoe Airport* (relatively high concentrations and high volumes), the runoff could have brought between 0.1 to 1kg of rBC to the lake every event. On the contrary, *Incline Village* runoff seems to be a small source of rBC to Lake Tahoe (~10g/event) despite high concentrations. Over the whole winter 2009, each site may have discharged between ~0.4 kg (*Kings Beach*) to ~5.4 kg (*Tahoe City*) of rBC, Table V.1. This is much higher than for Angora Creek (~1kg/year), even though the discharge of the creek is 20 to 1000 times larger than at the runoff sites.

Distribution of rBC concentrations for samples collected at different times of the precipitation event of January 22th at three locations (*Kings Beach*, *Incline Village* and *South Tahoe Airport*) shows higher concentrations at the beginning of the event than at the end, demonstrating an initial flushing effect (Figure VI.4).

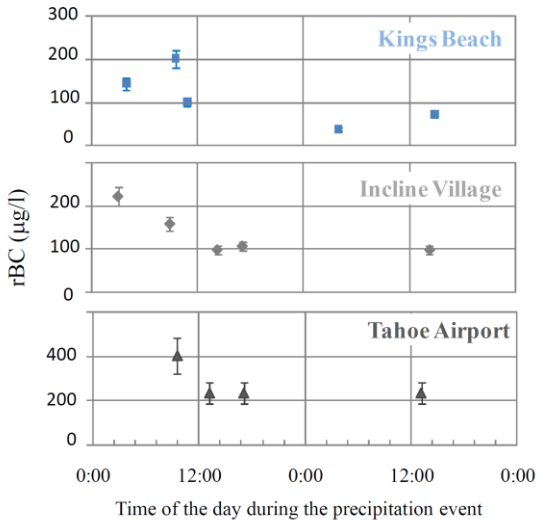

Figure VI.4: Distribution of rBC concentrations in µg/l during the single storm event of January 22, 2009 at three SWM sites (Kings Beach, Incline Village and Tahoe Airport). A first "flushing" effect is visible, followed by a tail of steady concentrations.

Free runoff. In samples collected from free runoff (surface water runoff, not from culverts), rBC concentrations were in the same order of magnitude as in SWM samples (culvert runoff). Replicate samples at one site and during one storm event had very similar concentrations (variability <10%), however, rBC concentrations varied from one site to another and from one day to another, sometimes by several orders of magnitude and depending on the total runoff volume (Figure VI.5). On February 23rd, we measured an averaged rBC concentration of 430 µg/l during a 24hrs period of intermittent rain which transported a total water volume of 340m^3 through the Bijou SWM site (chosen as reference for runoff volume). On March 2nd, runoff sampled during steady rain conditions and higher runoff volume (3060 m^3) had lower concentrations than during the first storm (average rBC concentration: 150 µg/l). On March 4th, occasional snow showers produced less water for runoff than the March 2nd event (400 m3) and rBC was comparatively more concentrated (average rBC concentration: 300 µg/l).

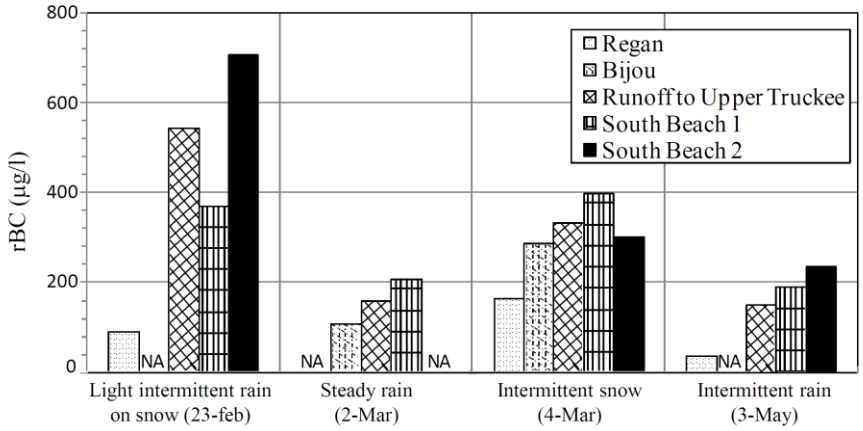

Figure VI.5: rBC concentrations in µg/l in runoff at the five South Lake Tahoe sites and the days (year 2009) and weather conditions during sampling.

Finally, on May 3rd, sampling took place after a two day period of scattered rain showers (~total runoff volume 400 m^3) but in this case rBC concentrations were also low (150 µg/l). Overall, concentrations during the major rain event of March 2nd, were lower than during the light precipitation events of February 23th and March 4th, suggesting dilution processes. However, low rBC concentrations also observed during the low volume runoff on May 3rd may indicate that urban rBC sources were smaller during the spring than in the winter (heavier road use, wood burning). Higher rBC concentrations and loads (due to higher flow rates) were also consistently found in sites close to Highway 50 (South Beach and Upper Truckee River), and the lower concentrations were observed for the commercial and residential sites (Bijou and Regan). Thus, the rBC concentrations appear directly related to traffic volume and may be used as an indicator for traffic pollution, as previously suggested by other studies (Jansen et al. 2005).

VI.2.3.3. rBC in the near-shore zone: linking runoff and middle lake

The near-shore zone (NSZ) of the lake (Figure VI.1C), is affected by runoff and river inputs and by mixing with the middle lake waters. Figure VI.6 shows rBC concentrations averaged for distances 1 and 10 m away from the shore for each site and event. The comparison of Figures VI.5 and VI.6 reveals concentrations one to three orders of magnitude lower in the NSZ than in

South Lake Tahoe runoff, with levels varying from 60 µg/l (March 4th 2007) to less than 5 µg/l (April 22nd 2007). Furthermore, we observed a lack of relationship between rBC concentrations in runoff and in NSZ waters at the four sites investigated, indicating that transfer processes from shore to lake are not straightforward.

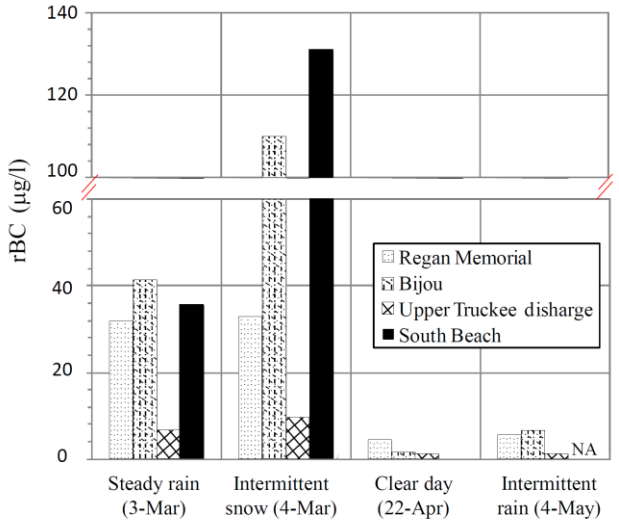

Figure VI.6: rBC concentration for near shore samples (lake samples) at the four South Lake Tahoe sites for the three storm events and one clear day monitored in the spring 2009, averaged for distances 1m and 10m away from shore.

The NSZ concentrations were inversely related to the discharge rate of the Upper Truckee River with lower concentrations associated with higher discharge rates from snowmelt {~3 m3/s in April up to 15 m3/s in May 2007`, \, #760}. This likely reflects dilution in the NSZ, which also displayed a sharp gradient (one to two orders of magnitude) in rBC concentrations 10 to 100 meters away from the shore, and lower rBC concentration in water from streams and from the Upper Truckee River. Overall, the analysis of stormwater runoff, stream and near-shore waters suggest that concentrations of rBC in the NSZ are mainly driven by pollution from vehicle emissions around the Lake and by direct urban runoff, probably overcoming natural rBC levels. The high concentrations (up to 600 µg/l) found in stormwater runoff have implications for water pollution in large cities where enormous amounts of rBC must be transferred from roadways and other surfaces by precipitation into urban water systems.

In the mid-lake, large perturbations in rBC concentrations appear to be connected with episodic events such as fires and snowmelt. However, considering that rBC nanoparticles should have very low water deposition rates (~1 m/year) it is surprising that concentrations in the lake remain relatively stable and do not build up. The rapid decrease in mid-lake concentrations following the pulse associated with the fire (Figure VI.3) is also unexpected knowing such low rates. In the NSZ, we hypothesize that rBC must be removed through interactions with larger particles and other colloidal species by a combination of adsorption and aggregation (Christian et al. 2008; Vesaratchanon et al. 2008; Koelmans et al. 2009), reducing the amount of rBC transferred to the mid-lake and driving the sharp gradient in rBC observed from 1 to 100 m from shore. Thus, an investigation of rBC concentrations in the top layer of NSZ sediments could reveal relatively high rBC content.

However, since Lake Tahoe is oligotrophic and with very low particulate concentrations (Swift et al. 2006), the adsorption of rBC on other colloids and its removal by aggregation in the middle of the lake is unlikely to account for the changes in concentration. We suggest that additional processes are also needed to explain those rapid changes. These processes may include alteration of rBC by UV irradiation (Lee et al. 2009; Hwang and Li 2010), uptake and agglomeration by biota (Baun et al. 2008; Tervonen et al. 2010), disaggregation and eventual mineralization (Nguyen et al. 2010). This implies that rBC is not transported over large distances as an hydrosol and that its transfer from continental pools to oceans likely occurs in association with sediments. Further studies of rBC and other colloids in lakes and rivers are needed to determine the ultimate mobility and fate of these ubiquitous particles through terrestrial water systems.

ACKNOWLEDGMENTS

We thank the anonymous reviewers as well as Martin Gysel (PSI, Switzerland) and Joshua Schwarz (NOAA, Boulder) whose their insightful comments have contributed to the significant improvement of the manuscript. We express our gratitude for the National Science Foundation,

the Desert Research Institute, and U.C. Davis for financial support and for support in sample collection and data analysis. Mid-lake samples were collected as part of the Lake Tahoe Interagency Monitoring Program (LTIMP), supported by funding to UCD from the Tahoe Regional Planning Agency and the Lahontan Regional Water Quality Control Board. Angora Creek samples were collected as part of the Angora Wildfire Water Quality Monitoring Project, supported by grants to DRI and UCD by the California State Water Board, the US Forest Service Lake Tahoe Basin Management Unit and the Lahontan Regional Water Quality Control Board. We also thank Todd Mihevc of DRI, and Raph Townsend, Brant Allen and Anne Liston from UC Davis for their assistance in sample collection and processing.

VI.3. INVESTIGATION OF rBC TRANSFER IN LAKE WATERS AT OTHER SITES

The comparison of rBC concentrations in Lake Tahoe with other high clarity and oligotrophic lakes may help to confirm our understanding of rBC fate in freshwater systems based on Lake Tahoe observations (section VI.2.). rBC measurements in Castle Lake (California), Crater Lake (Oregon) and Lake Superior (Minnesota), each subject to differing effects of anthropogenic disturbances and climatic changes on water properties, are thus presented here, Figure VI.7. Estimations of eventual clarity losses due to rBC inputs are shown in Appendices B.

Figure VI.7: Map of Crater Lake (OR), Castle Lake (CA) and Lake Tahoe (NV, CA) locations in the western United States.

VI.3.1. Castle Lake

Castle Lake is a shallow and oligotrophic glacial cirque lake located in California, close to Mount Shasta, also showing exceptional clarity. Its depth is 34 meters, and its area 0.19km^2. The lake was sampled in October 2009 by Dr. Alan Heyvaert from surface to bottom (0-25 meters, 13 samples) and analyzed at DRI for rBC in April 2010. rBC concentrations in Castle Lake (0.15±0.03 µg/l) were about a factor of 3 higher than Lake Tahoe's average concentrations and

comparable to the high concentrations measured subsequent to the Angora fire in July 2007 (Figure VI.8, left).

Overall, Castle Lake's concentration profile showed rather homogeneous values in the top 10 meters (~0.16±0.02 µg/l), then dropping to ~0.11 µg/l at 15m depth. Concentrations at the bottom increased again to ~20 µg/l which may suggest that the sediments were enriched in rBC, and that particles were not removed from water column until reaching the bottom of the lake (34 m), but rather accumulating.

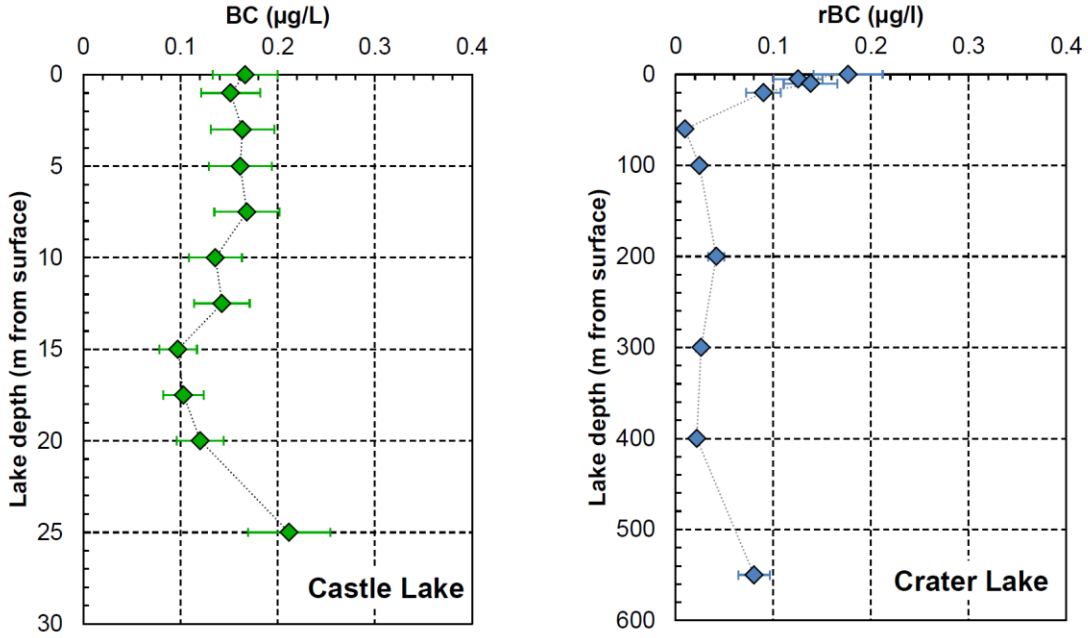

Figure VI.8: Fall 2009 rBC concentrations lake profiles of Castle Lake (left) and Crater Lake (right). Watch the difference in depth scale.

VI.3.2. Crater Lake

Crater Lake occupies a depression formed during the volcanic eruption of Mount Mazama volcano ~7700 YBP and is located in southern Oregon. Situated at an elevation of 1883m, it has a maximum depth of about 600m, and an area of 53km^2. The lake has no inlet and outlet and is annually recharged from evaporation and seepage by snowmelt. It is known for its exceptional water clarity which exceeds Lake Tahoe's.

Sampling and analyze of rBC in the lake were conducted in September 2009 with field support from Mark Buktenica and Scott Girdner (National Park Service) from the top of the lake to bottom (maximum depth = 593m). Analysis were conducted in April 2010, on a total of 10 samples, Figure VI.9. Geometric mean concentrations measured along the profile were comparable with levels observed in Lake Tahoe (lower than 0.05µg/l, cf. Figure VI.1). In contrast to Lake Tahoe, however, rBC concentrations were substantially higher in the top 20 meters (0.13 ± 0.04µg/l on average) than in the rest of the water column (0.03 ± 0.02µg/l). At comparable depths (from 0 to 20m), those concentrations were in the same order of magnitude as the concentrations measured in Castle Lake.

Crater Lake is known to be well stratified in summer and to be partially mixed by winds in the top 200m during winter. Cold down-welling may occur at this time, reaching the bottom when surface waters get cold enough to sink, e.g. from winter to spring (Crawford and Collier 1997; Larson et al. 2007). Sampling occurred in September, i.e. during the period (summer – fall) of established thermal stratification for the water of Crater Lake. Perhaps not surprisingly, rBC shows a stratified pattern as well, implying that excess rBC inputs to the lake exist during the dry summer season. Moreover, these higher concentrations in the top layers also suggest that rBC is aggregated, cleared, diluted or degraded before getting to the lower depths of the Lake. In fact, the minimal concentration measured in the water column was found at 60 meters depth (0.01 µg/l, close to the detection limit of the SP2). This concentration decrease is unexpected given with the known resistance of rBC towards degradation processes but confirms observations made in Lake Tahoe (see section VI.2).

An increase in concentrations at the bottom of the Lake similar to Castle Lake, suggests that the sediment may act as a source of rBC to the water column or represent a transfer boundary. This condition, however, was not observed at Lake Tahoe’s bottom.

VI.3.3. Great Lakes

Lake Superior is the largest of the five Great Lakes of North America (area 82,400km^2, maximum depth 410m) and is bounded to the north by the Canadian province of Ontario and the U.S state of Minnesota, and to the south by the U.S. states of Wisconsin and Michigan. Lake Superior, known as an oligotrophic lake, was sampled for rBC in collaboration with Elisabeth Minor and the University of Minnesota Duluth in 2009 at two periods of the year: in June, when the water column was isothermal, and in August, when the column was stratified. Four locations where investigated: two on the open surface of the Lake, one at the discharge of the Ontonagon River and one at the discharge of the Baptism River, Figure VI.9. The two open water sites were sampled at ~5m depth and ~150m depth.

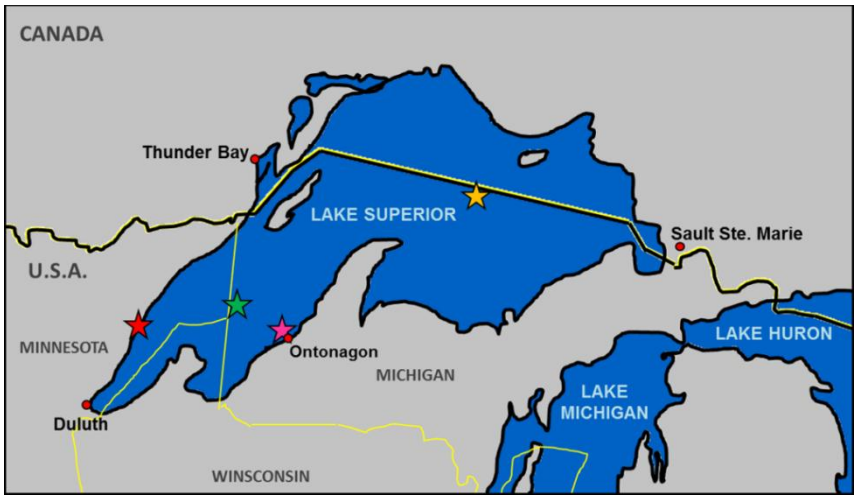

Figure VI.9: Map of Lake Superior sampling sites (stars). Two sites are open lakes (East, orange and West, green), one is at the mouth of the Ontonagon River (magenta), and the last one is at the mouth of the Baptism River (red).

rBC concentrations were in the same range as the concentrations found in Lake Tahoe, with geometric mean of 0.05 ± 0.02 µg/l, Figure VI.10. Mid-lake locations showed rBC surface concentrations in the same range than the one observed out of the river mouths, and were lower than surface levels observed at both Crater Lake and Castle Lake. At depth, the difference between isothermal and thermally stratified states of the lake was marked by a two-fold increase in rBC concentrations. At the surface, the difference between these two states was more variable from one site to another: an increase was observed at the Baptist River mouth and eastern open lake sites (306% and 200% respectively) and a decrease at the Ontonagon mouth and western

open lake sites (37% and 60% respectively). More sampling would be required before drawing further conclusions from these results.

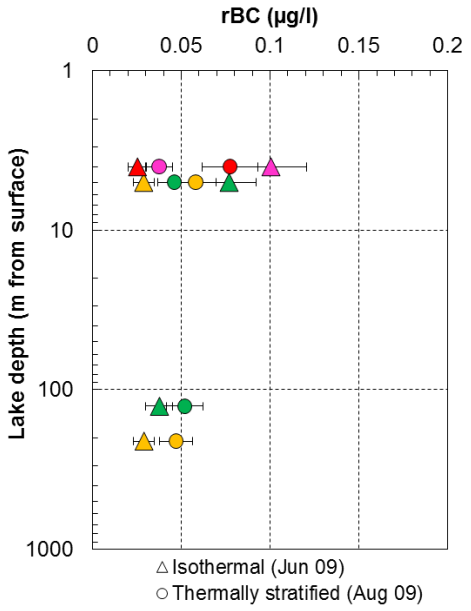

Figure VI.10: rBC concentrations in the Lake Superior, for isothermal and thermally stratified periods. Orange and green are open lake samples, magenta is at the mouth of the Ontonagon River, and red the mouth of the Baptism River.

VI.4. INTERPRETATION OF rBC SOURCES TO OLIGOTROPHIC LAKES AND TRANSFER PROCESSES TO SEDIMENTS

The analysis of Lake Tahoe and three other oligotrophic lakes water samples showed presence of rBC in low concentrations at all depths. Concentrations were found to be in the same range in deep water layers of Crater Lake, Lake Tahoe and Lake Superior, with geometric means of 0.05 ± 0.02 µg/l. Our in-depth investigation conducted at Lake Tahoe demonstrated that the transfer of rBC to freshwater environments can be induced by snow/urban runoff and dry deposition of smoke from fires. Inputs by runoff on fire scars did not seem, however, to be significantly contributing to Lake Tahoe rBC levels.

The analysis of rBC concentration in lake profiles as a function of water depth and time (Figure VI.3 + Appendices A) also showed that rBC was removed from the water column or degraded at a rate faster than expected. Moreover, the smaller lakes (Crater Lake, Castle Lake) had greater

surface concentrations in the top 20 meters (0.15 ± 0.05 µg/l), that then decreased with depth, notably in Crater Lake, suggesting rBC dispersion by mixing and inputs from shore not transferred to the mid-lake but rather deposited or degraded in the nearshore water column. This relatively fast loss or clearing rate in water is in contradiction with the common thought that rBC nanoparticle is a very refractory compound with very long lifetime. However, it confirms observations made in Lake Tahoe with the rapid decrease in concentrations subsequent to high inputs from the Angora fire (section VI.2.3).

Lastly, the observation that concentrations were rarely found under 0.02 µg/l indicates a background of rBC concentrations which is not degraded or cleared from water column. The concentration increase seen at the bottom of Crater Lake and Castle Lake confirms that rBC may accumulate at or above the sediment surface, which can then act as a source of rBC to the bottom waters of the lake, maybe through bioturbation.

Chapter VII. rBC in lake sediments: a potential archive to investigate past fire history

Black carbon has been observed unaltered in soils and sediments dated thousands of years old (section II.2.3.) and has been used as a proxy for local combustion (Muri et al. 2002; Elmquist et al. 2007). However, rBC nanoparticle measurements have never been applied for this purpose in those media. Our study of sources and fate of rBC in four oligotrophic lakes (Chapter VI) suggested that although partially cleared from the water columns, rBC may be transferred to the bottom of the lakes, and substantially to sediments. We thus applied the SP2-method (Chapter III) to a Lake Tahoe sediment core. Specifically, we investigated the possibility of differentiating the rBC nanoparticles from charcoal in sediments. In addition to charcoal measurements, this differentiation allows the apportionment between sources dominated by the atmosphere (small rBC nanoparticles emitted in the gas phase and travelling over long distances) and sources dominated by local burning (bigger char-BC fragments transported from fire scars to nearby ecosystems mostly by runoff and aquatic transport). This differentiation is discussed further by Thevenon et al. (2010) in terms of past fire regime determination, pyrogenic carbon cycle and human-climate interaction.

The study of rBC nanoparticles in the Lake Tahoe sediment core was possible at DRI during summer 2009. The core was extracted with a Soutar box corer, deployed from the University of California, Davis, RV John LeConte and was previously dated and analyzed for mercury, lead and charcoal (Heyvaert et al. 2000).

VII.1. LAKE TAHOE SEDIMENTS ANALYSIS

For this study, the sediment core LT91-1 of ~45cm long was extracted from a depth of 400m in the middle of Lake Tahoe and was used for rBC analysis and charcoal, Figure VII.1. This and the other cores were previously aliquoted every 1 to 5cm (28 aliquots), dried, mixed for homogeneous composition and analyzed notably for lead (Pb) and mercury (Hg) (Heyvaert et al. 2000).

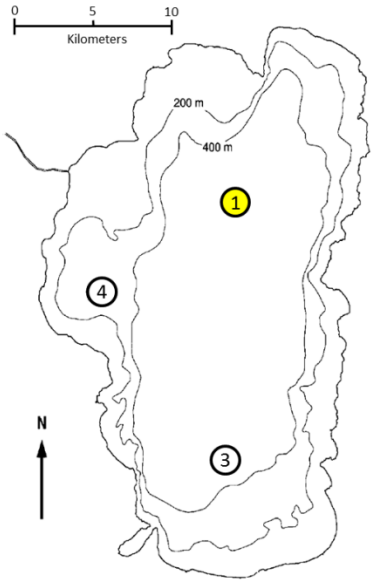

Figure VII.1: Bathymetric profile of Lake Tahoe (modified from Heyvaert et al. (2000)). Sediment sampling locations are indicated for cores (1) LT-91-1, (3) LT-91-3, and (4) LT-91-4. Core #1 was used for rBC measurements (in yellow), all the cores were used for Hg and Pb. Depth contours are given in meters.

VII.1.1. rBC measurements.

In contrast to conventional measurements of rBC in sediments and soils, the SP2 shows no biases induced by sample burning or oxidation steps. The procedure for sediment analysis was thus adapted from regular discrete water samples procedure. We sampled 20 to 80mg from each of the aliquots and applied a 1000 times dilution with ultra-pure water to decrease rBC and particle concentrations. Seven samples collected at a same depth were prepared with similar dilution factor. The samples were run on the SP2 with usual water samples procedure (described in section III.1.) with a standard and laboratory replicate run every 10 samples. Concentrations are reported in ppm ($\mu g/g_{sediment}$).

VII.1.2. Dating

The depth/age relationship used was the one reported by Heyveart et al. (2000) and based on sedimentation rates calculated from ^{210}Pb and ^{14}C and few event markers. Briefly, the top three dates shown in Figures VII.2,3,4 are derived from SCFCS interpretation (Segmented application of the Constant Flux with Constant Sedimentation rate model) of ^{210}Pb data; the 1860 date was located by sediment markers indicating the onset of historical logging; and the 1450 date was estimated from ^{14}C data. High mass sedimentation rates occurred during the logging era from 1860 to 1900. However, high-resolution dating by ^{210}Pb is not highly accurate in this system (Heyvaert et al. 2000), so modern dates shown on the figures are considered relatively accurate at the decadal scale but should not be over-interpreted.

VII.2. RESULTS AND DISCUSSION

VII.2.1. rBC concentrations in sediments

rBC averaged concentration measured in Lake Tahoe was 28 ± 8 ppm for the last 100 years and 15.6 ± 3.1 before 1900, Figure VII.2. The variability of the concentrations between field replicates was rather high and standard deviation at each depth ranged from 5% to 70%, with an average of 33% ± 13%. However, significant rBC trend with depth was still visible in the record notably in the top 10 cm, and showed increased rBC since the first half of the century (~1930), with a spike in the 1970s.

Averaged over the last century (since the year 1900), those concentrations corresponds to a rBC flux of ~0.03 g/m^2/yr. This value is comparable to pre-industrial and modern fluxes measured by Elmquist et al. (2007) in the Swedish Lake of Aspvreten averaging ~0.07 and ~0.05 g/m^2/yr respectively. However, it is ten times lower than rBC fluxes reconstructed at the Aspvreten during the Industrial Revolution (1870-1930, up to 0.35 g/m^2/yr).

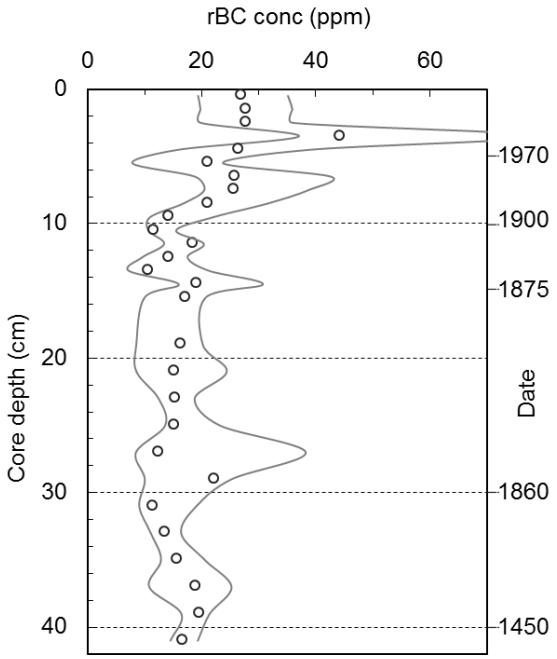

Figure VII.2: Median rBC concentrations (circles) versus core depth. Lines show 10 and 90%percentiles. Time scale (cal. yr.) is reported on the right axe.

VII.2.2. Comparison with the charcoal record

Charcoal is produced during biomass burning and is transferred to the aquatic environment mainly through runoff on fire-scars (cf. section II.3.5). It is thus commonly used to reconstruct local history of fire activity in a hydrologic basin, and was previously reported for this lake (Heyvaert, PhD Dissertation) through optical grain-counting. While we conclude in III.1 that rBC also records fire activity, the rBC and charcoal profiles in this sediment core do not show similar variability, Figure VII.3. Specifically, the layer showing very high charcoal counts at the end of the 19^{th} century, a period of important tree logging activity (Heyvaert et al. 2000), is not seen in the rBC record. Similarly, the peak observed in the rBC record around the 1970s seems to occurs later in the charcoal record.

Overall, and despite the high standard deviation of rBC field replicates, this comparison suggests that rBC and charcoal inputs to Lake Tahoe are not driven by the same sources and/or transport processes.

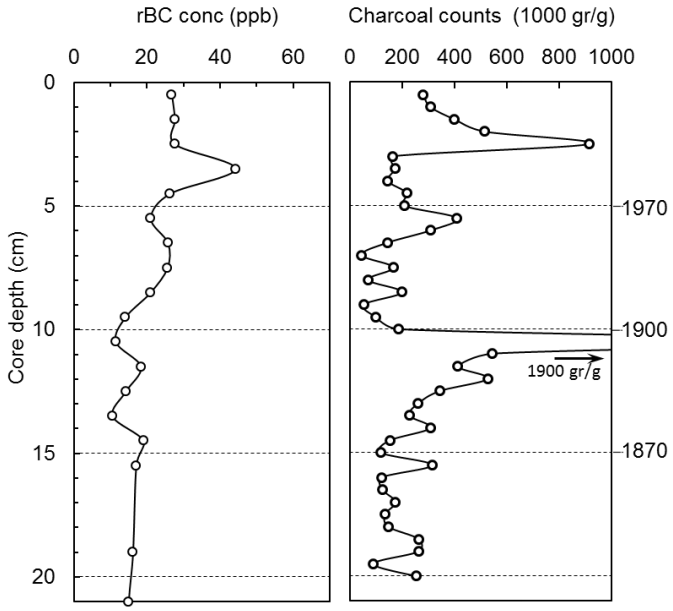

Figure VII.3: Comparison of rBC concentrations in µg/g (left) and charcoal counts in # of grains per gram (right) in the top 20 cm of the sediment core. Dated layers are indicated on the right scale.

VII.2.3. Comparison with lead and mercury records.

rBC variability is found to share more features in common with the Pb and Hg measured in this sediment core than with charcoal counts, Figure VII.4.

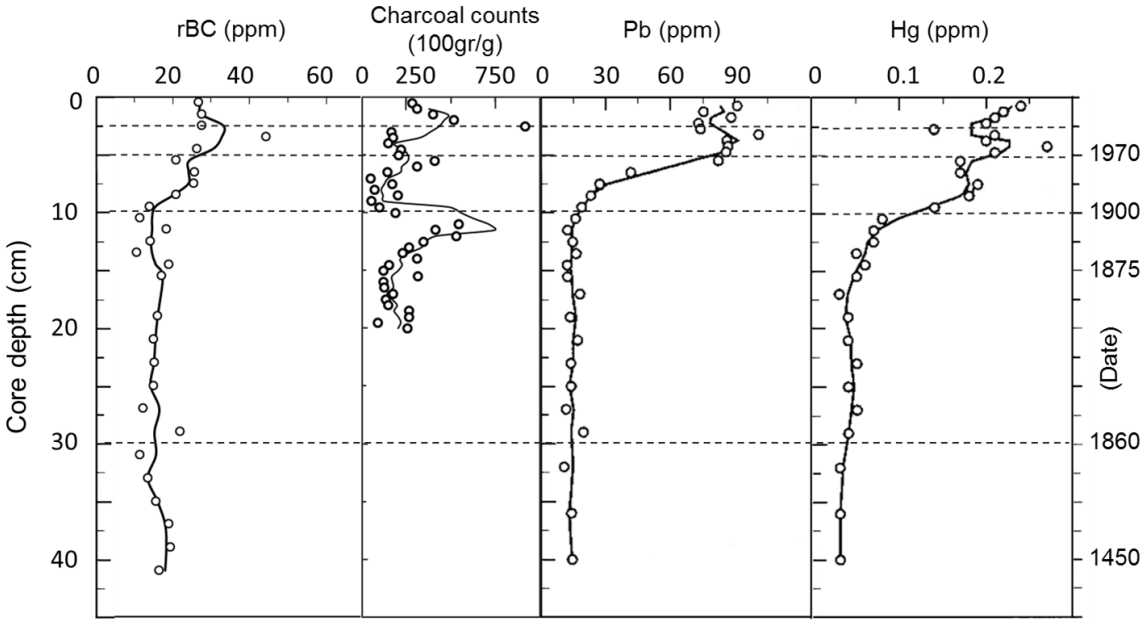

Figure VII.4: Lake Tahoe profiles (LT-91-1) of rBC, Pb and Hg concentrations, with the data smoothed by a three-term moving average, and of charcoal counts, smoothed by a five-term moving average. Approximate deposition dates are shown for reference on the right scale.

Notably, rBC, Hg, and Pb show similar increases in concentrations around 1900. rBC concentrations start to increase slightly after Hg concentrations, and almost simultaneously as Pb concentrations. After this increase, the variability of rBC seems to share more of the variability of Hg than Pb, except for the top measurements, showing stable concentrations for rBC and Pb and not for Hg.

According to Heyvaert et al. (2000), the increase in Pb concentrations from about 1920 to 1980 corresponds to increasing consumption of leaded gasoline in the Tahoe basin from the time of its introduction in 1923 and until EPA regulations in 1973.

On the other hand, Hg is known as a global pollutant and Hg emissions to the atmosphere have peaked in the 1970s in the mid-northern latitudes, specifically in the USA, as revealed by a firn air record from Summit, Greenland (Faïn et al. 2009). Since Heyvaert et al. (2000) found no Hg source in the vicinity of the Tahoe basin which could have been linked to the early rise in the Hg record, this peak is likely corresponding to the setting of the Clean Air Act (1970), which drastically limited the industrial use of Hg. Consequently, Hg recorded in Lake Tahoe sediments may be an indicator of global and regional pollution related to long-distance atmospheric transport by prevailing winds, in contrast to Pb, which is more locally derived. However, it has to be noted that the speed of deposition of Hg may vary with lake biology and diagenesis and may thus induce artifacts in the record (Outridge et al. 2007).

VII.3. CONCLUSIONS AND PERSPECTIVES TO RBC IN LAKE SEDIMENTS

This rBC sediment study suggests that despite loss and/or degradation processes observed in the water column (Chapter VI), rBC is transferred to sediments. The fate and stability of rBC particles in water is still not well understood, and is even less once in the sediment. However, assuming that rBC loss and/or degradation processes occurring in lake waters were constant over the period investigated, we show that sediment recorded a decadal variability in rBC

deposition, with increased concentrations since ~1900. Nonetheless, a comparison with the charcoal record shows that rBC variability is not overwhelmed by local fire activity and indicates that rBC is not sensitive to runoff inputs from the watershed (carrying the charcoal particles). rBC inputs to the Lake are thus likely dominated by dry and wet deposition, which are also the main inputs to the lake expected for Pb and Hg (Heyvaert et al., 2000). Comparisons with Pb and Hg records confirm that rBC inputs to Lake Tahoe likely happen at both local and regional scales, with probable anthropogenic contributions. The measurements of rBC in the sediments of a non anthropogenically-modified lake, far from local fires sources, would thus give information on emissions of rBC at a regional/global scale exclusively.

Chapter VIII. Conclusions and perspectives

Throughout this Ph.D. dissertation, we demonstrate that rBC can be used as a combustion proxy in Antarctica ice cores, and potentially in lacustrine sediment cores.

In Antarctica, the reconstruction of rBC records over the cal. yr. 1800-2000 period is shown to vary in space and time. The two high-resolution records retrieved from the low-elevation sites of WAIS and Law Dome show a clear annual co-variability since cal. yr. 1970. However, in the case of lower time-resolution sites investigated on the East-Antarctic Plateau, annual variability in rBC deposition do not relate from one site to another. Additionally, rBC concentrations among those sites are increasing with elevation, as an effect of decreased accumulation with altitude. Sub-annual to annual variability of the East Antarctic Plateau records is therefore expected to be dependent upon processes such as precipitation, wind blowing, ablation, and was assumed to be inappropriate. However, relatively stable accumulations over the cal. yr. 1800-2000 period suggests that accumulation is not a driving factor for temporal trends in rBC deposition to Antarctica. In fact, a periodicity corresponding to ENSO (2-8yr) and independent from atmospheric transport is found to modulate the rBC variability of WAIS, Law Dome, and most of the Plateau records. At Law Dome, this rBC-ENSO signal is delayed from the ENSO signal recorded by Na, indicating that ENSO may affect fires with a time lag probably linked to vegetation growth. On the East Antarctic Plateau, the long-term (20-40yr) variability of ENSO (NADA) seems to be driving the general trends in rBC concentrations in half of the records. However, none of these sites exhibit correlations of rBC deposition with ENSO indexes on an annual time scale. We attribute this lack of correlation to the dual effect of ENSO on vegetation, inducing drought on one side of the Pacific and floods on the other side, rendering a potential ENSO-fire signal very disparate.

On a decadal scale, the rBC records share more common features among the investigated sites. Notably, most of the Plateau sites exhibit relatively low concentrations from 1890 to 1910, high

concentrations until 1940 and an increasing trend at the end of the 21st century. While Law Dome record reveals a similar variability with the Plateau sites from 1890 to 1940, it is not the case with the WAIS record. However, WAIS and Law Dome show a similar trend from the 1950's to the end of the century, a result consistent with decadal variability in grassland and biofuel rBC emission inventories from Australia and South America, and with an increase in SH anthropogenic emissions (Ito and Penner 2005; Lamarque et al. 2010). The Law Dome record has features common to both WAIS and the Plateau sites. This may suggest that different sectors of Antarctica record emissions and/or atmospheric transport from different locations. An array of records from other areas of the polar continent could therefore improve the knowledge on rBC SH emission history over the last two centuries. Additionally, global transport models may also improve the understanding of rBC origin and deposition to Antarctica.

In the future, and with a careful investigation of accumulation changes, the investigation of long-term rBC records from Antarctica has the potential to reveal links between climate, atmospheric transport, and fire emissions in the southern hemisphere.

In the northern hemisphere on the contrary, where rBC is produced by biomass burning and by fossil fuel combustion, rBC records may record other information. The study of rBC concentrations in Lake Tahoe revealed high contribution from urban pollution to the lake waters, which injected urban runoff into the Lake of rBC concentrations up to four orders of magnitude higher than background concentrations. These high concentrations decreased after a large input of rBC from dry-deposition of the smoke of a large local wildfire, which showed that rBC could be removed or degraded in the water column within few weeks. However, a low-level background in rBC concentrations was found to remain year-round in the Lake, and comparable to measurements made in the other oligotrophic lakes of Castle Lake, Crater Lake and Lake Superior, guessing that the background in rBC pool is stabilized by organic matter "steric effects". Measurements in Lake Tahoe's sediments show that rBC is transferred to the bottom water of the lake and substantially to the sediments. rBC and charcoal records show different variability and

hence reveal that different sources influence both proxies. It is likely that, charcoal is recording local burning and is carried to the Lake through runoff, streams and rivers, while rBC ultimately deposited to sediments is likely carried to the Lake by smoke and with wet and dry deposition. Moreover, rBC patterns exhibited similarities with lead and mercury depth profiles in this lake, indicating that rBC inputs to Lake Tahoe may be driven not only by local sources, but also by regional emissions.

To further conclude, the comparison of this rBC sedimentary record with traditional BC and EC measurements performed with methods such as TOC or CTO-375, need to be performed to determine the exact nature of rBC measured with the SP2. In the longer-term perspective, the measurement of Lake rBC should be extended to eutrophic lakes and polluted environments. Moreover, the analysis of rBC in fluvial waters and runoff waters of seashore metropolitan areas may help to evaluate the transfer of rBC to oceans and further to the deep oceanic-sediments.

Appendices

A. MIDDLE LAKE TAHOE rBC MEASUREMENTS

18 depth profiles of rBC in the middle lake Tahoe were collected from March 2007 to August 2009, Figure A1. As described in the article in section VI.2., each profile was composed of a batch of approximately 12 samples from lake depths ranging from 0 to 450m. A duplicate sample was collected at depth 10m.

The rBC depth variability seemed to be dependent on the mixing state of the lake which is related to the broad timing of runoff phases over Lake Tahoe Basin. Runoff phases also influenced the temporal variability (lower during calm periods): over one or two months, the rBC distribution depth could switch from dispersed concentrations (April 2007) to homogeneous concentrations (May 2007). Overall, concentrations ranged from 0.02 to 0.45µg/l with a geometric mean of 0.05µg/l. Maximum concentrations occurred in July-August 2007. This increase was observed shortly after the Angora fire, which burnt 12.5 km² of forest at the end of June to beginning of July 2007 (more details in section VI.2.). In November 2007, the concentrations were almost back to the geometric mean observed over the 2-years sampling period, suggesting that rBC was rapidly transferred from the upper layers of the lake to lower layers, despite its small size and expected low-settling velocities.

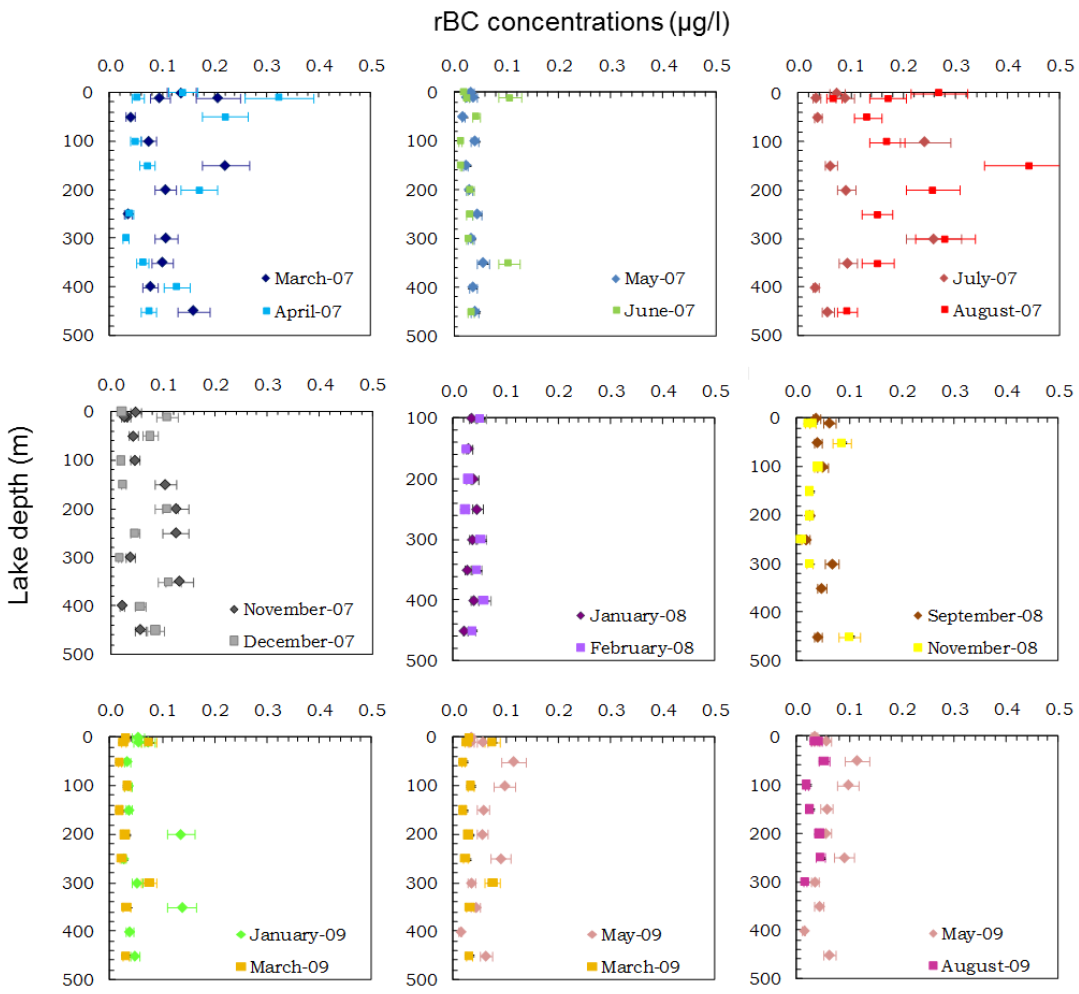

Figure A 1: BC in middle lake profiles from surface to 450 meters depth at various times of the year. Profiles are combined by periods of two months for more readability.

B. WATER CLARITY ISSUES IN LAKE TAHOE

a. Context

Lake Tahoe is world-renowned for its clarity and deep blue color. Over the last half-century, parts of the lake basin have been developed for residential and commercial use, and the lake has undergone progressive eutrophication and loss in clarity, Figure B1. The growing water quality problems of the lake have been studied intensively since the early 1960s (Coats et al. 2008) and have attracted considerable political attention. Presently, the annual average Secchi depth is approximately 23 m. Although this clarity indicator has shown steadier levels during the last five years, it has been declining during the last 34 years (Figure B1). Maintaining the clarity is necessary for aesthetic, economic, public health, and environmental reasons. Lake Tahoe is designated as an "Outstanding National Resources Water" by the Environmental Protection Agency which requires that California and Navada States prohibit development altering the essential character of the water and maintain water quality at current levels.

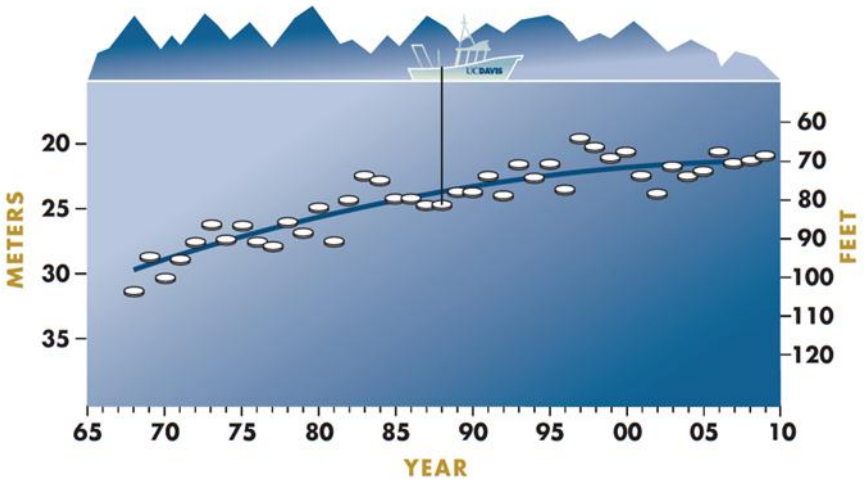

Figure B 1: Secchi depths as an indicator of water clarity loss in Lake Tahoe (annual state of the lake report 2010, Tahoe environmental research center, UC, Davis)

b. Transmittance and turbidity measurements

Turbidity. Water turbidity gives information on the water sample scattering coefficient and is known to be correlated to the number and size of particles of the near shore zone (NSZ). It is expressed in Nephelometric Turbidity Units (NTU) based on an empirical relationship to standard concentrations of formazin in water. For this study, turbidity was measured during the sampling of the Lake Tahoe NSZ (cf. section VI.2.) at depths varying from 10 to 50 cm, with a turbidity sensor (Hach 2100 AN, Loveland, Colorado) installed on the research vessel. The sensor was also brought back to the lab for turbidity measurements of black carbon standards, to evaluate the part of turbidity due to rBC nanoparticles exclusively.

Transmittance. Light transmission was also measured in the NSZ samples, as an indicator of combined light scattering and absorption in water –thus dependent on the number and size of the particles and colloids in the sample. rBC is a strong light-absorbent (section II.1.3), and consequently it may impact water clarity by reducing light transmission. With the aim of determining the part of light attenuation due to rBC only, rBC standards (Aquablack) were prepared and measured for transmittance in the lab. Transmittance was measured with a WETLabs C-star Light Transmissometer (Philomath, OR) which consisted of a light source emitting a narrow beam into a water sample and of a receptor measuring how much light is transmitted after the beam had travelled through the sample (typically 30cm).

c. Results

Turbidity. Turbidity values measured in the NSZ of South Lake Tahoe (Figure B2) during this study ranged from 0.26 NTU to 720 NTU with a geometric mean of ~6 NTU over the whole transects at the four measurement sites and for four storms.

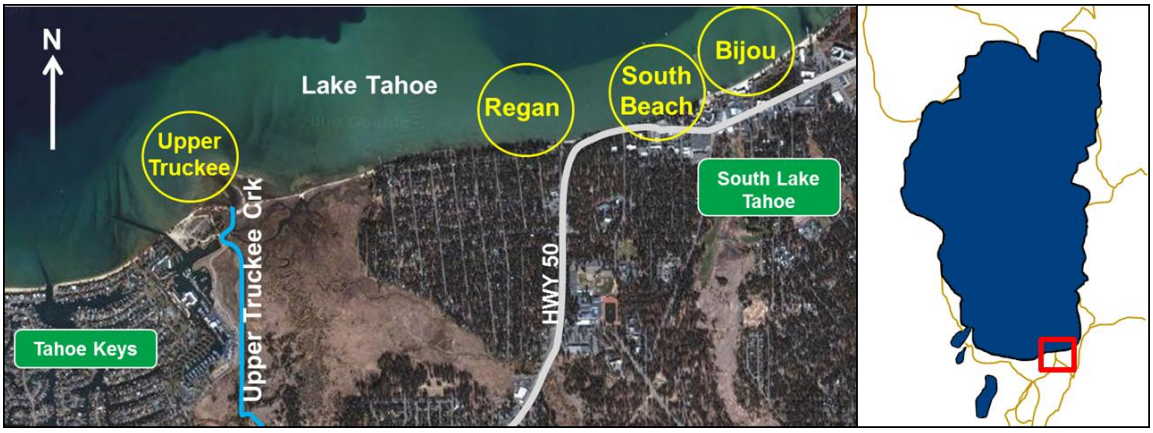

Figure B 2: Map of South Lake Tahoe off shore sites.

On the Figure B3 is plotted the turbidity at all sites (compiled for the four sampling days) as a function of distance from shore (data for ~1 and ~10 meters are averaged together as well as data for ~50 and ~100 meters). Compared with variations of rBC, in the same conditions, it is evident that turbidity values and rBC values are somehow correlated. A Spearman's rank correlation of rBC values with turbidity values shows strong correlations (Figure B4, at *Regan* and *South Beach* sites). However, since rBC is brought to the lake in the same time as other attenuating light constituents, we cannot conclude that rBC is at the origin of those variations in turbidity.

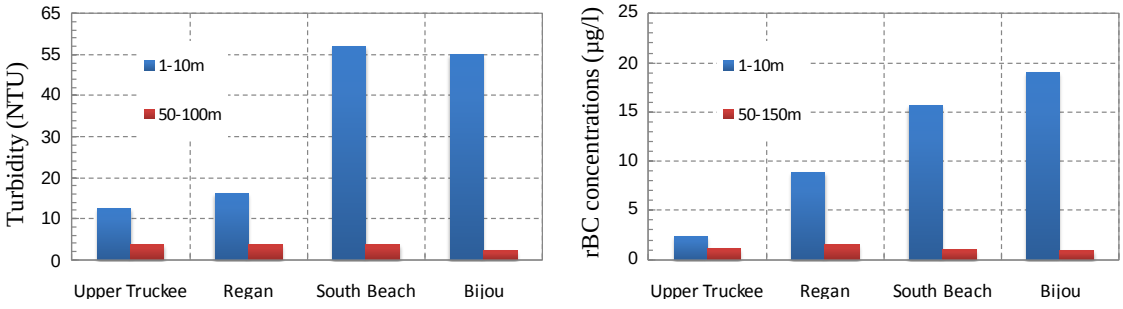

Figure B 3: Turbidity (left) and rBC concentrations (right) for South Lake Tahoe NSZ samples compiled as function of the site and the distance from the shore (1-10 meters) and (50-100 meters).

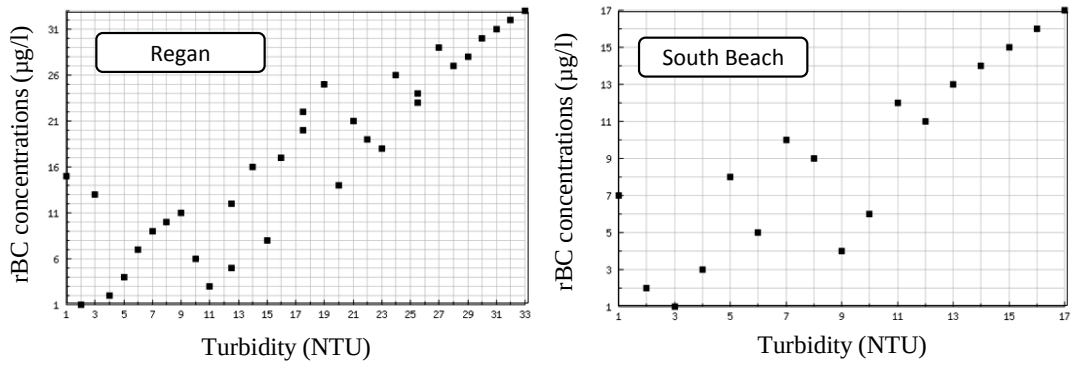

Figure B 4: Spearman's Rank correlation plot between turbidity and BC concentrations at two South Lake Tahoe sites (Regan and South Beach)

We investigated in the laboratory the impact of rBC on the water turbidity. The turbidity of several standards was determined (Figure B5), demonstrating that rBC particles do not influence water turbidity when their concentrations are under 10 µg/l. Concentrations higher than this threshold were seen on the NSZ (section VI.2.); however, it is still 10 to 100 times higher than concentrations found away from the influence of the shore and deep in the water column.

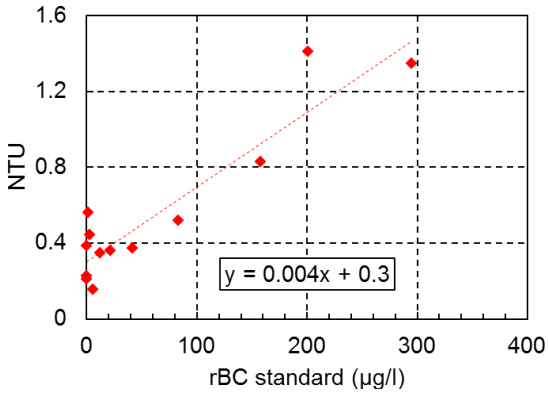

Figure B 5: Turbidity (NTU) in function of the concentrations (µg/l) of a BC standard

Transmittance. Just as with turbidity, rBC nanoparticles affect the transmission of light through water only at elevated concentrations. Figure B.6 shows that rBC concentrations of 200 µg/l reduces light transmission by 50%. A concentration of 10 µg/l reduces light transmission only by

5%, and concentrations lower than 3 µg/l have an effect of less than a percent. Even though water in the NSZ of Lake Tahoe can have rBC concentrations as high as 6 µg/l, the average annual concentrations in the shore and the middle lake observed during this study were always lower than 3 µg/l. Limited effect of rBC particles is thus expected on water transmittance in lake Tahoe.

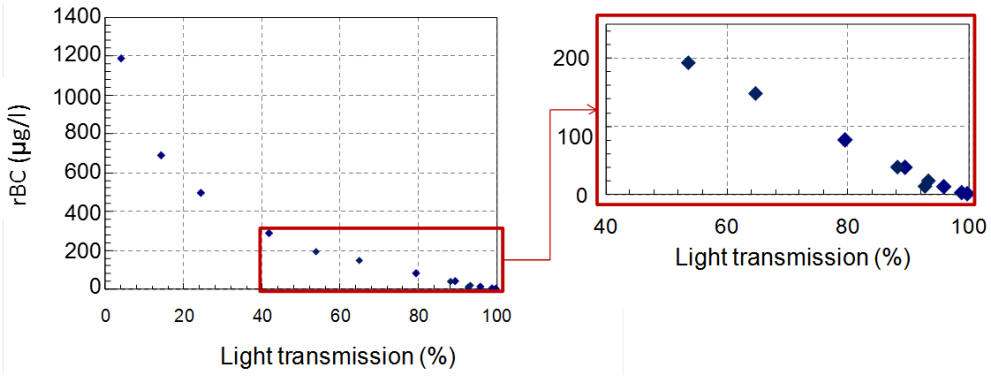

Figure B 6: Light transmittance as a function of BC standard concentrations, and close up of the lower concentration range (right).

d. Conclusions on water clarity

Turbidity and transmittance experiments assessed the effect of rBC nanoparticles on light attenuation in water. Significant effect on water clarity is only expected for very high concentrations and it is likely that rBC only plays a negligible role in the overall Lake Tahoe water clarity decline. Complementary experiments are, however, needed. Notably, lab measurements of light attenuation by other rBC material (e.g. different from Aquablack, such as fullerene soot) may give different results. Moreover, the sizes of the particles may also be a factor to take into account, and needs further investigation.

References

. "U.S. Geological Survey NWIS website;." from http://waterdata.usgs.gov/nwis.

Albrecht, B. A. (1989). "Aerosols, Cloud Microphysics, and Fractional Cloudiness." Science **245**(4923): 1227-1230.

Allen-King, R. M., P. Grathwohl and W. P. Ball (2002). "New modeling paradigms for the sorption of hydrophobic organic chemicals to heterogeneous carbonaceous matter in soils, sediments, and rocks." Advances in Water Resources **25**(8-12): 985-1016.

Alley, R. B., P. U. Clark, P. Huybrechts and I. Joughin (2005). "Ice-sheet and sea-level changes." Science **310**(5747): 456-460.

Alley, R. B., D. A. Meese, et al. (1993). "Abrupt increase in Greenland snow accumulation at the end of the Younger Dryas event." Nature **362**(6420): 527-529.

Andersen, K. K., A. Svensson, et al. (2006). "The Greenland Ice Core Chronology 2005, 15-42 ka. Part 1: constructing the time scale." Quaternary Science Reviews **25**(23-24): 3246-3257.

Andreae, M. O. and A. Gelencser (2006). "Black carbon or brown carbon? The nature of light-absorbing carbonaceous aerosols." Atmospheric Chemistry and Physics **6**: 3131-3148.

Andreae, M. O., C. D. Jones and P. M. Cox (2005). "Strong present-day aerosol cooling implies a hot future." Nature **435**(7046): 1187-1190.

Andreae, M. O. and P. Merlet (2001). "Emission of trace gases and aerosols from biomass burning." Global Biogeochemical Cycles **15**(4): 955-966.

Andreae, M. O., D. Rosenfeld, P. Artaxo, A. A. Costa, G. P. Frank, K. M. Longo and M. A. F. Silva-Dias (2004). "Smoking Rain Clouds over the Amazon." Science **303**(5662): 1337-1342.

Anklin, M., R. C. Bales, E. Mosley-Thornpson and K. Steifen (1998). "Annual accumulation at two sites in northwest Greenland during recent centuries." Journal of Geophysical Research **103**(D22): 28775-28783.

Anschütz, H., A. Sinisalo, E. Isaksson, J. R. McConnell, S.-E. Hamran, M. M. Bisiaux, D. Pasteris, T. A. Neumann and J.-G. Winther (2011). "Variation of accumulation rates over the last eight centuries on the East Antarctic Plateau derived from volcanic signals in ice cores." Journal of Geophysical Research **116**(D20): D20103.

Anschütz, H., K. Mueller, E. Isaksson, J. R. McConnell, H. Fischer, H. Miller, M. Albert and J. G. Winther (2009). "Revisiting sites of the South Pole Queen Maud Land Traverses in East Antarctica: Accumulation data from shallow firn cores." Journal of Geophysical Research-Atmospheres **114**.

Aristarain, A. J. and R. J. Delmas (1998). "Ice record of a large eruption of Deception Island Volcano (Antarctica) in the XVIITH century." Journal of Volcanology and Geothermal Research **80**(1-2): 17-25.

Arthern, R. J., D. P. Winebrenner and D. G. Vaughan (2006). "Antarctic snow accumulation mapped using polarization of 4.3-cm wavelength microwave emission." Journal of Geophysical Research-Atmospheres **111**(D6).

Baldock, J. A. and R. J. Smernik (2002). "Chemical composition and bioavailability of thermally altered Pinus resinosa (Red pine) wood." Organic Geochemistry **33**(9): 1093-1109.

Balzter, H., F. Gerard, C. George, G. Weedon, W. Grey, B. Combal, E. Bartholome, S. Bartalev and S. Los (2007). "Coupling of Vegetation Growing Season Anomalies and Fire Activity with Hemispheric and Regional-Scale Climate Patterns in Central and East Siberia." Journal of Climate **20**(15): 3713-3729.

Bamber, J. L., J. L. Gomez-Dans and J. A. Griggs (2009). "Antarctic 1 km Digital Elevation Model (DEM) from Combined ERS-1 Radar and ICESat Laser Satellite Altimetry." Boulder, Colorado USA: National Snow and Ice Data Center. Digital Media.

Banta, J. R. and J. R. McConnell (2007). "Annual accumulation over recent centuries at four sites in central Greenland." Journal of Geophysical Research **112**(D10): D10114.

Banta, J. R., J. R. McConnell, M. M. Frey, R. C. Bales and K. Taylor (2008). "Spatial and temporal variability in snow accumulation at the West Antarctic Ice Sheet Divide over recent centuries." Journal of Geophysical Research **113**(D23): D23102.

Barnola, J. M., D. Raynaud, Y. S. Korotkevich and C. Lorius (1987). "Vostok ice core provides 160,000-year record of atmospheric CO2." Nature **329**(6138): 408-414.

Baun, A., S. N. Sørensen, R. F. Rasmussen, N. B. Hartmann and C. B. Koch (2008). "Toxicity and bioaccumulation of xenobiotic organic compounds in the presence of aqueous suspensions of aggregates of nano-C60." Aquatic Toxicology **86**(3): 379-387.

Bertler, N., P. A. Mayewski, et al. (2005). "Snow chemistry across Antarctica." Annals of Glaciology **41**(1): 167-179.

Bisiaux, M. M., R. Edwards, A. C. Heyvaert, J. M. Thomas, B. Fitzgerald, R. B. Susfalk, S. G. Schladow and M. Thaw (2011). "Stormwater and fire as sources of black carbon nanoparticles to Lake Tahoe." Environmental Science & Technology **45**(6): 2065-2071.

Bisiaux, M. M., R. Edwards, et al. (2011). "Large scale changes in 20th Century black carbon deposition to Antarctica." Atmospheric Chemistry and Physics Discussions.

Bond, T. C. and R. W. Bergstrom (2006). "Light Absorption by Carbonaceous Particles: An Investigative Review." Aerosol Science and Technology **40**(1): 27 - 67.

Bond, T. C., D. G. Streets, K. F. Yarber, S. M. Nelson, J.-H. Woo and Z. Klimont (2004). "A technology-based global inventory of black and organic carbon emissions from combustion." Journal of Geophysical Research **109**(D14): D14203.

Bond, W. J., F. I. Woodward and G. F. Midgley (2005). "The global distribution of ecosystems in a world without fire." New Phytologist **165**(2): 525-538.

Bowman, D. M. J. S., J. K. Balch, et al. (2009). "Fire in the Earth System." Science **324**(5926): 481-484.

Brown, J. K. and J. K. Smith (2000). Wildland fire in ecosystems: effects of fire on flora, USDA Forest Service Gen. Tech. Rep. RMRS-GTR-42. **2:** 25.

Buckley, D. R., K. J. Rockne, A. Li and W. J. Mills (2004). "Soot Deposition in the Great Lakes: Implications for Semi-Volatile Hydrophobic Organic Pollutant Deposition." Environmental Science & Technology **38**(6): 1732-1739.

Budner, D. and J. Cole-Dai (2003). "The number and magnitude of large explosive volcanic eruptions between 904 and 1865 A.D.: Quantitative evidence from a new South Pole ice core." Volcanism and the Earth's Atmosphere. Geophysical Monograph **139**(*1*65–176).

Buiron, D. (2010). Dynamique climatique cotière en région Antarctic au cours des 50000 dernières années. PhD dissertation. Grenoble, Joseph Fourier University.

Burkhard, L. P., P. M. Cook and M. T. Lukasewycz (2008). "Organic carbon-water concentration quotients (Pi(soc)s and pi(poc)s): Measuring apparent chemical disequilibria and exploring the impact of black carbon in Lake Michigan." Environmental Science & Technology **42**(10): 3615-3621.

Carmona-Moreno, C., A. Belward, J.-P. Malingreau, A. Hartley, M. Garcia-Alegre, M. Antonovskiy, V. Buchshtaber and V. Pivovarov (2005). "Characterizing interannual variations in global fire calendar using data from Earth observing satellites." Global Change Biology **11**(9): 1537-1555.

Certini, G. (2005). "Effects of fire on properties of forest soils: a review." Oecologia **143**(1): 1-10.

Chappellaz, J., J. M. Barnola, D. Raynaud, Y. S. Korotkevich and C. Lorius (1990). "Ice-core record of atmospheric methane over the past 160,000 years." Nature **345**(6271): 127-131.

Cheney, P. and A. Sullivan (2008). Grassfires: fuel, weather and fire behaviour. Collingwood, Victoria, CSIRO publishing

Cheng, C.-H., J. Lehmann, J. E. Thies, S. D. Burton and M. H. Engelhard (2006). "Oxidation of black carbon by biotic and abiotic processes." Organic Geochemistry **37**(11): 1477-1488.

Christian, P., F. Von der Kammer, M. Baalousha and T. Hofmann (2008). "Nanoparticles: structure, properties, preparation and behaviour in environmental media." Ecotoxicology **17**(5): 326-343.

Chung, C. E., V. Ramanathan, D. Kim and I. A. Podgorny (2005). "Global anthropogenic aerosol direct forcing derived from satellite and ground-based observations." Journal of Geophysical Research **110**(D24): D24207.

Chýlek, P., B. Johnson and H. Wu (1992). "Black carbon concentration in Byrd station ice core - From 13,000 to 700 years before present." Annales Geophysicae-Atmospheres Hydrospheres and Space Sciences **10**(8): 625-629.

Chýlek, P., V. Ramaswamy and R. J. Cheng (1984). "Effect of graphitic carbon on the albedo of clouds." Journal of the Atmospheric Sciences **41**(21): 3076-3084.

Chýlek, P., V. Srivastava, L. Cahenzli, R. G. Pinnick, R. L. Dod, T. Novakov, T. L. Cook and B. D. Hinds (1987). "Aerosol and Graphitic Carbon Content of Snow." Journal of Geophysical Research **92**(D8): 9801-9809.

Clark, J. S. and P. D. Royall (1995). "Particle-Size Evidence for Source Areas of Charcoal Accumulation in Late Holocene Sediments of Eastern North American Lakes." Quaternary Research **43**(1): 80-89.

Clarke, A. D. and K. J. Noone (1985). "Soot in the Artic snowpack - A cause for perturbations in radiative-transfer " Atmospheric Environment **19**(12): 2045-2053.

Coats, R., M. Larsen, A. Heyvaert, J. Thomas, M. Luck and J. Reuter (2008). "Nutrient and sediment production, watershed characteristics, and land use in the Tahoe basin, California-Nevada." Journal of the American Water Resources Association **44**(3): 754-770.

Cohen-Ofri, I., R. Popovitz-Biro and S. Weiner (2007). "Structural Characterization of Modern and Fossilized Charcoal Produced in Natural Fires as Determined by Using Electron Energy Loss Spectroscopy." Chemistry – A European Journal **13**(8): 2306-2310.

Cole-Dai, J. H., E. Mosley-Thompson, S. P. Wight and L. G. Thompson (2000). "A 4100-year record of explosive volcanism from an East Antarctica ice core." Journal of Geophysical Research-Atmospheres **105**(D19): 24431-24441.

ColeDai, J. H., E. MosleyThompson and L. G. Thompson (1997). "Annually resolved southern hemisphere volcanic history from two Antarctic ice cores." Journal of Geophysical Research-Atmospheres **102**(D14): 16761-16771.

Cooke, W. F. and J. J. N. Wilson (1996). "A global black carbon aerosol model." Journal of Geophysical Research **101**(D14): 19395-19409.

Cozic, J., B. Verheggen, S. Mertes, P. Connolly, K. Bower, A. Petzold, U. Baltensperger and E. Weingartner (2007). "Scavenging of black carbon in mixed phase clouds at the high alpine site Jungfraujoch." Atmospheric Chemistry and Physics **7**(7): 1797-1807.

Crawford, G. B. and R. W. Collier (1997). "Observations of a deep mixing event in Crater Lake, Oregon." Limnology and Oceanography **42**(2): 299-306.

Cross, E. S., T. B. Onasch, et al. (2010). "Soot Particle Studies--Instrument Inter-Comparison--Project Overview." Aerosol Science and Technology **44**(8): 592 - 611.

Crutzen, P. J. and M. O. Andreae (1990). "Biomass burning in the tropics: Impact on atmospheric chemistry and biogeochemical cycles." Science **250**(4988): 1669-1678.

Curran, M. A. J., T. D. van Ommen and V. Morgan (1998). "Seasonal characteristics of the major ions in the high accumulation DSS ice core, Law Dome, Antarctica." Annals of Glaciology **22**(8): 83-794.

Daly, C., R. P. Neilson and D. L. Phillips (1994). "A statistical topographic model for mapping climatological precipitation over mountainous terrain." Journal of Applied Meteorology **33**(2): 140-158.

Davis, C. H., Y. H. Li, J. R. McConnell, M. M. Frey and E. Hanna (2005). "Snowfall-driven growth in East Antarctic ice sheet mitigates recent sea-level rise." Science **308**(5730): 1898-1901.

DeBano, L. F., D. G. Neary and P. F. Ffolliott (1998). Fire ecology; Wildfires; Soil ecology; Fire management; Ecosystem management New York, J. Wiley.

Delmas, R. J., M. Legrand, A. J. Aristarain and F. Zanolini (1985). "Volcanic deposits in Antarctic snow and ice." Journal of Geophysical Research-Atmospheres **90**(D7): 2901-2920.

Dickens, A. F., Y. Gélinas and J. I. Hedges (2004). "Physical separation of combustion and rock sources of graphitic black carbon in sediments." Marine Chemistry **92**(1-4): 215-223.

Dickens, A. F., Y. Gelinas, C. A. Masiello, S. Wakeham and J. I. Hedges (2004). "Reburial of fossil organic carbon in marine sediments." Nature **427**(6972): 336-339.

Dittmar, T. (2008). "The molecular level determination of black carbon in marine dissolved organic matter." Organic Geochemistry **39**(4): 396-407.

Dube, O. P. (2009). "Linking fire and climate: interactions with land use, vegetation, and soil." Current Opinion in Environmental Sustainability **1**(2): 161-169.

Duncan, B. N., R. V. Martin, A. C. Staudt, R. Yevich and J. A. Logan (2003). "Interannual and seasonal variability of biomass burning emissions constrained by satellite observations." Journal of Geophysical Research **108**(D2): 4100.

Elmquist, M., G. Cornelissen, Z. Kukulska and Ö. Gustafsson (2006). "Distinct oxidative stabilities of char versus soot black carbon: Implications for quantification and environmental recalcitrance." Global Biogeochemical Cycles **20**(2): GB2009.

Elmquist, M., I. Semiletov, L. D. Guo and O. Gustafsson (2008). "Pan-Arctic patterns in black carbon sources and fluvial discharges deduced from radiocarbon and PAH source apportionment markers in estuarine surface sediments." Global Biogeochemical Cycles **22**(2): -.

Elmquist, M., Z. Zencak and O. Gustafsson (2007). "A 700 Year Sediment Record of Black Carbon and Polycyclic Aromatic Hydrocarbons near the EMEP Air Monitoring Station in Aspvreten, Sweden." Environmental Science & Technology **41**(20): 6926-6932.

Elmquist, M. G., O.; Andersson, P. (2004). "Quantification of sedimentary black carbon using the chemothermal oxidation method: an evaluation of ex situ pretreatments and standard additions approaches." Limnology Oceanography -Methods **2**: 417−427.

Faïn, X., C. P. Ferrari, et al. (2009). "Polar firn air reveals large-scale impact of anthropogenic mercury emissions during the 1970s." Proceedings of the National Academy of Sciences **106**(38): 16114-16119.

Falk, D. A., E. K. Heyerdahl, P. M. Brown, T. W. Swetnam, E. K. Sutherland, Z. Gedalof, L. Yocom and T. J. Brown (2010). " Fire and climate variation in western North America from fire-scar and tree-ring networks." PAGES news **18**(2): 70-72.

Feingold, G., H. Jiang and J. Y. Harrington (2005). "On smoke suppression of clouds in Amazonia." Geophysical Research Letters **32**(2): L02804.

Ferretti, D. F., J. B. Miller, et al. (2005). "Unexpected Changes to the Global Methane Budget over the Past 2000 Years." Science **309**(5741): 1714-1717.

Flanner, M. G., C. S. Zender, J. T. Randerson and P. J. Rasch (2007). "Present-day climate forcing and response from black carbon in snow." Journal of Geophysical Research-Atmospheres **112**(D11): 17.

Flannigan, M. D., M. A. Krawchuk, W. J. de Groot, B. M. Wotton and L. M. Gowman (2009). "Implications of changing climate for global wildland fire." International Journal of Wildland Fire **18**(5): 483-507.

Flores-Cervantes, D. X., D. L. Plata, J. K. MacFarlane, C. M. Reddy and P. M. Gschwend (2009). "Black carbon in marine particulate organic carbon: Inputs and cycling of highly recalcitrant organic carbon in the Gulf of Maine." Marine Chemistry **113**(3-4): 172-181.

Forbes, M. S., R. J. Raison and J. O. Skjemstad (2006). "Formation, transformation and transport of black carbon (charcoal) in terrestrial and aquatic ecosystems." Science of the Total Environment **370**(1): 190-206.

Fountain, A. G., T. A. Neumann, P. L. Glenn and T. Chinn (2004). "Can climate warming induce glacier advance in Taylor Valley, Antarctica?" Journal of Glaciology **50**(171): 556-564.

Fraser, M. P. and K. Lakshmanan (2000). "Using levoglucosan as a molecular marker for the long-range transport of biomass combustion aerosols." Environmental Science & Technology **34**(21): 4560-4564.

Frezzotti, M., M. Pourchet, et al. (2005). "Spatial and temporal variability of snow accumulation in East Antarctica from traverse data." Journal of Glaciology **51**(172): 113-124.

Frezzotti, M., S. Urbini, M. Proposito, C. Scarchilli and S. Gandolfi (2007). "Spatial and temporal variability of surface mass balance near Talos Dome, East Antarctica." Journal of Geophysical Research-Earth Surface **112**(F2).

Gao, C., A. Robock, et al. (2006). "The 1452 or 1453 AD Kuwae eruption signal derived from multiple ice core records: Greatest volcanic sulfate event of the past 700 years." Journal of Geophysical Research-Atmospheres **111**(D12).

Gavin, D. G., D. J. Hallett, F. S. Hu, K. P. Lertzman, S. J. Prichard, K. J. Brown, J. A. Lynch, P. Bartlein and D. L. Peterson (2007). "Forest fire and climate change in western North

America: insights from sediment charcoal records." Frontiers in Ecology and the Environment **5**(9): 499-506.

Genthon, C. and G. Krinner (2001). "Antarctic surface mass balance and systematic biases in general circulation models." Journal of Geophysical Research-Atmospheres **106**(D18): 20653-20664.

Genthon, C., O. Magand, G. Krinner and M. Fily (2009). "Do climate models underestimate snow accumulation on the Antarctic plateau? A re-evaluation of/from in situ observations in East Wilkes and Victoria Lands." Annals of Glaciology **50**(50): 61-65.

Ghil, M., M. R. Allen, et al. (2002). "Advanced spectral methods for climatic time series." Review of Geophysics **40**(1): 1003.

Gillett, N. P., A. J. Weaver, F. W. Zwiers and M. D. Flannigan (2004). "Detecting the effect of climate change on Canadian forest fires." Geophysical Research Letters **31**(18): L18211.

Giovinetto, M. B. and H. J. Zwally (2000). Spatial distribution of net surface accumulation on the Antarctic ice sheet. Annals of Glaciology, Vol 31, 2000. K. Steffen. **31:** 171-178.

Glassman, I. (1996). "Environmental Combustion Considerations." Combustion (3rd ed.), Academic Press, San Diego.

Goodwin, I. D., T. D. van Ommen, M. A. J. Curran and P. A. Mayewski (2004). "Mid latitude winter climate variability in the South Indian and southwest Pacific regions since 1300 AD." Climate Dynamics **22**(8): 783-794.

Govaerts, Y. M., J. M. Pereira, B. Pinty and B. Mota (2002). "Impact of fires on surface albedo dynamics over the African continent." Journal of Geophysical Research **107**(D22): 4629.

Grenfell, T. C., D. K. Perovich and J. A. Ogren (1981). "Spectral albedos of an alpine snowpack." Cold Regions Science and Technology **4**(2): 121-127.

Grenfell, T. C., S. G. Warren and P. C. Mullen (1994). "Reflection of solar-radiation by the Antarctic snow surface at ultraviolet, visible, and near-infrared wavelenghts." Journal of Geophysical Research-Atmospheres **99**(D9): 18669-18684.

Gustafsson, O. and P. M. Gschwend (1998). "The flux of black carbon to surface sediments on the New England continental shelf." Geochimica Et Cosmochimica Acta **62**(3): 465-472.

Gustafsson, O., F. Haghseta, C. Chan, J. MacFarlane and P. M. Gschwend (1997). "Quantification of the dilute sedimentary soot phase: Implications for PAH speciation and bioavailability." Environmental Science & Technology **31**(1): 203-209.

Hadley, O. L., Corrigan, C. E., Kirchstetter, T. W., Cliff, S. S., Ramanathan, V. (2010). "Measured black carbon deposition on the Sierra Nevada snow pack and implication for snow pack retreat." Atmospheric Chemistry and Physics **10**(15).

Hamer, U., B. Marschner, S. Brodowski and W. Amelung (2004). "Interactive priming of black carbon and glucose mineralization." Organic Geochemistry **35**(7): 823-830.

Hammer, C. U., H. B. Clausen and H. Tauber (1986). "Ice-core dating of the Pleistocene-Holocene boundary applied to a calibration of the C-14 time scale." Radiocarbon **28**(2A): 284-291.

Hansen, J. and L. Nazarenko (2004). "Soot climate forcing via snow and ice albedos." Proceedings of the National Academy of Sciences of the United States of America **101**(2): 423-428.

Harrison, S. P., J. R. Marlon and P. J. Bartlein (2010). Fire in the Earth System. Changing Climates, Earth Systems and Society. J. Dodson, Springer Netherlands**:** 21-48.

Helsen, M. M., M. R. van den Broeke, R. S. W. van de Wal, W. J. van de Berg, E. van Meijgaard, C. H. Davis, Y. Li and I. Goodwin (2008). "Elevation changes in Antarctica mainly determined by accumulation variability." Science **320**(5883): 1626-1629.

Heyvaert, A. C., J. E. Reuter, D. G. Slotton and C. R. Goldman (2000). "Paleolimnological reconstruction of historical atmospheric lead and mercury deposition at Lake Tahoe, California-Nevada." Environmental Science & Technology **34**(17): 3588-3597.

Hockaday, W. C., A. M. Grannas, S. Kim and P. G. Hatcher (2007). "The transformation and mobility of charcoal in a fire-impacted watershed." Geochimica Et Cosmochimica Acta **71**(14): 3432-3445.

Hofstede, C. M., R. S. W. van de Wal, et al. (2004). "Firn accumulation records for the past 1000 years on the basis of dielectric profiling of six cores from Dronning Maud Land, Antarctica." Journal of Glaciology **50**(169): 279-291.

Horwath, M. and R. Dietrich (2009). "Signal and error in mass change inferences from GRACE: the case of Antarctica." Geophysical Journal International **177**(3): 849-864.

Houghton, R. A. (2003). "Revised estimates of the annual net flux of carbon to the atmosphere from changes in land use and land management 1850–2000." Tellus Series B-Chemical and Physical Meteorology **55**(2): 378-390.

Hwang, Y. S. and Q. Li (2010). "Characterizing Photochemical Transformation of Aqueous nC60 under Environmentally Relevant Conditions." Environmental Science & Technology **44**(8): 3008-3013.

IPCC (2007). Climate change 2007: The Physical Science Basis. Contribution of working group I to the fourth assessment report of the Intergovernmental Panel on Climate Change. Climate Change 2007: . S. Solomon, D.Qin, M. Manninget al. Cambridge, United Kingdom and New York, NY, USA., Cambridge University Press

Isaksson, E., M. van den Broeke, J.-G. Winther, L. Karlöf, J. Pinglot and N. Gundestrup (1999). "Accumulation and proxy-temperature variability in Dronning Maud Land, Antarctica, determined from shallow firn cores." Annals of Glaciology **29**: 17-22.

Isaksson, E., M. R. van den Broeke, J. G. Winther, L. Karlof, J. F. Pinglot and N. Gundestrup (1999). Accumulation and proxy-temperature variability in Dronning Maud Land, Antarctica, determined from shallow firn cores. Annals of Glaciology, Vol 29, 1999. T. H. Jacka. **29:** 17-22.

Ishiguro, T., Y. Takatori and K. Akihama (1997). "Microstructure of diesel soot particles probed by electron microscopy: First observation of inner core and outer shell." Combustion and Flame **108**(1-2): 231-234.

Ito, A. and J. E. Penner (2004). "Global estimates of biomass burning emissions based on satellite imagery for the year 2000." Journal of Geophysical Research **109**(D14): D14S05.

Ito, A. and J. E. Penner (2005). "Historical emissions of carbonaceous aerosols from biomass and fossil fuel burning for the period 1870-2000." Global Biogeochemical Cycles **19**(2): GB2028.

Jacobson, M. Z. (2001). "Strong radiative heating due to the mixing state of black carbon in atmospheric aerosols." Nature **409**(6821): 695-697.

Jansen, K. L., T. V. Larson, J. Q. Koenig, T. F. Mar, C. Fields, J. Stewart and M. Lippmann (2005). "Associations between Health Effects and Particulate Matter and Black Carbon in Subjects with Respiratory Disease." Environmental Health Perspectives **113**(12): 1741-1746.

Jassby, A. D., C. R. Goldman, J. E. Reuter and R. C. Richards (1999). "Origins and scale dependence of temporal variability in the transparency of Lake Tahoe, California-Nevada." Limnology and Oceanography **44**(2): 282-294.

Jouzel, J., V. Masson-Delmotte, et al. (2007). "Orbital and Millennial Antarctic Climate Variability over the Past 800,000 Years." Science **317**(5839): 793-796.

Jouzel, J., L. Merlivat, M. Pourchet and C. Lorius (1979). "A continuous record of artificial tritium fallout at the South Pole (1954-1978)." Earth and Planetary Science Letters **45**(1): 188-200.

Justice, C. O., L. Giglio, et al. (2002). "The MODIS fire products." Remote Sensing of Environment **83**(1-2): 244-262.

Karlöf, L., J. G. Winther, et al. (2000). "A 1500 year record of accumulation at Amundsenisen western Dronning Maud Land, Antarctica, derived from electrical and radioactive measurements on a 120 m ice core." Journal of Geophysical Research-Atmospheres **105**(D10): 12471-12483.

Kasischke, E. S., N. L. Christensen and B. J. Stocks (1995). "Fire, Global Warming, and the Carbon Balance of Boreal Forests." Ecological Applications **5**(2): 437-451.

Kaspari, S. D., M. Schwikowski, M. Gysel, M. G. Flanner, S. Kang, S. Hou and P. A. Mayewski (2011). "Recent increase in black carbon concentrations from a Mt. Everest ice core spanning 1860-2000 AD." Geophysical Research Letters **38**(L04703).

Kaufman, Y. J. and I. Koren (2006). "Smoke and pollution aerosol effect on cloud cover." Science **313**(5787): 655-658.

Kim, S. W., L. A. Kaplan, R. Benner and P. G. Hatcher (2004). "Hydrogen-deficient molecules in natural riverine water samples - evidence for the existence of black carbon in DOM." Marine Chemistry **92**(1-4): 225-234.

Kirchstetter, T. W. and T. Novakov (2007). "Controlled generation of black carbon particles from a diffusion flame and applications in evaluating black carbon measurement methods." Atmospheric Environment **41**(9): 1874-1888.

Kitzberger, T., P. M. Brown, E. K. Heyerdahl, T. W. Swetnam and T. T. Veblen (2007). "Contingent Pacificâ€“Atlantic Ocean influence on multicentury wildfire synchrony over western North America." Proceedings of the National Academy of Sciences **104**(2): 543-548.

Kochtubajda, B., M. Flanningan, J. Gyakum, R. Stewart, K. Logan and T. Nhuyen (2009). "Lightning and Fires in the Northwest Territories and Responses to Future Climate Change." ARCTIC, North America, **59**: 211-221.

Koelmans, A. A., B. Nowack and M. R. Wiesner (2009). "Comparison of manufactured and black carbon nanoparticle concentrations in aquatic sediments." Environmental Pollution **157**(4): 1110-1116.

Koren, I., Y. J. Kaufman, L. A. Remer and J. V. Martins (2004). "Measurement of the Effect of Amazon Smoke on Inhibition of Cloud Formation." Science **303**(5662): 1342-1345.

Krawchuk, M. A. and M. A. Moritz (2011). "Constraints on global fire activity vary across a resource gradient." Ecology **92**(1): 121-132.

Krebs, P., G. Pezzatti, S. Mazzoleni, L. Talbot and M. Conedera (2010). "Fire regime: history and definition of a key concept in disturbance ecology." Theory in Biosciences **129**(1): 53-69.

Kuhlbusch, T. A. J. (1995). "Method for determining black carbon in residues of vegetation fires." Environmental Science & Technology **29**(10): 2695-2702.

Kuhlbusch, T. A. J. (1998). "Black carbon and the carbon cycle." Science **280**(5371): 1903-1904.

Kuhlbusch, T. A. J. and P. J. Crutzen (1995). "Toward a global estimate of black carbon in residues of vegetation fires representing a sink of atmospheric CO2 and a source of O2 " Global Biogeochemical Cycles **9**(4): 491-501.

Lamarque, J. F., T. C. Bond, et al. (2010). "Historical (1850-2000) gridded anthropogenic and biomass burning emissions of reactive gases and aerosols: methodology and application." Atmospheric Chemistry and Physics **10**(15): 7017-7039.

Lambert, F., B. Delmonte, et al. (2008). "Dust-climate couplings over the past 800,000 years from the EPICA Dome C ice core." Nature **452**(7187): 616-619.

Langmann, B., B. Duncan, C. Textor, J. Trentmann and G. R. van der Werf (2009). "Vegetation fire emissions and their impact on air pollution and climate." Atmospheric Environment **43**(1): 107-116.

Langway, C. C., K. Osada, H. B. Clausen, C. U. Hammer and H. Shoji (1995). "A 10-century comparison of prominent bipolar volcanic events in ice cores." Journal of Geophysical Research-Atmospheres **100**(D8): 16241-16247.

Larson, G. L., R. Collier and M. W. Buktenica (2007). "Long-term limnological research and monitoring at Crater Lake, Oregon." Hydrobiologia **574**: 1-11.

Law, K. S. and A. Stohl (2007). "Arctic Air Pollution: Origins and Impacts." Science **315**(5818): 1537-1540.

Lee, J., M. Cho, J. D. Fortner, J. B. Hughes and J.-H. Kim (2009). "Transformation of Aggregated C60 in the Aqueous Phase by UV Irradiation." Environmental Science & Technology **43**(13): 4878-4883.

Legrand, M. and R. J. Delmas (1987). "A 220-year continuous record of volcanic H2SO4 in the Antarctic ice-sheet." Nature **327**(6124): 671-676.

Legrand, M. and P. Mayewski (1997). "Glaciochemistry of polar ice cores: A review." Rev. Geophys. **35**(3): 219-243.

Lehmann, J., J. Skjemstad, S. Sohi, J. Carter, M. Barson, P. Falloon, K. Coleman, P. Woodbury and E. Krull (2008). "Australian climate-carbon cycle feedback reduced by soil black carbon." Nature Geoscience **1**(12): 832-835.

Lewis, K., W. P. Arnott, H. Moosmüller and C. E. Wold (2008). "Strong spectral variation of biomass smoke light absorption and single scattering albedo observed with a novel dual-wavelength photoacoustic instrument." J. Geophys. Res. **113**(D16203).

Li, J., S.-P. Xie, E. R. Cook, G. Huang, R. D'Arrigo, F. Liu, J. Ma and X.-T. Zheng (2011). "Interdecadal modulation of El Nino amplitude during the past millennium." Nature Climate Change **1**(2): 114-118.

Li, Y., J. Cole-Dai and L. Zhou (2009). "Glaciochemical evidence in an East Antarctica ice core of a recent (AD 1450-1850) neoglacial episode." Journal of Geophysical Research-Atmospheres **114**.

Limpert, E., W. A. Stahel and M. Abbt (2001). "Log-normal Distributions across the Sciences: Keys and Clues." BioScience **51**(5): 341-352.

Liousse, C., B. Guillaume, et al. (2010). "Updated African biomass burning emission inventories in the framework of the AMMA-IDAF program, with an evaluation of combustion aerosols." Atmospheric Chemistry and Physics **10**(19): 9631.

Liu, X., B. Xu, T. Yao, N. Wang and G. Wu (2008). "Carbonaceous particles in Muztag Ata ice core, West Kunlun Mountains, China." Chinese. Sci. Bull. **53**(21): 3379-3386.

Lohmann, R., K. Bollinger, M. Cantwell, J. Feichter, I. Fischer-Bruns and M. Zabel (2009). "Fluxes of soot black carbon to South Atlantic sediments." Global Biogeochemical Cycles **23**: 13.

Lohmann, R., K. Bollinger, M. Cantwell, J. Feichter, I. Fischer-Bruns and M. Zabel (2009). "Fluxes of soot black carbon to South Atlantic sediments." Global Biogeochemical Cycles **23**.

Lorius, C., J. Jouzel and D. Raynaud (1993). "Glacials-interglacials in Vostok: climate and greenhouse gases." Global and Planetary Change **7**(1-3): 131-143.

Magand, O., C. Genthon, M. Fily, G. Krinner, G. Picard, M. Frezzotti and A. A. Ekaykin (2007). "An up-to-date quality-controlled surface mass balance data set for the 90 degrees-180 degrees E Antarctica sector and 1950-2005 period." Journal of Geophysical Research-Atmospheres **112**(D12).

Mann, H. B. (1945). "Nonparametric tests against trend." Econometrica **13**: 245-259.

Mannino, A. and H. R. Harvey (2004). "Black carbon in estuarine and coastal ocean dissolved organic matter." Limnology and Oceanography **49**(3): 735-740.

Marlon, J. R., P. J. Bartlein, C. Carcaillet, D. G. Gavin, S. P. Harrison, P. E. Higuera, F. Joos, M. J. Power and I. C. Prentice (2008). "Climate and human influences on global biomass burning over the past two millennia." Nature Geoscience **1**(10): 697-702.

Martin, D. A. and J. A. Moody (2001). "Comparison of soil infiltration rates in burned and unburned mountainous watersheds." Hydrological Processes **15**(15): 2893-2903.

Masiello, C. A. (2004). "New directions in black carbon organic geochemistry." Marine Chemistry **92**(1-4): 201-213.

Masiello, C. A. and E. R. M. Druffel (1998). "Black carbon in deep-sea sediments." Science **280**(5371): 1911-1913.

McConnell, J. R. (2010). "New Directions: Historical black carbon and other ice core aerosol records in the Arctic for GCM evaluation." Atmospheric Environment **44**(21-22): 2665-2666.

McConnell, J. R., A. J. Aristarain, J. R. Banta, P. R. Edwards and J. C. Simões (2007). "20th-Century doubling in dust archived in an Antarctic Peninsula ice core parallels climate change and desertification in South America." Proceedings of the National Academy of Sciences **104**(14): 5743-5748.

McConnell, J. R., R. Edwards, et al. (2007). "20th-century industrial black carbon emissions altered arctic climate forcing." Science **317**(5843): 1381-1384.

McConnell, J. R., G. W. Lamorey, S. W. Lambert and K. C. Taylor (2002). "Continuous Ice-Core Chemical Analyses Using Inductively Coupled Plasma Mass Spectrometry." Environmental Science & Technology **36**(1): 7-11.

McConnell, J. R., R. Edwards and R. Banta (2005). A novel method for high-resolution, broad spectrum ice core analyses using ICP-OES and dual HR-ICP-MS. European Geophysical Society XXX General Assembly, Geophysical Research Abstracts.

Meese, D. A., A. J. Gow, P. Grootes, M. Stuiver, P. A. Mayewski, G. A. Zielinski, M. Ram, K. C. Taylor and E. D. Waddington (1994). "The Accumulation Record from the GISP2 Core as an Indicator of Climate Change Throughout the Holocene." Science **266**(5191): 1680-1682.

Middelburg, J. J., J. Nieuwenhuize and P. van Breugel (1999). "Black carbon in marine sediments." Marine Chemistry **65**(3-4): 245-252.

Mieville, A., C. Granier, C. Liousse, B. Guillaume, F. Mouillot, J. F. Lamarque, J. M. Grégoire and G. Pétron (2010). "Emissions of gases and particles from biomass burning during the 20th century using satellite data and an historical reconstruction." Atmospheric Environment **44**(11): 1469-1477.

Ming, J., H. Cachier, C. Xiao, D. Qin, S. Kang, S. Hou and J. Xu (2008). "Black carbon record based on a shallow Himalayan ice core and its climatic implications." Atmospheric Chemistry and Physics **8**(5): 1343-1352.

Mitra, S., T. S. Bianchi, B. A. McKee and M. Sutula (2002). "Black carbon from the Mississippi River: Quantities, sources, and potential implications for the global carbon cycle." Environmental Science & Technology **36**(11): 2296-2302.

Moermond, C. T. A., J. J. G. Zwolsman and A. A. Koelmans (2005). "Black carbon and ecological factors affect in situ biota to sediment accumulation factors for hydrophobic organic compounds in flood plain lakes." Environmental Science & Technology **39**(9): 3101-3109.

Monaghan, A. J., D. H. Bromwich, et al. (2006). "Insignificant change in Antarctic snowfall since the International Geophysical Year." Science **313**(5788): 827-831.

Moore, J. C., H. Narita and N. Maeno (1991). "A continuous 770-years record of volcanic activity from East Antarctica." Journal of Geophysical Research-Atmospheres **96**(D9): 17353-17359.

Moosmüller, H., R. K. Chakrabarty and W. P. Arnott (2009). "Aerosol light absorption and its measurement: A review." Journal of Quantitative Spectroscopy and Radiative Transfer **110**(11): 844-878.

Morgan, V., M. Delmotte, T. van Ommen, J. Jouzel, J. r. m. Chappellaz, S. Woon, V. r. Masson-Delmotte and D. Raynaud (2002). "Relative Timing of Deglacial Climate Events in Antarctica and Greenland." Science **297**(5588): 1862-1864.

Morgan, V. I., I. D. Goodwin, D. M. Etheridget and C. W. Wookey (1991). "Evidence from Antarctic ice cores for recent increases in snow accumulation." Nature **354**(6348): 58-60.

Morgan, V. I., C. W. Wookey, J. Li, T. D. vanOmmen, W. Skinner and M. F. Fitzpatrick (1997). "Site information and initial results from deep ice drilling on Law dome, Antarctica." Journal of Glaciology **43**(143): 3-10.

Moriondo, M., P. Good, R. Durao, M. Bindi, C. Giannakopoulos and J. Corte-Real (2006). "Potential impact of climate change on fire risk in the Mediterranean area." Journal Climate Research **31**(1): 85-95.

Mosley-Thompson, E., J. F. Paskievitch, A. J. Gow and L. G. Thompson (1999). "Late 20th Century increase in South Pole snow accumulation." Journal of Geophysical Research-Atmospheres **104**(D4): 3877-3886.

Moteki, N. and Y. Kondo (2007). "Effects of mixing state on black carbon measurements by laser-induced incandescence." Aerosol Science and Technology **41**(4): 398-417.

Moteki, N. and Y. Kondo (2010). "Dependence of Laser-Induced Incandescence on Physical Properties of Black Carbon Aerosols: Measurements and Theoretical Interpretation." Aerosol Science and Technology **44**(8): 663-675.

Mouillot, F. and C. B. Field (2005). Fire history and the global carbon budget: a 1°× 1° fire history reconstruction for the 20th century, Blackwell Science Ltd. **11:** 398-420.

Müller, K., S.-E. Hamran, A. Sinisalo and J.-O. Hagen (2010). "L-band microwave penetration depth in polar snow, firn, and ice." Submitted to Transactions on Geoscience and Remote Sensing.

Müller, K., A. Sinisalo, H. Anschuetz, S.-E. Hamran, J.-O. Hagen, J. R. McConnell and D. R. Pasteris (Submitted). "An 860 km surface mass-balance profile on the East Antarctic plateau derived by GPR." Annals of Glaciology **51**(55): 1-8.

Muri, G., B. Cermelj, J. Faganeli and J. Holc (2002). "Determination of black carbon in lacustrine and coastal marine sediments by thermal oxidation." Acta Chimica Slovenica **49**(1): 29-42.

Neary, D. G., C. C. Klopatek, L. F. DeBano and P. F. Ffolliott (1999). "Fire effects on belowground sustainability: a review and synthesis." Forest Ecology and Management **122**(1-2): 51-71.

Nguyen, B. T. and J. Lehmann (2009). "Black carbon decomposition under varying water regimes." Organic Geochemistry **40**(8): 846-853.

Nguyen, B. T., J. Lehmann, W. C. Hockaday, S. Joseph and C. A. Masiello (2010). "Temperature Sensitivity of Black Carbon Decomposition and Oxidation." Environmental Science & Technology **44**(9): 3324-3331.

Nguyen, T. H., R. A. Brown and W. P. Ball (2004). "An evaluation of thermal resistance as a measure of black carbon content in diesel soot, wood char, and sediment." Organic Geochemistry **35**(3): 217-234.

Nitschke, C. R. and J. L. Innes (2008). "Climatic change and fire potential in South-Central British Columbia, Canada." Global Change Biology **14**(4): 841-855.

Oerter, H., F. Wilhelms, F. Jung-Rothenhausler, F. Goktas, H. Miller, W. Graf and S. Sommer (2000). Accumulation rates in Dronning Maud Land, Antarctica, as revealed by dielectric-profiling measurements of shallow firn cores. Annals of Glaciology, Vol 30, 2000. K. Hutter. **30:** 27-34.

Önöz, B. and M. Bayazit (2003). "The Power of Statistical Tests for Trend Detection." Turkish J. Eng. Env. Sci. **27**: 247-251.

Outridge, H. Sanei, Stern, Hamilton and F. Goodarzi (2007). "Evidence for Control of Mercury Accumulation Rates in Canadian High Arctic Lake Sediments by Variations of Aquatic Primary Productivity." Environmental Science & Technology **41**(15): 5259-5265.

Pace, G., D. Meloni and A. di Sarra (2005). "Forest fire aerosol over the Mediterranean basin during summer 2003." Journal of Geophysical Research **110**(D21): D21202.

Paillard, D., L. Labeyrie, and P. Yiou (1996). "Macintosh program performs time-series analysis." Eos Trans. AGU **77**(39): 379.

Palmer, A. S., T. D. van Ommen, M. A. J. Curran, V. Morgan, J. M. Souney and P. A. Mayewski (2001). "High-precision dating of volcanic events - (AD 1301-1995) using ice cores from Law Dome, Antarctica." Journal of Geophysical Research-Atmospheres **106**(D22): 28089-28095.

Parrenin, F., J.-M. Barnola, et al. (2007). "The EDC3 chronology for the EPICA Dome C ice core." Climate of the Past **3**(3): 485-497.

Penner, J. E., S. Y. Zhang, et al. (2002). "A comparison of model -and satellite-derived aerosol optical depth and reflectivity." J. Atmos. Sci. **59**: 441-460.

Pessenda, L. C. R., S. E. M. Gouveia and R. Aravena (2001). " Radiocarbon dating of total soil organic matter and humin fraction, and comparison with 14C ages of fossil charcoal." Radiocarbon **43**(2): 561-567.

Picciotto, E., G. Grozaz and W. d. Breuck (1971). "Accumulation on the South Pole Queen Maud Land Traverse, 1964-1968. Antarctic Snow and Ice Studies II. ." Antarc. Res. Ser.(16): 257-315.

Podgorny, I. A., F. Li and V. Ramanathan (2003). "Large Aerosol Radiative Forcing due to the 1997 Indonesian Forest Fire." Geophysical Research Letters **30**(1): 1028.

Pomeroy, J. W., T. D. Davies, H. G. Jones, P. Marsh, N. E. Peters and M. Tranter (1999). "Transformations of snow chemistry in the boreal forest: accumulation and volatilization." Hydrological Processes **13**(14-15): 2257-2273.

Posfai, M. l. and P. R. Buseck (2010). "Nature and Climate Effects of Individual Tropospheric Aerosol Particles." Annual Review of Earth and Planetary Sciences **38**(1): 17-43.

Preece, N. (2002). "Aboriginal fires in monsoonal Australia from historical accounts." Journal of Biogeography **29**(3): 321-336.

Pyne, S. J. (2001). "The Fires This Time, and Next." Science **294**(5544): 1005-1006.

Raisbeck, G. M., F. Yiou, O. Cattani and J. Jouzel (2006). "10Be evidence for the Matuyama-Brunhes geomagnetic reversal in the EPICA Dome C ice core." Nature **444**(7115): 82-84.

Ramanathan, V. and G. Carmichael (2008). "Global and regional climate changes due to black carbon." Nature Geoscience **1**(4): 221-227.

Ramanathan, V., P. J. Crutzen, J. T. Kiehl and D. Rosenfeld (2001). "Atmosphere - Aerosols, climate, and the hydrological cycle." Science **294**(5549): 2119-2124.

Reid, J. S., R. Koppmann, T. F. Eck and D. P. Eleuterio (2005). "A review of biomass burning emissions part II: intensive physical properties of biomass burning particles." Atmospheric Chemistry and Physics **5**: 799-825.

Ren, J., C. Li, S. Hou, C. Xiao, D. Qin, Y. Li and M. Ding (2010). "A 2680 year volcanic record from the DT-401 East Antarctic ice core." Journal of Geophysical Research-Atmospheres **115**.

Ren, J. W., J. Y. Sun and D. H. Qin (2004). Preliminary results of ionic concentrations in snow pits along the Zhongshan-Dome A traverse route, Antarctica. Annals of Glaciology, Vol 39, 2005. J. Jacka. **39:** 155-160.

Richardson, C., E. Aarholt, S. E. Hamran, P. Holmlund and E. Isaksson (1997). "Spatial distribution of snow in western Dronning Maud Land, East Antarctica, mapped by a ground-based snow radar." Journal of Geophysical Research-Solid Earth **102**(B9): 20343-20353.

Rignot, E., J. L. Bamber, M. R. Van Den Broeke, C. Davis, Y. Li, W. J. Van De Berg and E. Van Meijgaard (2008). "Recent Antarctic ice mass loss from radar interferometry and regional climate modelling." Nature Geoscience **1**(2): 106-110.

Russell-Smith, J., C. P. Yates, et al. (2007). "Bushfires 'down under': patterns and implications of contemporary Australian landscape burning." International Journal of Wildland Fire **16**(4): 361-377

Savarino, J. and M. Legrand (1998). "High northern latitude forest fires and vegetation emissions over the last millennium inferred from the chemistry of a central Greenland ice core." Journal of geophysical Research Atmospheres **103**(D7): 8267-8279.

Schmidt, M. W. I. and A. G. Noack (2000). "Black carbon in soils and sediments: Analysis, distribution, implications, and current challenges." Global Biogeochemical Cycles **14**(3): 777-793.

Schmidt, M. W. I., J. O. Skjemstad, C. I. Czimczik, B. Glaser, K. M. Prentice, Y. Gelinas and T. A. J. Kuhlbusch (2001). "Comparative analysis of black carbon in soils." Global Biogeochemical Cycles **15**(1): 163-167.

Schmidt, M. W. I., J. O. Skjemstad, E. Gehrt and I. Kögel-Knabner (1999). "Charred organic carbon in German chernozemic soils." European Journal of Soil Science **50**(2): 351-365.

Schneider, J., U. Kirchner, S. Borrmann, R. Vogt and V. Scheer (2008). "In situ measurements of particle number concentration, chemically resolved size distributions and black carbon content of traffic-related emissions on German motorways, rural roads and in city traffic." Atmospheric Environment **42**(18): 4257-4268.

Schultz, M. G., A. Heil, J. J. Hoelzemann, A. Spessa, K. Thonicke, J. G. Goldammer, A. C. Held, J. M. C. Pereira and M. van het Bolscher (2008). "Global wildland fire emissions from 1960 to 2000." Global Biogeochemical Cycles **22**(2): GB2002.

Schwarz, J. P., R. S. Gao, et al. (2006). "Single-particle measurements of midlatitude black carbon and light-scattering aerosols from the boundary layer to the lower stratosphere." Journal of Geophysical Research-Atmospheres **111**(D16): 15.

Schwarz, J. P., J. R. Spackman, et al. (2010). "The Detection Efficiency of the Single Particle Soot Photometer." Aerosol Science and Technology **44**(8): 612-628.

Schwarz, J. P., J. R. Spackman, R. S. Gao, L. A. Watts, P. Stier, M. Schulz, S. M. Davis, S. C. Wofsy and D. W. Fahey (2010). "Global-scale black carbon profiles observed in the remote atmosphere and compared to models." Geophys. Res. Lett. **37**(18): L18812.

Scott, A. C. (1989). "Observations on the nature and origin of fusain." International Journal of Coal Geology **12**(1-4): 443-475.

Scotter, D. (1970). "Soil temperatures under grass fires." Soil Research **8**(3): 273-279.

Seiler, W. and P. J. Crutzen (1980). "Estimates of gross and net fluxes of carbon between the biosphere and the atmosphere from biomass burning." Climatic Change **2**(3): 207-247.

Seinfeld (1998). Atmospheric chemistry and physics: From air pollution to climate change. New York, Wiley.

Seinfeld, J. (2008). "Atmospheric science - Black carbon and brown clouds." Nature Geoscience **1**(1): 15-16.

Shneour, E. A. (1966). "Oxidation of Graphitic Carbon in Certain Soils." Science **151**(3713): 991-992.

Shrestha, G., S. J. Traina and C. W. Swanston (2010). " Black Carbon's Properties and Role in the Environment: A Comprehensive Review." Sustainability **2(1)**: 294-320.

Simpson, M. J. and P. G. Hatcher (2004). "Determination of black carbon in natural organic matter by chemical oxidation and solid-state 13C nuclear magnetic resonance spectroscopy." Organic Geochemistry **35**(8): 923-935.

Singer, B. S., H. Guillou, B. R. Jicha, C. Laj, C. Kissel, B. L. Beard and C. M. Johnson (2009). "40Ar/39Ar, K-Ar and 230Th-238U dating of the Laschamp excursion: A radioisotopic tie-point for ice core and climate chronologies." Earth and Planetary Science Letters **286**(1-2): 80-88.

Skeie, R. B., T. Berntsen, G. Myhre, C. A. Pedersen, J. Ström, S. Gerland and J. A. Ogren (2011). "Black carbon in the atmosphere and snow, from pre-industrial times until present." Atmos. Chem. Phys. **11**(14): 6809- 6836.

Skjemstad, J., P. Clarke, J. Taylor, J. Oades and S. Mcclure (1996). "The chemistry and nature of protected carbon in soil." Australian Journal of Soil Research **34**(2): 251-271.

Slowik, J. G., E. S. Cross, et al. (2007). "An inter-comparison of instruments measuring black carbon content of soot particles." Aerosol Science and Technology **41**(3): 295-314.

Sneed, S. B., P. A. Mayewski and D. A. Dixon (2011). "An emerging technique: multi-ice-core multi-parameter correlations with Antarctic sea-ice extent." Annals of Glaciology **52**(57): 347-354.

Sodemann, H. and A. Stohl (2009). "Asymmetries in the moisture origin of Antarctic precipitation." Geophys. Res. Lett. **36**(22): L22803.

Stanmore, B. R., J. F. Brilhac and P. Gilot (2001). "The oxidation of soot: a review of experiments, mechanisms and models." Carbon **39**(15): 2247-2268.

Stenni, B., M. Proposito, R. Gragnani, O. Flora, J. Jouzel, S. Falourd and M. Frezzotti (2002). "Eight centuries of volcanic signal and climate change at Talos Dome (East Antarctica)." Journal of Geophysical Research-Atmospheres **107**(D9).

Stephens, M., N. Turner and J. Sandberg (2003). "Particle identification by laser-induced incandescence in a solid-state laser cavity." Applied Optics **42**(19): 3726-3736.

Stohl, A. (2006). "Characteristics of atmospheric transport into the Arctic troposphere." J. Geophys. Res. **111**(D11): D11306.

Suglia, S. F., A. Gryparis, R. O. Wright, J. Schwartz and R. J. Wright (2008). "Association of black carbon with cognition among children in a prospective birth cohort study." American Journal of Epidemiology **167**(3): 280-286.

Svensson, A., K. K. Andersen, et al. (2008). A 60 000 year Greenland stratigraphic ice core chronology. Climate of the Past, Copernicus publications **4 (1):** 47-57.

Svensson, A., K. K. Andersen, et al. (2006). "The Greenland Ice Core Chronology 2005, 15-42 ka. Part 2: comparison to other records." Quaternary Science Reviews **25**(23-24): 3258-3267.

Swift, T., J. Perez-Losada, S. Schladow, J. Reuter, A. Jassby and C. Goldman (2006). "Water clarity modeling in Lake Tahoe: Linking suspended matter characteristics to Secchi depth." Aquatic Sciences - Research Across Boundaries **68**(1): 1-15.

Tervonen, K., G. Waissi, E. J. Petersen, J. Akkanen and J. V. Kukkonen (2010). Analysis of fullerene-C60 and kinetic measurements for its accumulation and depuration in Daphnia magna, John Wiley & Sons, Inc. **29:** 1072-1078.

Thevenon, F., F. S. Anselmetti, S. M. Bernasconi and M. Schwikowski (2009). "Mineral dust and elemental black carbon records from an Alpine ice core (Colle Gnifetti glacier) over the last millennium." Journal of Geophysical Research **114**(D17): D17102.

Thevenon, F., D. Williamson, E. Bard, F. S. Anselmetti, L. Beaufort and H. Cachier (2010). "Combining charcoal and elemental black carbon analysis in sedimentary archives: Implications for past fire regimes, the pyrogenic carbon cycle, and the human-climate interactions." Global and Planetary Change **72**(4): 381-389.

Thomas, E. R., G. J. Marshall and J. R. McConnell (2008). "A doubling in snow accumulation in the western Antarctic Peninsula since 1850." Geophysical Research Letters **35**(1): L01706.

Traufetter, F., H. Oerter, H. Fischer, R. Weller and H. Miller (2004). "Spatio-temporal variability in volcanic sulphate deposition over the past 2 kyr in snow pits and firn cores from Amundsenisen, Antarctica." Journal of Glaciology **50**(168): 137-146.

Turner, J., P. Convey, R. Bindschadler, G. di Prisco, E. Fahrbach, J. Gutt, D. A. Hodgson, P. A. Mayewski and C. P. Summerhayes (2009). "Antarctic climate change and the environment." Antarctic Science **21**(6): 541-563.

Turner, M. G., E. A. H. Smithwick, K. L. Metzger, D. B. Tinker and W. H. Romme (2007). "Inorganic nitrogen availability after severe stand-replacing fire in the Greater Yellowstone ecosystem." Proceedings of the National Academy of Sciences **104**(12): 4782-4789.

van de Berg, W. J., M. R. van den Broeke, C. H. Reijmer and E. van Meijgaard (2006). "Reassessment of the Antarctic surface mass balance using calibrated output of a regional atmospheric climate model." Journal of Geophysical Research-Atmospheres **111**(D11).

van der Werf, G. R., J. T. Randerson, L. Giglio, G. J. Collatz, P. S. Kasibhatla and A. F. Arellano Jr. (2006). "Interannual variability in global biomass burning emissions from 1997 to 2004." Atmospheric Chemistry and Physics **6**(11): 3423-3441.

van der Werf, G. R., J. T. Randerson, et al. (2010). "Global fire emissions and the contribution of deforestation, savanna, forest, agricultural, and peat fires (1997-2009)." Atmos. Chem. Phys. **10**(23): 11707-11735.

van der Werf, G. R., J. T. Randerson, L. Giglio, N. Gobron and A. J. Dolman (2008). "Climate controls on the variability of fires in the tropics and subtropics." Global Biogeochemical Cycles **22**(3): GB3028.

van Ommen, T. D. and V. Morgan (2010). "Snowfall increase in coastal East Antarctica linked with southwest Western Australian drought." Nature Geoscience **3**(4): 267-272.

Vaughan, D. G. (2005). "How does the antarctic ice sheet affect sea level rise?" Science **308**(5730): 1877-1878.

Vaughan, D. G., J. L. Bamber, M. Giovinetto, J. Russell and A. P. R. Cooper (1999). "Reassessment of net surface mass balance in Antarctica." Journal of Climate **12**(4): 933-946.

Vautard, R. and M. Ghil (1989). "Singular spectrum analysis in nonlinear dynamics, with applications to paleoclimatic time series." Physica D: Nonlinear Phenomena **35**(3): 395-424.

Velicogna, I. (2009). "Increasing rates of ice mass loss from the Greenland and Antarctic ice sheets revealed by GRACE." Geophysical Research Letters **36**.

Vesaratchanon, J. S., A. Nikolov and D. T. Wasan (2008). "Sedimentation of concentrated monodisperse colloidal suspensions: Role of collective particle interaction forces." Journal of Colloid and Interface Science **322**(1): 180-189.

Vinther, B. M., H. B. Clausen, et al. (2006). "A synchronized dating of three Greenland ice cores throughout the Holocene." J. Geophys. Res. **111**(D13): D13102.

Wang, Z., J. Chappellaz, K. Park and J. E. Mak (2010). "Large Variations in Southern Hemisphere Biomass Burning During the Last 650 Years." Science **330**(6011): 1663-1666.

Warren, S. G. and A. D. Clarke (1990). "Soot in the atmosphere and snow surface of Antarctica." Journal of Geophysical Research-Atmospheres **95**(D2): 1811-1816.

Weingartner, E., H. Burtscher and U. Baltensperger (1997). "Hygroscopic properties of carbon and diesel soot particles." Atmospheric Environment **31**(15): 2311-2327.

Westerling, A. L., H. G. Hidalgo, D. R. Cayan and T. W. Swetnam (2006). "Warming and Earlier Spring Increase Western U.S. Forest Wildfire Activity." Science **313**(5789): 940-943.

Whitlock, C. and P. J. Bartlein (2003). Holocene fire activity as a record of past environmental change. Developments in Quaternary Sciences. S. C. P. A.R. Gillespie and B. F. Atwater, Elsevier. **Volume 1:** 479-490.

Whitlock, C. and C. Larsen (2002). Charcoal as a Fire Proxy. Tracking Environmental Change Using Lake Sediments. J. P. Smol, H. J. B. Birks and W. M. Last, Springer Netherlands. **3:** 75-97.

Whitlock, C. and W. Tinner (2010). "Editorial: Fire in the Earth System." Pages news **18**: 55-56.

Wilhelms, F., J. Kipfstuhl, H. Miller, K. Heinloth and J. Firestone (1998). "Precise dielectric profiling of ice cores: a new device with improved guarding and its theory." Journal of Glaciology **44**(146): 171-174.

Williams, A. A. J., D. J. Karoly and N. Tapper (2001). "The Sensitivity of Australian Fire Danger to Climate Change." Climatic Change **49**(1): 171-191.

Wolbach, W., S., , R. S. Lewis and E. Anders (1985). "Cretaceous Extinctions: Evidence for Wildfires and Search for Meteoritic Material." Science **230**(4722): 167-170.

Wolff, E. W. and H. Cachier (1998). "Concentrations and seasonal cycle of black carbon in aerosol at a coastal Antarctic station." Journal of Geophysical Research-Atmospheres **103**(D9): 11033-11041.

Yang, H., C. Liu, D. F. Yang, H. S. Zhang and Z. G. Xi (2009). "Comparative study of cytotoxicity, oxidative stress and genotoxicity induced by four typical nanomaterials: the role of particle size, shape and composition." Journal of Applied Toxicology **29**(1): 69-78.

Zhang, R. Y., A. F. Khalizov, J. Pagels, D. Zhang, H. X. Xue and P. H. McMurry (2008). "Variability in morphology, hygroscopicity, and optical properties of soot aerosols during atmospheric processing." Proceedings of the National Academy of Sciences of the United States of America **105**(30): 10291-10296.

Zielinska, B., J. Sagebiel, W. P. Arnott, C. F. Rogers, K. E. Kelly, D. A. Wagner, J. S. Lighty, A. F. Sarofim and G. Palmer (2004). "Phase and size distribution of polycyclic aromatic hydrocarbons in diesel and gasoline vehicle emissions." Environ. Sci. Technol. **38**: 2557-2567.

Ziolkowski, L. A. and E. R. M. Druffel (2010). "Aged black carbon identified in marine dissolved organic carbon." Geophysical Research Letters **37**(16): L16601.